

UNIVERSIDADE DE SÃO PAULO
INSTITUTO DE QUÍMICA

Programa de Pós-Graduação em Ciências Biológicas (Bioquímica)

ANA PAULA DE JESUS SANTOS

**Identification of new human mesenchymal stem
cell biomarkers by aptamers**

Versão da tese corrigida

São Paulo

Data do depósito na SPG:

20/02/20

ANA PAULA DE JESUS SANTOS

**Identification of new human mesenchymal stem
cell biomarkers by aptamers**

Identificação de novos biomarcadores de
células tronco mesenquimais de origem humana por meio de
antêmeros

*Tese apresentada ao Instituto de Química da
Universidade de São Paulo para Obtenção do Título
de Doutora em Ciências Biológicas (Bioquímica)*

Orientador: Prof. Dr. Alexander Henning Ulrich

São Paulo

2020

Autorizo a reprodução e divulgação total ou parcial deste trabalho, por qualquer meio convencional ou eletrônico, para fins de estudo e pesquisa, desde que citada a fonte.

Ficha Catalográfica elaborada eletronicamente pelo autor, utilizando o programa desenvolvido pela Seção Técnica de Informática do ICMC/USP e adaptado para a Divisão de Biblioteca e Documentação do Conjunto das Químicas da I

Bibliotecária responsável pela orientação de catalogação da publicação:
Marlene Aparecida Vieira - CRB - 8/5562

S231i Santos, Ana Paula
Identification of new human mesenchymal stem cell biomarker by aptamers . / Ana Paula Santos. - São Paulo, 2020.
109 p.

Tese (doutorado) - Instituto de Química da Universidade de São Paulo. Departamento de Bioquímica.
Orientador: Ulrich, Alexander Henning

1. CB210.9.3.1.1. I. T. II. Ulrich, Alexander Henning, orientador.

DEDICATÓRIAS

*Aos meus pais,
por toda a dedicação e
fortuna de tê-los em minha vida*

AGRADECIMENTOS

Ao concluir esta fase de crescimento profissional e pessoal, chego aqui agradecendo à minha sorte de ter muitas pessoas acerca de mim, que caminharam junto comigo após longos desafios, dificuldades, esperança, alegrias e muita superação.

Agradeço aos meus pais, Clarice e Edvar, pelo caminho percorrido para chegar nessa fase de minha vida e mostrar ao mundo que tudo é possível graças ao amor e à educação. À minha mãe, por toda força e luta trabalhando desde os quinze anos de idade, dedicando sua vida a proporcionar educação, alegrias, conquistas e melhora de vida a mim e à nossa família. Ao meu pai, por todo seu trabalho, amor e devoção ao preservar nossa família como bem maior.

Agradeço à minha família pela compreensão e amor, especialmente à minha tia Cleonice e à minha madrinha Isabel pela presença e entendimento de todo meu esforço. Às minhas primas Girleide e Jakeline, e sua mãe presente em alma, pelo amor e carinho.

Gostaria de agradecer imensamente ao meu orientador e professor Henning Ulrich pelas oportunidades, aprendizado, admiração e confiança no meu trabalho desenvolvido até os dias de hoje. Tive a chance de crescimento e superação em seu laboratório.

Um agradecimento à família Bottino, Vera Maria e Haylton por acreditar e me ajudar sempre em toda à minha trajetória de vida. À Maria Augusta, minha amiga-irmã e à Maria Clara, minha maior incentivadora.

Agradeço ao meu namorado Ignacio com sua presença, amor, orgulho e motivação em uma fase tão difícil e trabalhosa como esta, obrigado por chegar à minha vida na hora certa trazendo toda a paz que o meu coração precisava.

Obrigada aos meus amigos da vida Camila, amiga da alma presente na minha vida pessoal e profissional há 12 anos. À Mariana, à Laís, ao Malson, à Elise, à Maryanne e ao

Bruno, meus amigos que Ribeirão Preto me presenteou e concedeu. E aos meus amigos que valorizaram minha dedicação e preservaram a amizade de infância.

Às minhas grandes conquistas de amizade, na altura dos trinta anos, que o doutorado me concedeu. Ágatha, minha amiga linda de grande coração, nos identificamos e seguimos nos ajudando desde o primeiro dia. Ana Teresa por sempre estar ao meu lado em todos os momentos, sendo uma grande amiga-irmã que Portugal me deu. Juliana, pela sabedoria e alegria misturada, mas sempre com todo carinho do mundo mesmo à distância. Maria Elisa, meu chaveirinho que foi entrando em minha vida e permaneceu nas etapas lindas e ruins da vida. Yahaira, minha amiga porto-riquenha de grande bagagem profissional, mas sempre pronta para os momentos de diversão. E ao Jean, amigo curioso de grande coração e vontade de aprender.

Aos meus colegas de laboratório e de colaboração Arquimedes Cheffer, Fernanda Coutinho, Erika Molina, Mona Oliveira, Isis Cristina, Maria Carolina, Laura Sardá, Ricardo Pereira e Talita Glaser. À Professora Claudiana Lameu, pelas oportunidades e momentos de amizade, ao seu grupo de pesquisa e às técnicas Denise Yamamoto, Zilda e Sirley.

Ao meu coorientador Dr. Matthias Schiemann, que me concedeu o espaço de seu laboratório na Alemanha, me proporcionou oportunidades de crescimento e de colaboração.

Ao Dr. Arthur Nery pelo trabalho desenvolvido, pela dedicação e ensinamento mesmo à distância.

Muito obrigada ao grupo alemão pelo suporte, ao meu aluno de mestrado Anton Mühlbauer, ao Dr. Immanuel Andrä e às técnicas Lynet, Corrine e Suzy. Todos foram muito prestativos. E aos amigos que a Alemanha me concedeu: Jeremy, Gustavo, Bárbara e Lívia.

Agradeço à Coordenação de Aperfeiçoamento de Pessoal de Nível Superior (CAPES) pelo apoio e pelos financiamentos do meu doutorado direto (CAPES PROEX - processo nº

88882.332985/2018-01) e doutorado sanduíche (CAPES PDSE - processo n° 88881.186506/2018-01), além da verba laboratorial.

Obrigada também, à Fundação de Amparo à Pesquisa do Estado de São Paulo (FAPESP) pela verba concedida ao laboratório.

*Life is not easy for any of us. But what of that? We must have
perseverance and above all confidence in ourselves.
We must believe that we are gifted for something, and
that this thing, at whatever cost, must be attained.*

Marie Curie

RESUMO

Santos, A. P. J. **Identificação de novos biomarcadores de células tronco mesenquimais de origem humana por meio de aptâmeros.** 2020. 109 p. Tese de Doutorado – Programa de Pós-Graduação em Ciências Biológicas (Bioquímica). Instituto de Química, Universidade em São Paulo.

Células tronco são células indiferenciadas que podem ser distinguidas de outros tipos celulares por meio da habilidade de se auto renovarem e de se diferenciarem em novos tipos celulares. Células tronco mesenquimais (MSC) são células tronco adultas encontradas em diferentes tecidos como tecido adiposo, polpa de dente e cordão umbilical. Estas células podem se autodividir em células idênticas ou se diferenciarem em células de origem mesodermal. Estas células têm sido estudadas em novas aplicações que envolvem terapia regenerativas. Embora resultados encorajadores tenham sido demonstrados, terapias que utilizam MSC ainda encontram uma grande barreira: a dificuldade no isolamento destas células a partir de um ambiente heterogêneo. MSC são caracterizadas por populações positivas em ensaios de imunomarcção para os epítomos membranares CD29, CD73, CD90 e CD105, presentes também em outros tipos celulares. Assim, o presente trabalho tem o objetivo de identificar novos biomarcadores de MSC de origem humana, utilizando aptâmeros de DNA produzidos pela técnica SELEX (Systematic Evolution of Ligands by EXponential Enrichment) como ferramenta. Nossos resultados mostraram que MSC de diferentes origens ligam-se a aptâmeros (oligonucleotídeos de DNA ou RNA que atuam como ligantes específicos de alvos moleculares) de DNA candidatos que atuam no isolamento de MSC por meio da técnica FACS de separação celular, promovendo uma maior indução de diferenciação em células específicas (condrócitos, osteócitos e adipócitos) comparada com a população total de MSC. Análises de citometria de fluxo mostraram que os aptâmeros candidatos se ligam a 50% das MSC de polpa de dente e não apresentam taxa de ligação significativa para fibroblastos e linfócitos de origem humana - utilizados como controles negativo. Além do

mais, imagens de imunofluorescência e confocal mostraram ligação na superfície da membrana de MSC e a marcação interna de monócitos a estes aptâmeros. Portanto, um aptâmero controle (CNTR APT) foi utilizado para comparar a especificidade dos aptâmeros ligados a células viáveis, mostrando a não ligação deste aptâmero a MSC. Porém, 40% da população de monócitos ligou-se ao CNTR APT. Uma normalização baseada na comparação entre as taxas de ligação entre células ligadas com aptâmeros candidatos e o aptâmero controle gerou uma taxa de especificidade entre 10-16 vezes maior para MSC contra 2,5 vezes para os monócitos. Deste modo, embora os resultados tenham mostrado uma taxa de ligação entre monócitos e aptâmeros, as MSC ligadas aos aptâmeros candidatos possuem uma maior taxa de especificidade devido a uma maior presença de antígenos que são expressos em ambas as células. Um ensaio de Pull Down seguido de espectrometria de massas foi utilizado para a identificação de biomarcadores que se ligariam aos aptâmeros candidatos, e que não seriam co-expressos por monócitos e por antígenos ligados ao aptâmero controle. Deste modo, a proteína ADAM17 foi identificada nas amostras de APT10 ligadas às MSC. Tal proteína está relacionada à inibição de uma cascata de sinalização da família de proteínas TGF β , responsável pela diferenciação de MSC. Assim, MSC com maior potencial tronco deveriam expressar ADAM17 em maior quantidade. Tal proteína apresenta um sítio catalítico que demonstra interagir com o APT10, de acordo com predição Docking entre proteína e DNA. Foi identificada também, a proteína VAMP3, que pertence a um complexo proteico transmembranar responsável pelos processos de endocitose e exocitose, e que podem ter um papel importante na liberação de citocinas e outras moléculas relacionadas às respostas imune e inflamatórias. Deste modo, o APT10 identificou proteínas importantes que devem estar relacionadas com a melhora de imunoterapias que utilizam MSC.

Palavras-chave: Células tronco mesenquimais, aptâmeros, Cell-SELEX, ADAM17, VAMP3.

ABSTRACT

Santos, A. P. J. **Identification of new human mesenchymal stem cell biomarker by aptamers.** 2020. 109 p. Doctorate Dissertation – Post-Graduate Program in Biological Sciences (Biochemistry). Chemistry Institute, University of São Paulo

Stem cells are undifferentiated cells that can be distinguished from others by their ability to self-renew and to differentiate into new specific cell types. Mesenchymal stem cells (MSC) are adult stem cells that can be obtained from different sources, such as adipose tissue, bone marrow, dental pulp, and umbilical cord. They can either replicate, originating new identical cells, or differentiate into cells of mesodermal origin and from other germ layers. MSC have been studied as new tools for regenerative therapy. Although encouraging results have been demonstrated, MSC-based therapies still face a great barrier: the difficulty of isolating these cells from heterogeneous environments. MSC are currently characterized by immunolabelling through a set of multiple surface membrane markers, including CD29, CD73, CD90 and CD105, which are also expressed by other cell types. Hence, the present work aimed to identify new specific biomarkers for the characterization of human MSC using DNA aptamers produced by the SELEX (Systematic Evolution of Ligands by EXponential Enrichment) technique. Our results showed that MSC from different origins bound to DNA candidate aptamers, that is, DNA or RNA oligonucleotides selected from random libraries that bind specifically to biological targets. Aptamer-bound MSC could be isolated by fluorescence-activated cell sorting (FACS) procedures, enhancing the induction of differentiation into specific phenotypes (chondrocytes, osteocytes and adipocytes) when compared to the whole MSC population. Flow cytometry analyses revealed that candidate aptamers bound to 50% of the MSC population from dental pulp and did not present significant binding rates to human fibroblasts or lymphocytes, both used as negative control. Moreover, immunofluorescence images and confocal analyses revealed staining of MSC by aptamers localized in the surface

membrane of these cells. The results also showed internal staining of human monocytes by our investigated aptamers. A non-specific control aptamer (CNTR APT) obtained from the random pool was then utilized to compare the specificity of the aptamers bound to the analyzed non-apoptotic cells, showing no staining for MSC. However, 40% of the monocytes bound to the CNTR APT. Normalized data based on the cells bound to candidate aptamers compared to those bound to the CNTR APT, revealed a 10 to 16-fold higher binding rate for MSC against 2-fold for monocytes. Despite its low specificity, monocyte-aptamer binding occurs probably due to the expression of shared markers with MSC, since monocytes are derived from hematopoietic stem cells and are important for the immune system ability to internalize/phagocyte external molecules. Given that, we performed a pull-down assay followed by mass spectrometry analysis to detect which MSC-specific protein or other target epitope not coexpressed by monocytes or the CNTR APT would bind to the candidate aptamer. Distinguishing between MSC and monocyte epitopes is important, as both cells are involved in immunomodulatory effects after MSC transplantations. ADAM17 was found to be a target of the APT10, emerging as a possible biomarker of MSC, since its involvement in the inhibition of the TGF β signaling cascade, which is responsible for the differentiation of MSC. Thus, MSC with a higher stemness profile should overexpress the protein ADAM17, which presents a catalytic site with affinity to APT10. Another target of Apt 10 is VAMP3, belonging to a transmembrane protein complex that is involved in endocytosis and exocytosis processes during immune and inflammatory responses. Overall, proteins identified as targets of APT10 may be cell surface MSC biomarkers, with importance for MSC-based cell and immune therapies.

Keywords: Mesenchymal stem cells, aptamers, Cell-SELEX, biomarkers, ADAM17, VAMP3.

ILLUSTRATIONS AND TABLES

Figure 1. Schematic representation of the functionality of aptamers	21
Figure 2. Schematic Cell-SELEX procedure with all relevant steps	22
Table 1.: Advantages and drawbacks of the aptamer applications	23
Table 2.: Sequences of DNA aptamers selected for AD-MSK by Cell SELEX technique	31
Figure 3. Setting of populations of different cell types by flow cytometry	42
Figure 4. Flow cytometry analysis of known MSC surface markers	43
Figure 5. Flow cytometry analysis of known lymphocyte surface markers	45
Figure 6. Flow cytometry analysis of known lymphocyte and monocyte surface markers	46
Figure 7. Verification of aptamer standard concentration by MSC binding rate analyses	49
Table 3. The average of binding rate of aptamers and cells	51
Figure 8. Flow cytometry analysis of the binding rate (%) of different cell types bound to aptamers	51
Figure 9. Quantitative flow cytometry analysis of apoptotic induction by staurosporine	54
Figure 10. Binding rate efficiency and specificity of candidate aptamers to lymphocytes, monocytes and MSC	57
Figure 11. Flow cytometry analysis of binding rates (%) of aptamers to DPMSC, UCMSC, PBMCs and monocytes	58
Figure 12. Immunofluorescence of DP-MSK and fibroblasts stained with aptamers	60
Figure 13. Co-staining analysis of DP-MSK bound to aptamers and specific surface marker epitopes by immunofluorescence microscopy	61
Figure 14. Confocal images of live and adhered UC-MSK, stained with a panel of aptamers and anti- CD90 surface marker.	63
Figure 15. Confocal microscopy of live PBMCs and isolated monocytes stained with a panel of aptamers	65
Figure 16. Characterization of stemness surface markers in human lymphocytes by flow cytometry	68
Figure 17. Characterization of stemness surface markers in human monocytes cells by flow cytometry.	70
Figure 18. Flow cytometry analysis of MSC surface marker profiles of fresh isolated aptamer positive population of MSC by flow cytometry	72

Figure 19. Flow cytometry analysis of MSC surface marker profile after <i>in vitro</i> culture of aptamer-sorted MSC	74
Figure 20. Flow cytometry analysis of MSC surface marker profile of fresh aptamer-restained MSC after <i>in vitro</i> cultivation	75
Figure 21. Cellular differentiation of heterogeneous MSC and aptamer-sorted MSC ..	78
Figure 22. Differentiation potential of MSC quantified by the tissue cytometry technique	80
Figure 23. Mean color intensity comparison for differentiated aptamer-sorted and non-sorted MSC by tissue cytometry technique	81
Figure 24. Confirmation of biotin-aptamer DNA linked to streptavidin-immobilized beads for affinity chromatography assay	84
Figure 25. Verification of membrane surface proteins bound to aptamers in a pull down assay with DP-MSD and blood cell lysates	86
Figure 26. Amino acid sequences of ADAM 17 and VAMP3 proteins found by spectrometry mass for MSC	90
Table 4.: Description of proteins identified by mass spectrometry when bound to the complex “APT10-MSD surface lysate” after a pull down assay.....	90
Figure 27. ADAM17 interaction with aptamer 10 model	92
Table 5: Scoring information of ADAM17 and aptamer interaction, as predicted by HDock	93
Figure 28. VAMP3 interaction with aptamer 10 model	95

ABBREVIATIONS

Embryonic stem cells - **(ESC)**

Mesenchymal stem cells - **(MSC)**

International Society of Cell Therapy - **(ISCT)**

Systematic Evolution of Ligands by Exponential Enrichment - **(SELEX)**

Polymerase chain reaction - **(PCR)**

Single strand DNA - **(ssDNA)**

Single strand RNA - **(ssRNA)**

Human MSC from adipose tissue - **(AD-MSC)**

Human MSC from umbilical cord - **(UC-MSC)**

Human MSC from dental pulp - **(DP-MSC)**

Phosphate buffered saline - **(PBS)**

6-carboxyfluorescein - **(6-FAM)**

Human peripheral blood mononuclear cells - **(PBMCs)**

Dimethyl sulfoxide - **(DMSO)**

Fluorescence-activated cell sorting - **(FACS)**

Aptamer-sorted MSC - **(APT-MSC)**

Undifferentiated MSC - **(UND MSC)**

Non-sorted differentiated MSC- **(CTL MSC)**

Dulbecco's Modified Eagle Medium - **(DMEM)**

Aptamer - **(APT)**

Control/random aptamer - **(CNTR APT)**

Acetonitrile - **(ACN)**

Formic acid - **(FA)**

Trifluoro acetic acid - **(TFA)**

Disintegrin and metalloproteinase domain-containing protein 17 (**ADAM17**)

Vesicle-associated membrane protein 3 - **(VAMP3)**

Analysis of Variance (**ANOVA**)

Forward scatter (**FSC**)

Side scatter (**SSC**)

Phycoerythrin (**PE**)

Allophycocyanin - **(APC)**

Phycoerythrin and a cyanine dye - **(PECy5)**

Pacific Blue - **(PB)**

Phycoerythrin-Texas Red - **(ECD)**

SUMÁRIO

1. INTRODUCTION	19
1.1 MESENCHYMAL STEM CELLS AND THEIR POTENTIAL FOR MEDICINE.....	20
1.2 APTAMERS.....	20
2. JUSTIFICATION	25
3. AIMS	27
4. MATERIALS AND METHODS	29
4.1 CULTURE OF MESENCHYMAL STEM CELLS	29
4.2 ISOLATION OF MSC FROM UMBILICAL CORD.....	29
4.3 ISOLATION OF PERIPHERAL BLOOD MONONUCLEAR CELLS FROM WHOLE BLOOD OR BUFFY COAT	30
4.4 CELLULAR STAINING WITH APTAMERS.....	30
4.5 FLOW CYTOMETRY ASSAY.....	32
4.6 IMMUNOFLUORESCENCE MICROSCOPY ANALYSIS	32
4.7 CELL DEATH ASSAY VIA APOPTOSIS.....	33
4.8 CHARACTERIZATION OF RECOVERED APTAMER-STAINED CELLS	33
4.9 MONOCYTE ISOLATION AND APTAMER-STAINING ANALYSIS.....	34
4.10 DIFFERENTIATION OF APTAMER-SORTED DP-MSC	34
4.11 PULL DOWN ASSAY WITH APTAMERS	35
4.12 MASS SPECTROMETRY OF APT10-STAINED MSC.....	36
4.13 BIOINFORMATIC ANALYSIS OF APT10 BOUND TO CANDIDATE BIOMARKERS	36
4.131 Prediction of aptamer 3D-structure	36
4.132 Homology model generation	37
4.133 Protein aptamer molecular docking.....	38
4.14 STATISTICAL ANALYSIS	38
5. RESULTS AND DISCUSSION	41
5.1 VALIDATION OF SURFACE MARKERS FROM HUMAN MSC, LYMPHOCYTES AND MONOCYTES.....	41
5.2 QUANTIFICATION OF APTAMER BINDING RATE ON HUMAN MSC FROM DIFFERENT ORIGINS	47
5.3 VERIFICATION OF APTAMER BINDING TO VIABLE CELLS	52
5.4 BINDING EFFICIENCY AND SPECIFICITY BETWEEN VIABLE CELLS AND CANDIDATE APTAMERS	55
5.5 ANALYSIS OF APTAMER BINDING SITES ON MSC	59
5.6 HEMATOPOIETIC STEM CELL LABELING IN PBMCs	66
5.7 CONFIRMATION OF THE SURFACE PROFILE OF FACS-SORTED APTAMER-STAINED MSC	71
5.8 DIFFERENTIATION POTENTIAL OF ISOLATED APTAMER-STAINED MSC.....	77
5.9 IDENTIFICATION OF SURFACE PROTEINS BOUND TO APTAMERS.....	82
5.10 ANALYSIS OF MSC BIOMARKERS BOUND TO SPECIFIC APTAMERS	87
5.11 BIOINFORMATIC ANALYSIS OF APT10 BINDING TO ADAM17 AND VAMP3	91
5. CONCLUSION.....	97
PERSPECTIVES	99
7. REFERENCES.....	101
8. LISTA DE ANEXOS.....	109

8.1 SÚMULA CURRICULAR.....	109
8.2 PUBLICAÇÕES.....	109

1. INTRODUCTION

The research on stem cells and their use for regenerative medicine therapies has grown in the last few years. Stem cells can be classified by their potential of differentiation as totipotent (able to differentiate into all types of embryonic and extraembryonic cells), pluripotent (able to differentiate into all three embryonic follicles), multipotent (able to differentiate into some cellular types of the embryonic follicle) and unipotent (able to differentiate into a single type of mature cell) (Wagers et al., 2004). Embryonic stem cells (ESC) are pluripotent stem cells that can differentiate into all types of somatic cells, forming all the three embryonic germ layers. On the other hand, adult stem cells, formed in the post-embryo stages, can originate only cells restricted to its original tissue (Can et al., 2008). Mesenchymal stem cells (MSC) are multipotent stem cells found in most adult tissues, such as adipose tissue, synovial membrane, dermis, periosteum, peripheral blood, menstrual blood, and in solid organs (liver, spleen, lung, among others) (Baer et al., 2012).

Although MSC are of great clinical relevance, there is a lack of a unique MSC marker that could be reliably used for isolation and purification of these cells. Thus, the isolation of MSC from a heterogeneous tissue environment has always been difficult, since their surface markers are also expressed by other cell types. Specific ligands such as small molecules, antibodies and peptides have been developed for specific molecular recognition. Nowadays, nucleic acid-related approaches are attracting significant interest for its possible application in many biological processes, such as diagnostic, technologic and therapeutic ones (Lauridsen et al., 2012). Recently, another type of molecular ligand called aptamer has drawn significant attention due to its many applications (Wu et al., 2012), such as the identification and isolation of specific targets. The most known commercially available aptamer is Pegaptanib (known as Macugen), an RNA aptamer that identifies vascular epidermal growth

factor (Ng et al., 2006), a cell receptor target. Moreover, it is sold by Pfizer for age-related macular degeneration therapy (Ng et al., 2006).

In this work, the aptamer technology appeared as a potential tool for purification and identification of MSC by a specific target interaction.

1.1 Mesenchymal Stem Cells and their Potential for Medicine

Mesenchymal stem cells (MSC) are multipotent stem cells that were initially characterized as plastic adherent and fibroblastoid cells found in many adult tissues, such as adipose tissue and solid organs (Friedenstein et al., 1970 ; Baer et al., 2012). In recent years, the focus on MSC has increased, since they show a great plasticity and potential for therapeutic applications (Nery et al., 2013).

The main criterium defined for the identification of MSC, according to the International Society of Cell Therapy (ISCT), is that those cells should express CD105, CD73 and CD90 surface markers and not express the markers CD45, CD34, CD14, CD11b, CD79 α , CD19 and HLA-DR surface molecules (Lin et al., 2012). Therefore, in addition to their plastic adherent (fibroblastic-like) properties, cultured MSC have been characterized as CD45⁻CD34⁻CD105⁺CD73⁺CD90⁺ cells (Dominici et al., 2006). Since a unique marker for MSC has not been identified yet, safe isolation and purification from heterogeneous tissue environments is still under development. This led to the conclusion that clinical applications of MSC depend on well-determined identification and isolation procedures.

1.2 Aptamers

Looking for novel catalytic mechanisms for the molecular recognition functionalities, ribozymes and DNA ligands drew significant attention for this subject. The aptamer ligands are single-stranded RNA or DNA oligonucleotides with high specificity and affinity for their

target molecules. Their ability to bind to molecular proteins originates from their sequence-encoded three-dimensional conformations and their capacity to form intermolecular interactions with the target (via hydrogen bonds, electrostatic and Van der Waals forces) (Seelam et al., 2019).

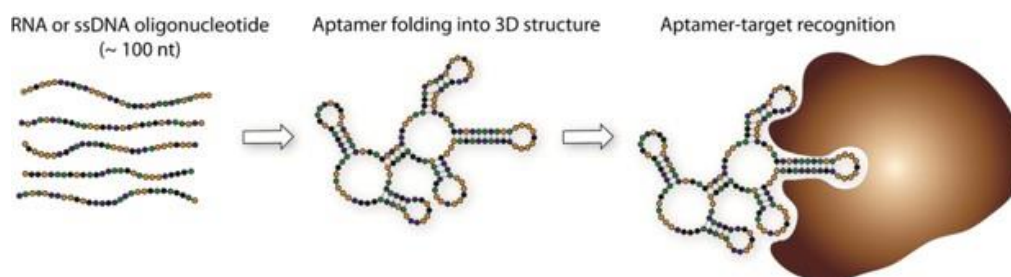


Figure 1. Schematic representation of the functionality of aptamers. The aptamer-target interaction is based on three dimensional interaction points, where hydrogen bonds, electrostatic and Van de Walls forces act. An aptamer 3D-structure is highly dependent on the ionic constitution of the environment. Adapted from Darmostuk et al., 2015.

In vitro evolution of oligonucleotide-libraries leads to the selection of oligonucleotides with desired recognition properties to a target molecule in a process called Systematic Evolution of Ligands by Exponential Enrichment (SELEX). SELEX consists of iterative rounds of DNA/RNA sequence selection that bind to a specific target, by favoring in vitro amplification of sequences with better affinity and selectivity for the target. This process is intermediated by amplification of selected sequences exerting an artificial selection pressure, and by negative selection rounds to subtract aptamers that might bind to sites other than the selection target. Targets can range from small molecules, metallic ions to a whole individual cell (Catherine et al., 2014; Ohuchi, 2012 and Ninjee et al., 2005).

The Cell-SELEX technique uses the whole individual cell as a target for the selection of an aptamer from an initial DNA library. All the cell surface epitopes are included in the process of aptamers selection against membrane proteins. Moreover these molecules are hard

to be purified and has great value for the biomarkers research (Nery et al., 2009 and Chang et al., 2013). Similar to conventional SELEX, an oligonucleotide library is incubated with specific targets for the Cell-SELEX; in this case, cells are used for the selection. The unbound DNA oligonucleotides are washed out and aptamers are separated from the target and amplified by PCR (Darmostuk et al., 2015). Many surface proteins and receptors are restricted to specific cell lineages, limiting them to a highly heterogeneous environment and granting differentiation upon stimulation (Ulrich et al., 2009). Aptamers bound specifically to non-identified epitopes are submitted to selection steps, followed by negative selection that uses other cell types to eliminate non-specific aptamers that might bind to shared surface epitopes. Therefore, Cell-SELEX is a technology of unbiased approach for biomarkers development that does not require knowledge about the target cell protein composition (Chang et al., 2013).

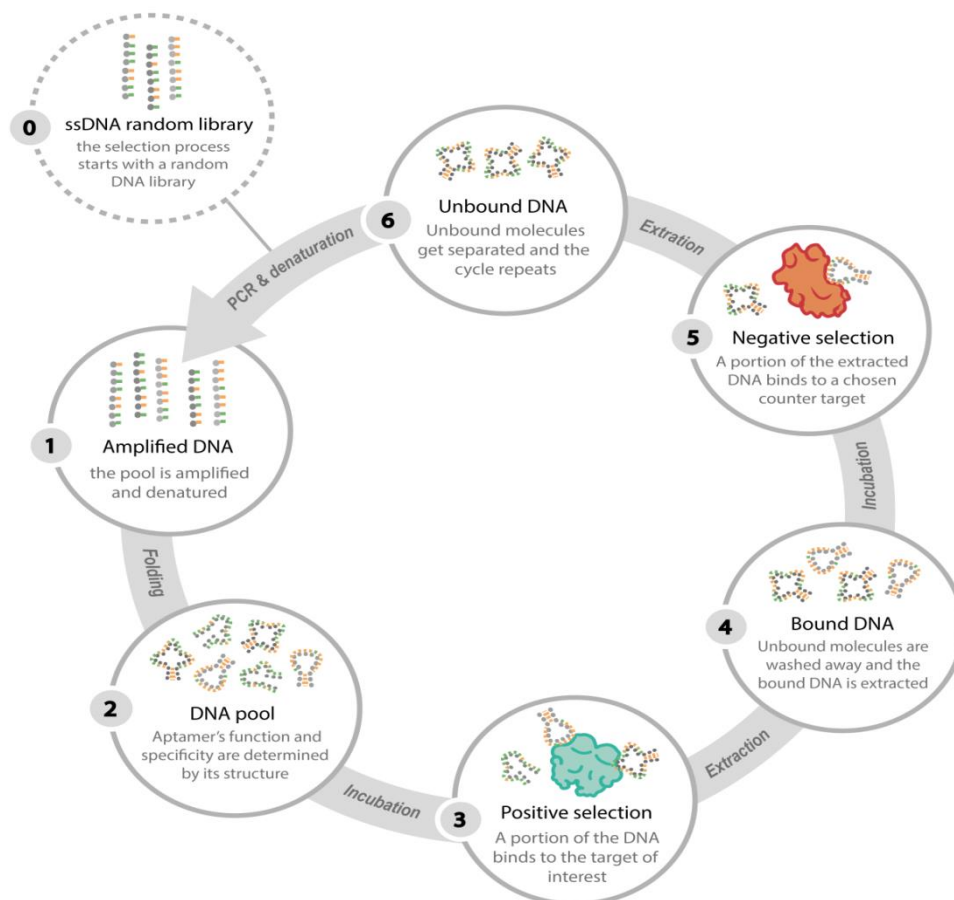


Figure 2. Schematic Cell-SELEX procedure with all relevant steps. The Cell-SELEX process utilizes iterative steps of negative and positive selections, eliminating unbound and non-specific aptamers from a DNA

library. Aptamers bound to the target cells are amplified and subjected to consecutive rounds until their stringency increase (Pereira et al., 2018)

Under optimal buffer conditions, the unpaired bases of aptamers (RNA or DNA) form local secondary structure motifs due to a base stacking and traditional base pairing. The combined secondary structures acquire a defined tertiary structure that is essential for target recognition and specificity (Hermann et al., 2000). In general, single strand (ss) DNA aptamers are more likely to be applicable because of their superior stability and resistance to enzymatic degradation, when compared to RNA aptamers. Additionally, the SELEX procedure benefits from the decreased number of enzymatic steps that are necessary for amplification, when compared to ssRNA (Marimuthu et al., 2012). The main advantages and some drawbacks of using aptamers as binding agents compared to antibodies are summarized in Table 1 (Zhou et al., 2017 and Keefe et al. 2010)

Table 1.: Advantages and drawbacks of the aptamer applications

Advantages	Drawbacks
<i>In vitro</i> production and selection	Rapid degradation by nucleases
Easy modification with functional groups	Rapid excretion via renal filtration
Greater stability (shelf life)	Aptamer cross-reactivity
Increased bioavailability due to small size	Limited target range (electrostatic repulsion)
Low immunogenicity	

Previous studies of our research group (Nery, 2013) identified ssDNA aptamers that could bind to MSC from human adipose tissue. This work established the selection of aptamers by the Cell-SELEX method in addition to a previous published separation technique (Giordano et al., 2001). The process involves the collection of binding ssDNA molecules and the disposal of non-binding or weak-binding molecules from the

combinatorial library (Daniels et al., 2003). The aptamer-purified cell source (CD29⁺/CD90⁺/CD45⁻) obtained by Nery (2013) was confirmed by specific morphology and in vitro differentiation assay. The identified sequences were filed in patent applications in Brazil (BR1020130217018), in the US (US14/915,170) and in the European Union (14839532-0). In this work, we will validate and characterize these sequences and identify the MSC target bound to the previously selected aptamers.

2. JUSTIFICATION

Research on stem cells has gained prominence due to the high potential for regeneration and self-renewal of these cells. The interest in this cell type has grown exponentially in recent years due to its great potential application in the regeneration of damaged tissues and organs. The growing number of research groups studying MSC and new researchers attracted by this field accelerate the scientific discovery and development of new cellular therapies (Dominici et al., 2006). Some examples of therapeutic treatments from bone marrow mesenchymal stem cells (BM-MSC) include cardiovascular repair, pulmonary fibrosis treatment, spinal and bone marrow lesions, and cartilage repair (Barry et al., 2004). Current methods of purification and extraction of MSC based on plastic adhesion require too much time for immediate therapeutic use in emergency procedures. Thus, it is necessary to develop new cell recognition techniques to facilitate the identification and isolation of these cells. Previous studies from our laboratory by Nery et al., 2013 (Doctoral Thesis defended), succeeded in the selection of aptamers for adipose tissue mesenchymal stem cells (AD-MSC). Now, it is necessary to characterize the selected aptamer and to identify biomarkers of MSC that might enhance the applicability of these cells to improve regenerative therapies.

3. AIMS

We proposed to characterize selected aptamers developed against MSC of the human adipose tissue and to compare the binding characteristics among different MSC types. Aptamer binding properties were used to identify new possible biomarkers of human MSC.

3.1 Specific aims

- To characterize aptamers selected for AD-MSC concerning the binding to MSC from different origins as well as to other cell types;
- To demonstrate the differentiation potential of aptamer-bound MSC;
- To identify a new biomarker of MSC according to the affinity of cells and candidate aptamers.

4. MATERIALS AND METHODS

4.1 Culture of mesenchymal stem cells

Human MSC from umbilical cord (UC-MSC) were obtained following protocols approved by the Ethical Committee of the Institute of Medical Microbiology, Immunology, and Hygiene - Technical University of Munich, Germany - and MSC from human dental pulp (DP-MSC) were gently provided by Professor Dr. Ulrich Sack from the University of Leipzig, Germany. The cells were cultivated in Mesenchymal Stem Cell Growth Medium (PromoCell®) in 100 mm² plates, at 37°C in an incubator (5% CO₂ and 95% relative humidity) for two weeks. The culture medium was changed every two days (followed by washes with phosphate buffered saline - PBS). At the end of two weeks, cells were trypsinized (0.25% Trysin - EDTA solution, Sigma Aldrich) for expansion or collected for flow cytometry experiments and fluorescence microscopy. Immunostaining against CD45 antigen expressed by blood-derived cells were used to verify the degree of contamination by blood cells. MSC were distinguished from other cell types by immunofluorescence analyses against CD29, CD34, CD90 and CD105 antigens (Yoshimura et al., 2006).

4.2 Isolation of MSC from Umbilical Cord

Fresh human umbilical cords were provided by the Medical Clinic of the Technical University of Munich (Klinikum rechts der Isar der Technischen Universität München), Germany, and washed in phosphate buffer saline (0.01M PBS, pH 7.4). Under sterile conditions, the stem cell bearing Wharton's jelly was collected, cut in small pieces and digested with 1 mg/mL solution of collagenase and hyaluronidase (Sigma Aldrich), diluted in PBS and incubated for 30 minutes at 37°C. To block the protease activity, cell suspension was filled with supplemented MSC medium and centrifuged at 300 X g for 5 minutes. The supernatant was discarded and the pellet was transferred to a pre-coated cell culture flask (75 cm³, Corning®)

containing supplemented MSC medium. Cells were allowed to attach to the plastic surface for 2 weeks without changing the medium.

4.3 Isolation of peripheral blood mononuclear cells from whole blood or buffy coat

Prior to separation, fresh human blood of different individuals was 1:2 diluted with PBS. Peripheral blood mononuclear cells (PBMC) were isolated using 50 mL LeucosepTM tubes and Ficoll solution (Biochrom) carefully overlaid into the diluted cell suspension. The mixture were centrifuged at 2500 x g for 20 minutes at 4°C. Cells and liquid components were separated in distinct layers according to their density. Between two liquid phases (Ficoll solution and blood plasma), a white layer of leukocytes was collected and the isolation of PBMC was completed after washing twice with PBS.

4.4 Cellular staining with aptamers

Aptamers were synthesized (Table 2) with a 6-carboxyfluorescein (6-FAM) fluorophore conjugated to the 5' end of the ssDNA. The sequences had an 18 carbon chain spacer to separate the 6-FAM fluorophore from the DNA strand. In this way, 15 sequences of ssDNA aptamers (IDT Síntese Biotecnologia) selected for AD-MSC by Cell-SELEX and one non-specific control aptamer (IBA Lifesciences) were synthesized for characterization purpose (Table 2). Cells were initially incubated with slow rolling in their appropriate medium for 30 minutes at 25°C for the recovery of surface epitopes. Following the cell centrifugation step at 300 X g for 5 minutes, 2×10^5 cells were resuspended in PBS (500 μ L). In parallel, 1 μ M solution of aptamers (conjugated with 6-FAM; $E_{m\acute{a}x}$: 495 nm - blue laser / $E_{x\acute{m}a}x$: 517 nm - green laser) has undergone a temperature folding process. The aptamer solution was diluted in selection buffer solution (1:5 dilution: 125 mM Hepes, 7 mM KCl, 9

mM CaCl₂ · 2H₂O, 6 mM MgCl₂, 725 mM NaCl, 50 mM glucose at pH 7.4) and incubated at 95°C for 20 minutes and subsequently cooled down to 25°C for 20 minutes (folding process). Finally, cells were incubated with the folded aptamers for 20 minutes under soft stirring, washed the aptamer-cell suspension and used the aptamer-stained cells for the detection methods described below.

Table 2.: Sequences of DNA aptamers selected for AD-MSC by Cell-SELEX technique.

DNA Sequence (5' – 3')	
APT1	6-FAM-C18-GGGAGACAAGAATAAGCGGACCCAAGCCGACCGCCCCCATGAGTCGGGGTGTAAAGGAGGCTCACAACAGGC
APT2	6-FAM-C18-GGGAGACAAGAATAAGCGGAGGGCCGCTGGAACAATGGGTTGCGCGGAAGGAGGCTCACAACAGGC
APT3	6-FAM-C18-GGGAGACAAGAATAAGCGGCACGGACGGGCGCACGCGCTTGAGCCCGGGGAAGGAGGCTCACAACAGGC
APT5	6-FAM-C18-GGGAGACAAGAATAAGCGGCAGGGGCGGGCCGATGCGCTTGAGCCCGGGGAAGGAGGCTCACAACAGGC
APT6	6-FAM-C18-GGGAGACAAGAATAAGCGGCCGAGGCCGACCGGTTCCCTTGAGTCGGGGTGAAGGAGGCTCACAACAGGC
APT7	6-FAM-C18-GGGAGACAAGAATAAGCGGCCGAAGGGCGTCGGAGCGGCCATCACAGGGGAAGGAGGCTCACAACAGGC
APT8	6-FAM-C18-GGGAGACAAGAATAAGCGGCCGGGGGCGTCGGAGCGGCCATCACAGGGGAAGGAGGCTCACAACAGGC
APT9	6-FAM-C18-GGGAGACAAGAATAAGCGGCCGGGGGCGTCGGAGCGCGCTCCAGGGGAAGGAGGCTCACAACAGGC
APT10	6-FAM-C18-GGGAGACAAGAATAAGCGGGCGGGGCGCCTGGAACGATGGGTTGCGCGGAAGGAGGCTCACAACAGGC
APT11	6-FAM-C18-GGGAGACAAGAATAAGCGGGCGGGGGCGCCGAGCGGCCATCGCAGGGGAAGGAGGCTCACAACAGGC
APT12	6-FAM-C18-GGGAGACAAGAATAAGCGGGCAGGCCGACCGGTTCCCTTGAGTCGGGGTGAAGGAGGCTCACAACAGGC
APT13	6-FAM-C18-GGGAGACAAGAATAAGCGGGGATCGCCTGGAACGATGGGTTGCGCACGAAGGAGGCTCACAACAGGC
APT14	6-FAM-C18-GGGAGACAAGAATAAGCGGGGCACCGCCCTGGAGCGATGGGCTCGGGCTGTAAGGAGGCTCACAACAGGC
APT15	6-FAM-C18-GGGAGACAAGAATAAGCGGGGCACCGCCCTGGAGCGATGGGCTCGGGCTGTAAGGAGGCTCACAACAGGC
APT16	6-FAM-C18-GGGAGACAAGAATAAGCGGGGCATCCCGTGGACCCATGGCGTGC CGGATAAGGAGGCTCACAACAGGC
CNTRAPT	6-FAM-C18-GGGCGCAGCAGGC

4.5 Flow cytometry assay

The binding of aptamers to MSC, PBMC and hematopoietic stem cells (HSC) was quantitatively analyzed by flow cytometry (CitoFLEX Mibi, plate loader, Beckman Coulter). Following the aptamer staining protocol previously described, cells were additionally stained with specific human monoclonal antibodies for 20 minutes. For MSC identification, the antibodies (BD Biosciences) used were anti-human CD73 (1:50; phycoerythrin or PE conjugated; Ex_{max} : 546 nm / Em_{max} : 578 nm), CD90 (1:50; allophycocyanin fluorophore or APC conjugated; Ex_{max} : 650 nm / Em_{max} : 660 nm) and CD105 (1:50; fluorochrome conjugated in tandem that combines phycoerythrin or PE - and a cyanine dye or Cy5 or PECy5; Ex_{max} : 482 nm / Em_{max} : 678 nm). For PBMCs, anti-human CD14 (1:10; Life Technologies; Pacific Blue or PB fluorophore; Ex_{max} 401 nm / Em_{max} 452 nm), CD14 (1:50; Dako; APC conjugated), CD45 (1:20, Dako; PB conjugated), CD4 (1:50; Beckman Coulter; Phycoerythrin-Texas Red® -X or ECD; Ex_{max} 488 nm / Em_{max} 613 nm), and CD8 (1:50; Beckman Coulter; PE conjugated) were used. For HSC, staining was performed with anti-human HLA-DR (1:50; Beckman Coulter; PB conjugated) and CD117 (1:15; Dako; APC conjugated). Annexin V (cellular protein that detect early apoptosis; 1:20; APC conjugated) was also added to the cell-aptamer solution for 15 minutes to identify apoptotic cells.

4.6 Immunofluorescence microscopy analysis

For the qualitative analysis of aptamer-bound cells, an immunofluorescence microscopy was performed using the same aptamer staining protocol. Cells were stained for 20 minutes with 1 μ M of the fluorescence-labelled aptamer solution. Afterwards, monoclonal antibodies anti-human CD90 (1:100; BD Biosciences, APC conjugated) and anti-human CD14 (1:5; Invitrogen, APC conjugated) were added for 20 minutes for MSC and PBMCs recognition, respectively. HOECHST 33342 DNA dye (1:10000, Thermo Scientific) was

added to the solution for 10 minutes. Adhered cells and cells in suspension were washed with PBS and analyzed in an 8 well chamber slide (Ibidi®) on a Confocal Leica SP5 microscope. All the antibodies were chosen in order not to overlap the emission wavelength of the aptamer fluorophore (6-FAM).

4.7 Cell death assay via apoptosis

Cell death rates of MSC and PBMCs were measured by flow cytometry (CytoFLEX Mibi) following staurosporine reagent protocol (Sigma Aldrich). This reagent induces cell death in human MSC in a time-dependent manner. 2 µg/mL staurosporine was standardized as the optimal concentration to quantify cell death. The time points of induction of cell death by staurosporine were 30 minutes, 1 hour or 2 hours of incubation at 37°C. We used DMSO as negative control of apoptosis induction and we made the analyses at the same time points of incubation. After staurosporine exposition time, MSC and PBMCs were stained with aptamers for 20 minutes (after the folding process) with annexin V (Life Technologies; 1:20; APC conjugated) for 15 minutes and with anti-human CD14 antibody (Life Technologies, PB conjugated) for 20 minutes prior to analysis.

4.8 Characterization of recovered aptamer-stained cells

To recover live aptamer-bound MSC for further analyses, it was performed a fluorescence-activated cell sorting (FACS) experiment, which is a specific flow cytometry method that allows the sorting of selected cell groups from a mixture into different containers. Initially, cells were stained with 6-FAM-conjugated aptamer, cell type-specific antibodies and the apoptosis detector annexin V (APC conjugated) or LIVE/DEAD Cell aqua stain (1:1000; Invitrogen; $E_{x_{\text{máx}}}$: 405 nm; $E_{m_{\text{máx}}}$: 512 nm), as previously described. For each experiment, we started with 2×10^6 cells. Sorted cells were tested for the anti-human CD90 (APC conjugated)

and CD105 (PECy5 conjugated) markers by regular flow cytometry to confirm their MSC profile. The analysis of isolated aptamer-stained MSC was performed one hour after collection of the cells and two weeks after cell culture under expansion conditions. FACS and regular flow cytometry experiments were carried out using the BD FACSAria II® (BD Biosciences) and CytoFLEX Mibi (Beckman Coulter) equipments, respectively.

4.9 Monocyte isolation and aptamer-staining analysis

Human monocytes were sorted from human PBMCs by FACS (BD FACSAria II®) using anti-human CD14 (1:10; APC conjugated) antibody as cell marker. Collected monocytes (CD14⁺ cell subpopulation) were incubated with aptamer solutions (APT1, APT3, APT10, APT15 and CNTR APT), immediately after the sorting. Stained cells were added to an 8 well chamber slide (Ibidi®), without attaching to the plastic surface, and were analyzed by immunofluorescence using a Confocal microscope (Leica SP5).

4.10 Differentiation of aptamer-sorted DP-MSc

Based on the binding rate results obtained by flow cytometry and immunomicroscopy, a FACS experiment was performed following the previously described protocol. For the isolation of aptamer-stained DP-MSc it was used the candidate aptamers APT1, APT3, APT9, APT10 and APT15. Sorted aptamer-bound MSC were kept in cell culture to evaluate their stem cell-differentiation potential. Each aptamer-sorted cell population was differentiated into chondrocytes, adipocytes and osteocytes during 14 days under specific culture medium (Chondrogenic, Adipogenic and Osteogenic differentiation medium, HyClone - GE Healthcare). After the differentiation procedure, MSC-derived chondrocytes, adipocytes and osteocytes were fixed in 4% paraformaldehyde (4% PFA) and stained with 1% (v/v) toluidine blue (pH 2.5), 0.5% (v/v) oil red-O (6:4 final diluted) and 2% (v/v) Alizarin Red S

(pH 4.1) for 30 minutes to detect the different cell types. The differentiation rate of sorted aptamer-MSC (APT-MSC) compared to undifferentiated MSC (UND MSC) and non-sorted differentiated MSC (CTL MSC) was analyzed using the TissueFAXS system (TissueGnostics).

4.11 Pull down assay with aptamers

DP-MSC were detached from cell culture flasks using TrypLE selected enzyme (1X) solution (Gibco®) for 3 minutes at 37°C, followed by its dilution with DMEM Low medium. Live DP-MSC have recovered their epitopes during 1 hour at 37°C in the same medium. After that, cell pellets were resuspended in 50mM tris-HCL, 150 mM NaCL buffer - pH 8.3 and sonicated for 2 minutes (0°C, 40 kHz, Branson®). The resultant DP-MSC were incubated with a protease inhibitor solution (Thermo Scientific) for 15 minutes and centrifuged for 15 minutes at 25°C, 10.000 X g. Resuspended pellets were incubated with 5 µM biotin-conjugated aptamer (one biotin molecule was conjugated to the 5' end of APT10 and CNTR APT DNA sequences) for 20 minutes. Aptamer-bound MSC were submitted to a pull down assay based on affinity chromatography. Biotin-APT-bound MSC were added to 50 µL of agarose resin bead (Fluka) composed by streptavidin molecules. MSC not bound to any aptamer were washed out by centrifugation (300 X g, 2 minutes). Resin beads were washed 3 times with selection buffer and submitted to a temperature denaturation process (95°C, 30 minutes) in 200 µL of 6M urea buffer (in PBS). Biotin-aptamer molecules bound to streptavidin agarose beads were recovered in the supernatant after centrifugation. Digested protein epitopes from DP-MSC bound to the biotin-aptamers were maintained at 4°C for the mass spectrometry preparation.

4.12 Mass spectrometry of APT10-stained MSC

Digested proteins from DP-MSC that bound to APT10 and CNTR APT were submitted to a SDS-PAGE (5% acrylamide stacking gel, 25 mA; and 16% acrylamide running gel, 30 mA) in 10% SDS loading buffer. After running in a 10% SDS, 0.25M Tris-HCl, 1.92M glycine buffer - pH 8.3, the gel was stained overnight with Comassie R-250 solution (Thermo Scientific) and destained for 2 hours (10% acetic acid and 30% ethanol). Stained bands were cut from the gel in 1 mm² small pieces and washed with a 40% acetonitrile (ACN) solution in 50 mM NH₄HCO₃ buffer (pH 7.0) in a thermomixer at 250 X g for 30 minutes. Samples received 60 µL of 10 mM Dithiothreitol (DDT) in 50 mM NH₄HCO₃ buffer (pH 7.0) prior digestion with 100 ng trypsin (from a 0.005 µg/µL stock) in 10 mM NH₄HCO₃ + 5% ACN for 16 hours at 37°C. The digestion reaction was stopped by adding 10% formic acid (FA). Samples were purified using columns previously activated with 100 µL of absolute ACN and equilibrated 3x with 100 µL of 0.1% FA. Purification was done by a centrifugation step of 4 minutes at 400 X g. Next, 3 washes with 100 µL of 0,1% FA were performed. Samples were eluted by concentration gradient, using 50% ACN and 0.1% trifluoro acetic acid (TFA) solution and 70% ACN and 0.1% TFA solution, respectively. Eluted samples were dried in a speed vaccum and the final product was analyzed by mass spectrometry at Easy nLC-LTQ-Orbitrap Velos (performed at CEFAP biomass, University of São Paulo).

4.13 Bioinformatic analysis of APT10 bound to candidate biomarkers

4.131 Prediction of aptamer 3D-structure

Aptamer tertiary structures were generated by a protocol inspired by the work of Jeddi *and* Saiz, 2017, where the secondary structure prediction supported the inference of a 3D-ssRNA structure, further modified to create the ssDNA aptamer.

The DNA aptamer sequences were converted into their respective RNA counterparts and used together with secondary structure information as input for tertiary structure prediction via RNA-Composer webservice (Biesiada et al., 2016 ; Popenda et al., 2012). Calculated structures were then converted to their respective DNA analogues using a script implemented with the 3DNA package (Lu *and* Olson, 2003), while Maestro (Schrödinger Drug Discovery, v2019.4) was used to edit the sugar moieties, add hydrogen atoms and generate the charges using the force-field (OPLS3e).

4.132 Homology model generation

Disintegrin and metalloproteinase domain-containing protein 17 (or ADAM17, UniProt code: P78536) core, ranging from the amino-acids Pro218 to Ile432, was modelled after ADAM10's ectodomain structure (PDB ID: 6BE6, resolution: 2.8 Å, (Seegar et al., 2017). ADAM17 and ADAM10's ectodomain cores share 30% sequence identity and 53% similarity. A template structure missing residues and loop fragments (residues 357 – 360) was modelled prior to homology modelling generation, using Prime (Jacobson et al.,2004). Loops underwent further refinement using extended sampling option and refining side-chains within 7.5 Å range. OPLS3e force-field and implicit solvent model (VSGB) was used in all calculations (Roos et al, 2019). ADAM17 metalloprotease domain (2DDF, resolution: 1.7 Å) was retrieved from the PDB and fixed using Protein Preparation Wizard. Engineered mutated residues were changed back to match the reference sequence (Ala266Ser, Gly353Val, Gln452Asn), and the product structure was then minimized. Three-dimensional protein structures were generated by homology modelling using the Prime program implemented in the Schrödinger Drug Discovery (v2019.4) software suite with standard options, using secondary-structure prediction options to guide the query-template alignment. Protein complexes were prepared using the protein preparation tool and further refined with a

restrained minimization step, allowing heavy atoms to vary within 0.5 Å of limit, in order to fix steric clashes. All models were inspected for Ramachandran outliers, which were fixed by energy minimization. Illustrations of structures were made with PyMol v2.3 (PyMOL system, Schrödinger).

4.133 Protein aptamer molecular docking

Docking of proteins with aptamers was carried out using the HDOCK webserver platform (Huang et al. 2014 ; Yan et al., 2017) by providing both the protein structural models and the predicted aptamer structures as PDB files. HDOCK is a shape complementarity-based docking algorithm specialized in the interaction between protein and nucleic acids. It calculates the minimal free-energy conformation for the protein-aptamer complex, which is provided as a 3D-complex output. Aptamer-protein complexes for each system were selected based on their energy values and underwent visual inspection and software analysis, to quantify the number and geometry of hydrogen-bonds, polar and hydrophobic interactions. Complexes where aptamers would bind in transmembrane regions were disregarded. The Nucplot software (McDonald et al., 1994 ; Luscombe et al., 1997) was used for identification and characterization of DNA-protein interactions, especially hydrogen bonds.

4.14 Statistical analysis

Flow cytometry and TissueFAXS results were submitted to statistical analysis of One Way Analysis of Variance (ANOVA) followed by post hoc Dunnett test or Bonferroni test, respectively, using Graph Prism 5.0 software (GraphPad Software, USA) . Significance of data was set at alpha lower than 0.05.

5. RESULTS AND DISCUSSION

5.1 Validation of surface markers from human MSC, Lymphocytes and Monocytes

MSC have been isolated from different human tissues, such as adipose tissue, dental pulp and umbilical cord, and were verified regarding a panel of surface antigens expression. The most frequently used positive surface markers expressed by MSC are CD73, CD90 and CD105. These proteins are used as indicator of MSC purity, which cannot be confirmed only by traditional colony microscopy. Therefore, UC-MSC were tested for the expression of CD73 (phycoerythrin [PE] conjugated) and CD90 (allophycocyanin [APC] conjugated) biomarker epitopes expression by flow cytometry analysis. We separated MSC from debris (Figure 3) based on the size and granularity of the cells, as shown by the forward scatter (FSC-A) channel versus the side scatter area environment (SSC-A) (the peak generated by the light through the cells). Doublets were then excluded by analyzing the width and the height signal of one scatter (FSC-W versus FSC-H).

Thereafter, the final gate for the fluorescence intensity of surface markers was obtained from the signal area in the y-axis gated (Figure 4A). Negative controls (MSC without antibodies) were defined as unstained cells despite their basal fluorescence (less than 1%). Basal fluorescence can be attributed to a general autofluorescence in the PE channel, which is stronger than in APC channel, since the longer wavelengths are generally less prone to detect autofluorescence. CD90⁺ and CD73⁺ MSC subpopulations were significantly shifted in the y-axis for both markers, which featured > 98% of cells positive for the respective antibodies (Figure 4B).

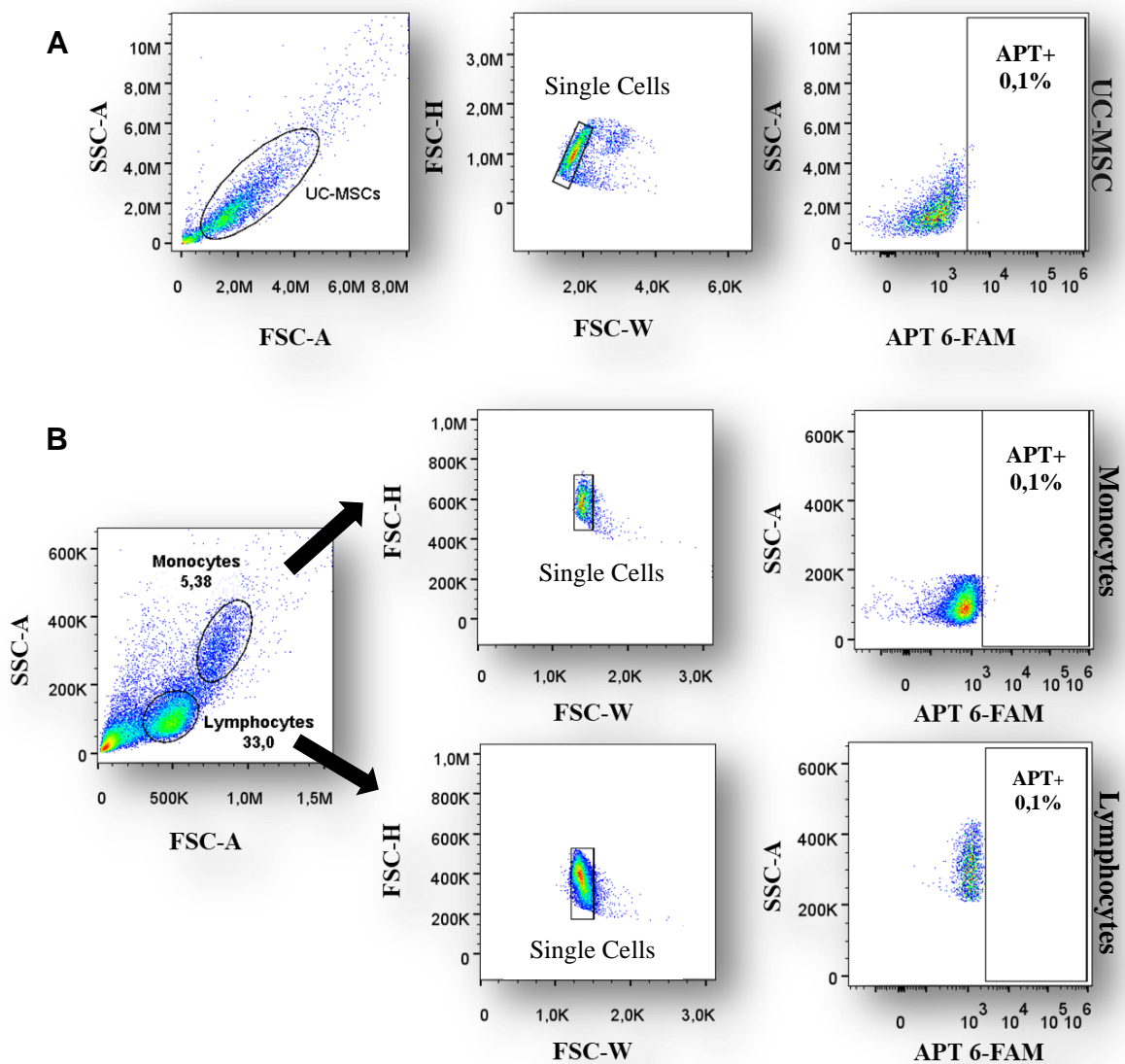


Figure 3. Setting of populations of different cell types by flow cytometry. A) Pseudocolor plots of MSC populations separated by the area of the signal generated by size and granularity (FSC-A versus SSC-A) of the cell's path in the laser (left) by flow cytometry; doublet cells exclusion (middle) by the size of the signal height and interval time (FSC-H versus FSC-W); unstained MSC (right) with negative cell population in the gate APT+ (positive for aptamer-stained cell) detected by the SSC-A scatter channel and 6-FAM fluorescence emission channel (aptamer positive); B) PBMCs separated in lymphocytes and monocytes populations according to the size and granularity of the cells (left); doublet cells exclusion by size (middle); unstained cells with no population at gate APT+ for stained cells (right).

This led to the assumption that isolated cells represented a MSC-containing sample. For all human MSC sources there were similar percentages for the specific surface markers

CD73 and CD90, as indicated in the representative image of UC-MSc (Figure 4). However, the overlap of surface antigens with other cell types, as fibroblastoid cells, must also be taken into consideration, since CD73 and CD90 protein expression alone cannot exclude a possible non-stem-like fibroblast contamination, as fibroblast preparations from different origins were shown to express both markers as well (Alt et al. 2011).

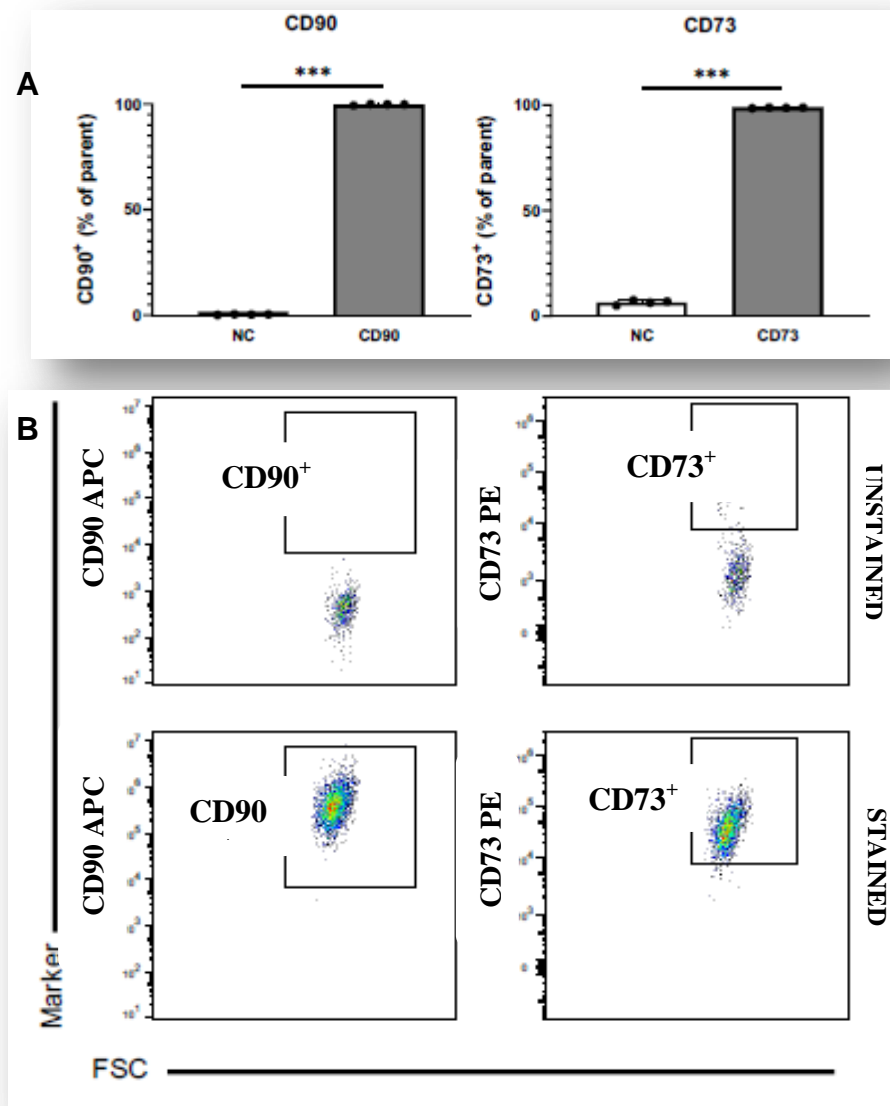


Figure 4. Flow cytometry analysis of known MSC surface markers. A) Pseudocolor plots of unstained UC-MSc (top) and anti CD90/CD73 stained MSC in percentage of live cells (98% of positive cells for the verified antigens); B) Quantitative and statistical analysis of the flow cytometry data image ($n = 4$, $P < 0.05$); NC = Negative control (unstained MSC).

Human peripheral blood mononuclear cells (PBMCs) were used as negative control for any potential unspecific aptamer staining, given that PBMCs also originate from the bone marrow. Hence, they reflect a highly heterogeneous cell compartment that has to be simplified and characterized for their use as a control. Human PBMCs are isolated from peripheral blood and identified as any other blood cell with a round nucleus (i.e. lymphocytes, monocytes, NK cells or dendritic cells) (Verhoeckx et al, 2015). Lymphocytes consist of T cells, B cells and NK cells, which can be used in therapies to recover a patient immune system response. However, cell populations employed are generally not of high purity due to the difficulty of isolating these cells (Neudorfer et al., 2007).

Lymphocytes and monocytes are especially easy to separate by FSC-SSC scatters based on their different size and granularity. Lymphocytes consist of T cells (CD45, CD4, CD8 and CD3), B cells (CD19) and NK cells. CD4⁺ T helper cells and cytotoxic CD8⁺ T cells represent the subdivided populations of T cells. CD45 is a type I transmembrane protein present in differentiated hematopoietic cells (except erythrocytes and plasma cells) under different isoforms, being mainly expressed by lymphocytes (Holmes, et al. 2006).

To verify lymphocyte population's gate in the FSC-SSC analysis, both T cell populations were investigated for the human CD4 (phycoerythrin-Texas Red-x [ECD] conjugated) and CD8 (PE conjugated) presence by flow cytometry (Figure 5). As indicated in the image of the pseudocolor plot (Figure 5A), both populations were detected in the lymphocyte gate with CD4⁺ subpopulation comprising $34 \pm 1,8\%$ and CD8⁺ cells comprising $26 \pm 1,2\%$ of cells (Figure 5B). This ratio is comparable to CD4⁺ and CD8⁺ T lymphocytes from peripheral blood, which ranges from 30 to 50% for CD4⁺ cells and 21 to 30% for CD8⁺ cells (Bliakher et al. 2005).

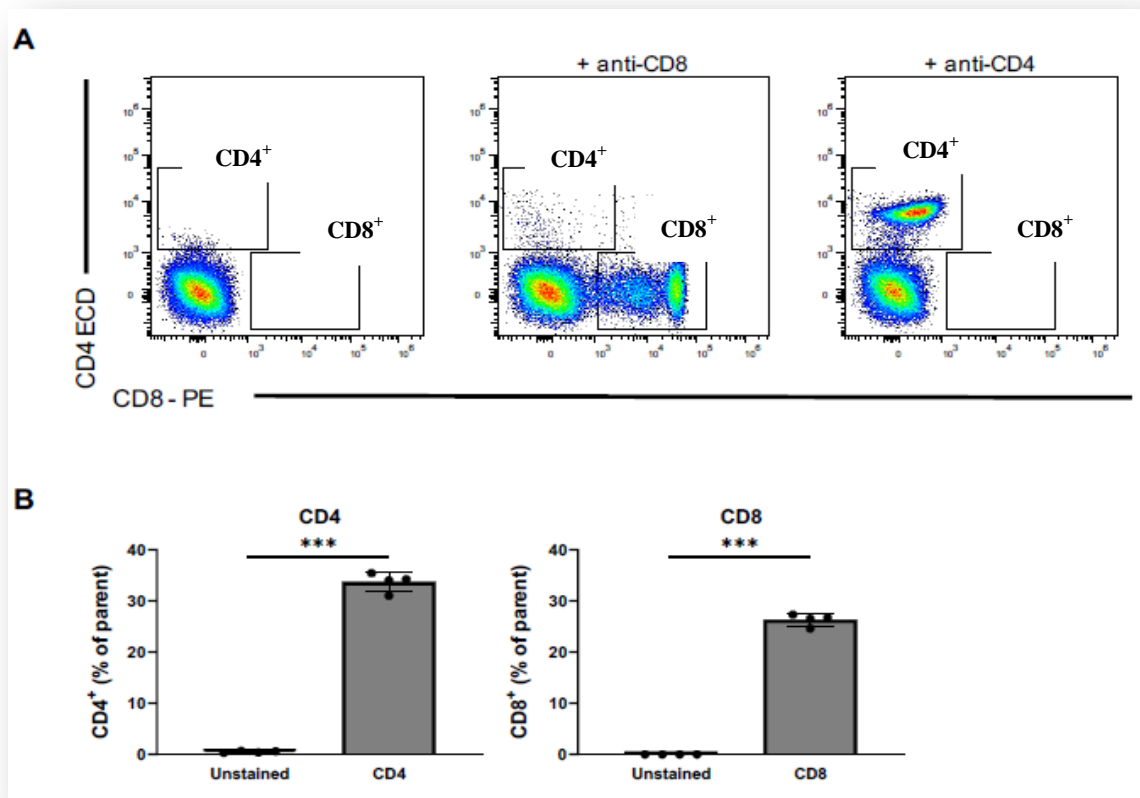


Figure 5. Flow cytometry analysis of known lymphocyte surface markers. A) Pseudocolor plots of unstained control PBMSs (left) and anti CD8/CD4 (in the middle and in the right, respectively) stained PBMCs samples; B) Quantitative and statistical analysis of the flow cytometry data (n = 4, P < 0.05).

Thereafter, the putative monocyte population was investigated for the anti-human CD14 (APC conjugated) marker, which also detects dendritic-like cells. CD14 was described as a monocyte/macrophage differentiation antigen present in the surface of myeloid cell lineages, such as monocytes, macrophages and dendritic cells. Therefore, monocytes showed significantly more CD14 antigen (> 90% of stained cells) than the lymphocytes population, where CD14 is virtually absent (Figure 6).

In the same experiment, we additionally discriminated lymphocyte population by the characterization of T cell and B cell specific markers CD3 (APC conjugated) and CD45 (APC

conjugated), respectively (Figure 6). Lymphocyte population showed a staining of 68% of the cells for CD3 and 53% for CD45 antigens (Figure 6B).

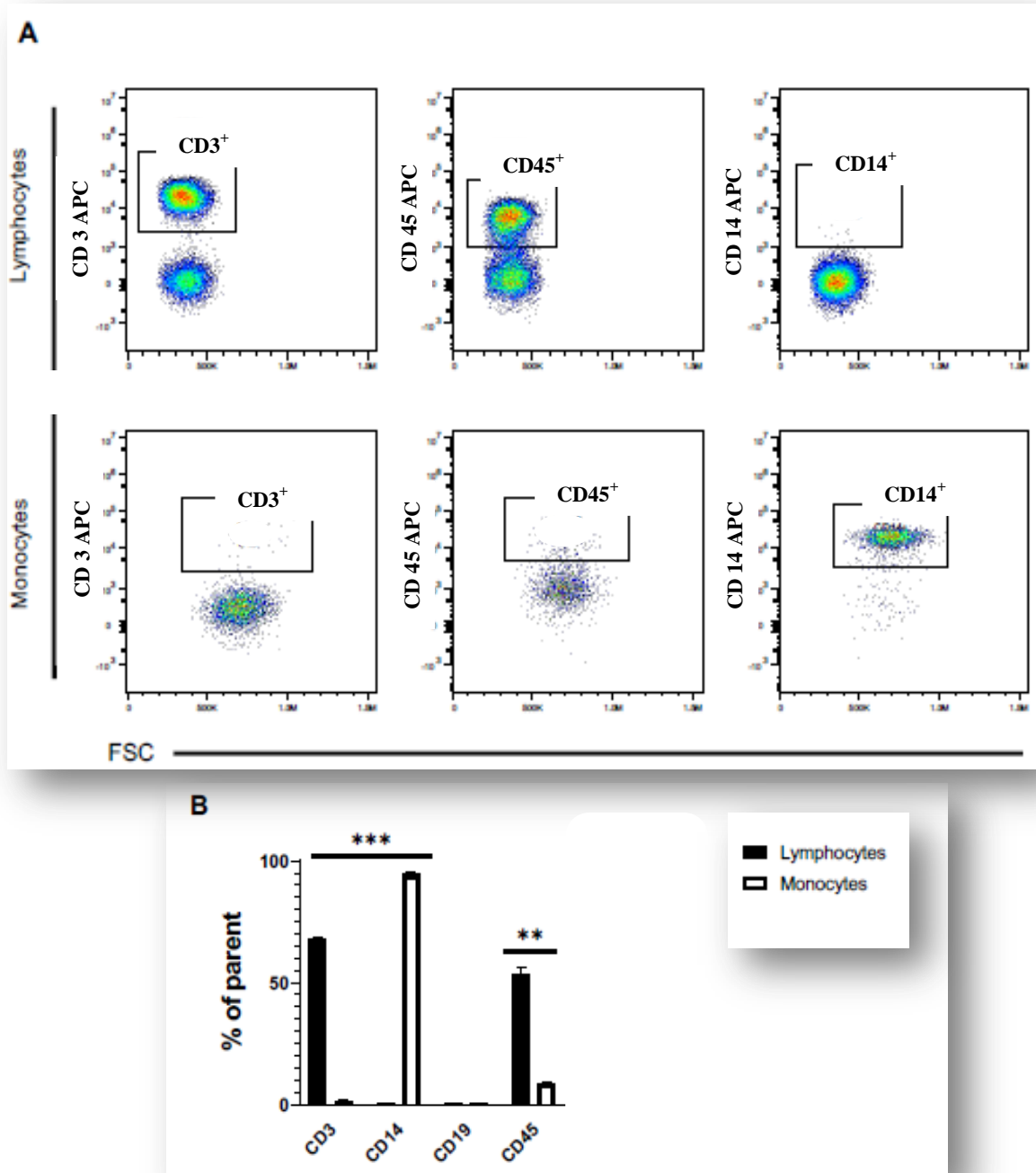


Figure 6. Flow cytometry analysis of known lymphocyte and monocyte surface markers. A) Pseudocolor plots of lymphocyte and monocyte populations, gated by size and granularity based on FSC-SSC scatters, stained and analyzed by APC-conjugated detection antibodies against CD3, CD45 and CD14 specific markers; B) Quantitative analysis of flow cytometry data, comprising all used markers (n=2) and statistical analysis $P < 0.05$.

CD3 antigen is part of the TCR/CD3 complex that facilitates T cell activation. It is generic to CD4⁺ and CD8⁺ cell population of T lymphocytes, exclusively expressed by lymphocyte populations (Chetty et al. 1994). On the other hand, CD45 antigen is a membrane-bound protein composed by an intracellular tyrosine phosphatase domain, presenting many isoforms. CD45 can be considered a pan-leukocyte marker due to its presence in hematopoietic stem cells, T cells, B cells, and also monocytes, even though, it is most prominently expressed by T cells in the lymphocytes compartment. Indeed, monocytes showed high percentage of cells stained for the CD14 marker while this antigen was absent in lymphocyte population. CD14 is a myeloid differentiation antigen expressed primarily by peripheral blood monocytes and macrophages (Haziot et al., 1988). This information was confirmed since only monocytes were 95% positive for CD14 population. Therefore, results suggested that FSC-SSC gates designated for lymphocytes and monocytes were accurate. Despite it, monocytes showed expression of the dendritic cell marker CD11c (data not shown, n=1), which has not been reported in human lymphocytes (Geissmann et al., 2003; Geissmann et al., 2010). CD14⁺ monocytes might also function as dendritic cell precursors by upregulating CD11c. Taken together, it is possible that the observed population resembled true monocytes, which are inherently plastic and express various surface antigens under certain conditions.

5.2 Quantification of aptamer binding rate on human MSC from different origins

The pool of aptamer sequences identifying AD-MSC was previously selected by the Cell-SELEX technique at our laboratory. This aptamer pool was sorted by Magnetic-Activated Cell Sorting (MACS) for the recognition of MSC, which resulted in positive CD90 and CD29, or only CD29 or CD90 surface markers subpopulations (flow cytometry data).

Besides that, after the aptamer pool sequencing, we confirmed, using the software “Mfold”, that each DNA oligonucleotide sequence had its predicted secondary structure (Zucker, 2003), which estimates the Gibbs free energy ($\Delta G^\circ < 0$) of the most stable secondary structures. Therefore, 32 aptamer sequences identified for AD-MSK were classified into different categories, according to their predicted secondary structures and their obtained analogue sequences: Class I, BR5, Class II, R12 and Class III, as defined by Dr. Arthur Nery and colleagues.

For the current work, based on pre-defined structural similarity, 15 aptamers were synthesized and studied for their characterization using different cell types, including MSC from multiple origins. We had chosen the aptamers sequences 3 and 5 from Class I, aptamer 6 from BR5 group, aptamers 7, 8 and 9 from Class II, aptamers 10, 11, 12 and 13 from R12 group, aptamers 14 and 15 from Class III, and aptamers 1, 2 and 16, which did not have predefined secondary structures to be classified into any of the classes/groups. We ordered the chemical synthesis of the aptamers (IDT - Integrated DNA Technologies) with a 6-FAM fluorophore (6- carboxyfluorescein) modification at the 5'-DNA terminus. And finally, we performed flow cytometry assays for the characterization of MSC-bound aptamers by testing cells from human lipoaspirate (AD-MSK) and DP-MSK, using human fibroblast cells as negative control.

First, we compared the binding rates of different amounts of aptamers using two concentrations of aptamer 9 (APT 9): 100 nM and 1 μ M for 1 billion of human DP-MSK (Figure 7). The DNA sequence was folded into its tertiary structure by a temperature “folding” process. Afterward, APT9 was incubated with DP-MSK and flow cytometry results showed that, when the aptamer concentration was increased, the binding rate of aptamer-stained MSC increases from 7.1% to 17.8%. For this assay, we excluded debris and doublets from the analysis, as described previously, resulting in an 84% of total analyzed cells. The

histogram graph (Figure 7A) and the pseudocolor plot (Figure 7B) showed the fluorescence intensity shift (represented by x axis: 6-FAM conjugated APT 9) between the negative control (unstained DP-MSC) and the APT 9 range concentration. We used APT 9 for the cell staining analysis, based on the preliminary results for AD-MSC performed by Dr. Arthur Nery (Nery, 2013). Therefore, the concentration of aptamers used for their binding characterization was defined as 1 μ M.

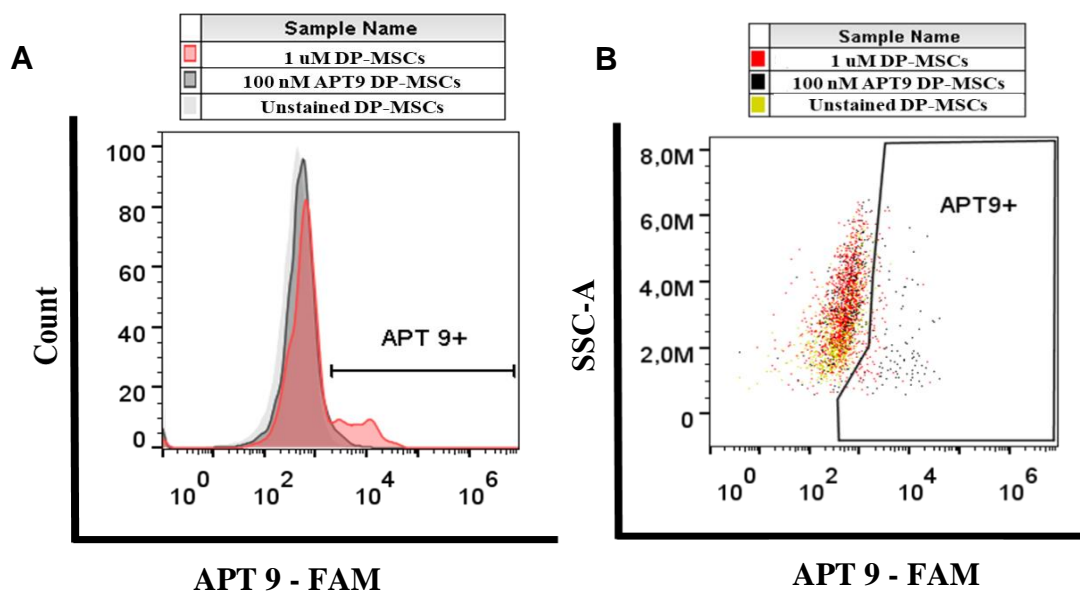


Figure 7. Verification of aptamer standard concentration by MSC binding rate analyses. Aptamer binding quantification by flow cytometry using DP-MSC to verify the standard concentration used for the aptamer characterization analysis, where 84% of cells were considered MSC population. A) Histogram analysis of DP-MSC bound to APT9: light grey peak represented unstained MSC (less than 1%), dark grey peak represented 100 nM APT9 (channel emission by 6-FAM conjugated fluorophore) bound to cells (7,1%), red color peak represents 1 μ M APT 9 stained MSC (17,8%); B) Pseudocolor plot representing the shift of events, evidenced by the appearance of a subpopulation of cells when stained with APT9: the same staining percentage performed by yellow color (unstained MSC), black color (100 nM APT9) and red color (1 μ M APT 9) events; y-axis analyzed by granularity on side scatter - SSC-A.

After setting the correct concentration of aptamers for further characterization analyses, we analyzed the aptamer staining for MSC from different origins. For that, we

checked by flow cytometry the binding rate of AD-MSK and DP-MSK (confirmed subpopulations positive to CD29, CD73 and CD90 surface markers) using the 15 selected aptamers. We also analyzed binding rate nature of human fibroblast cells and aptamers for a negative control comparison, based on their similar structural morphology (Figure 8). Using the same flow cytometry analysis strategies, we excluded debris and doublets from the total number of cells in order to find the binding rate of 1 μM aptamers (6-FAM conjugated) to the human cell types (DP-MSK, AD-MSK and fibroblast).

Results showed that aptamers with similar structures (e.g. Class II, represented by aptamers 7 and 9) had a higher binding rate to MSK depending on the cell origin (Figure 8A). APT10 presented the highest average binding rate to all MSK types: 50.5% of stained DP-MSK, 41% of stained AD-MSK and 5.7% of stained fibroblasts. Moreover, we verified that DP-MSK were the cell type with best binding rate results.

Aptamer binding to fibroblast revealed only a small percentage of stained cells. We showed that APT1, APT2, APT3, APT5, APT6, APT7, APT8, APT9, APT10, APT11, APT12, APT13, APT14, APT15 and APT16 presented a $42\% \pm 1.4$ average binding to DP-MSK, $24.3\% \pm 1.8$ average binding to AD-MSK, and $2.8\% \pm 0.6$ average binding to fibroblasts (Table 3).

Besides that, the analysis also showed that the stained cell subpopulation clearly shifted when bound to aptamers. When analyzing APT10 stained cells in a single representative experiment (Figure 8B), we found that from a total of 63.5% viable cells, 69.8% of DP-MSK were stained for the aptamer. The subpopulation shift was not pronounced following staining of fibroblasts. A population of 80% viable cells showed 16.8% of APT10-stained cells, due to unspecific staining through auto fluorescence emission in this replicate.

Table 3. The average of binding rate of aptamers and cells.

	DP-MSCs	AD-MSCs	Fibroblasts
APT1	42,8%	23,2%	3,3%
APT2	29,7%	22,7%	0,4%
APT3	36%	20,9%	0,8%
APT5	38%	19,2%	0,6%
APT6	38,2%	17,5%	0,4%
APT7	50,2%	23,5%	7,9%
APT8	41,6%	22,3%	2,3%
APT9	49,3%	28,6%	6,5%
APT10	50,5%	40,9%	5,7%
APT11	44,4%	21,5%	4,6%
APT12	41,8%	31,6%	2,1%
APT13	42,5%	24,7%	1,3%
APT14	40,9%	25,1%	0,7%
APT15	42,3%	21%	3,6%
APT16	40,4%	22%	2,4%

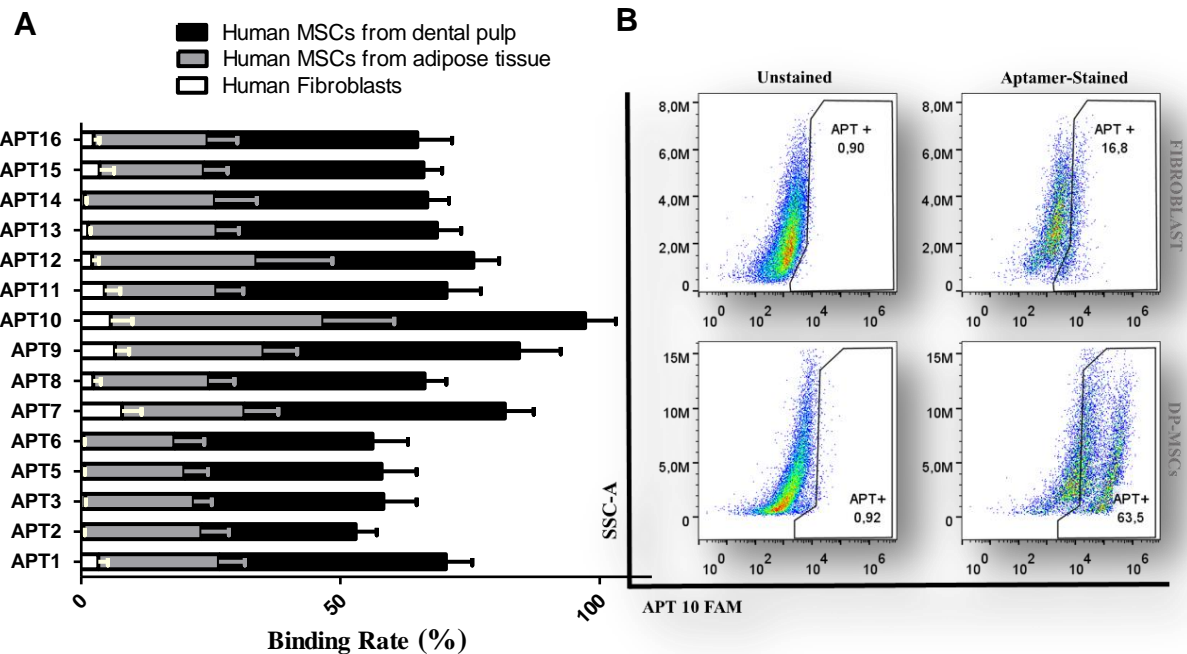


Figure 8. Flow cytometry analysis of aptamer binding rates (%) to diverse cell types. A) Binding of aptamer (1 μ M) (as 6- fluorescein-isothiocyanate fluorescence emission) to DP-MSC (black), AD-MSC (grey) and fibroblast cells negative control (white); the average binding rate of 15 aptamers were 42%, 24.% and 2.5% for DP-MSC, AD-MSC and fibroblast cells, respectively; B) Pseudocolor plots with a comparison between

APT10-stained cells; on the left are cells in the absence of aptamer staining (fibroblasts above and DP-MSC below) with less than 1% of positive cells in the APT⁺ region, gated for aptamer-stained cells; on the right are the aptamer-stained cells with 63.5% of DP-MSC (below) and 16.8% of fibroblasts (right) APT10-stained cells

The aptamers with higher binding rates presented well defined structured stem loops according to their predicted secondary structures. Cell profile analysis showed a subpopulation of cells that can be related to conserved groups of cells with higher (or different) replication characteristics and differentiation potential than the cells purified by classical methods (Baghaei et al. 2017). Therefore, aptamers with similar secondary structures could recognize MSC biomarkers with differential expression rates, according to cell origin.

5.3 Verification of aptamer binding to viable cells

We investigated whether the selected aptamers for human DP-MSC would bind to dead or apoptotic cells, since the DNA oligonucleotides can potentially bind, non-specifically, to intracellular molecules (Figure 9B). Staurosporine (*Streptomyces staurospores*) is a non-selective protein kinase inhibitor that is frequently used to induce cell death in a wide range of cells (Kabir et al. 2002). In this work, staurosporine was used to induce cell death, which was monitored by means of annexin V-APC staining. Annexin V is an indicator of apoptosis that binds to exposed phosphatidylserine (PS) on the plasma membrane surface when the membrane asymmetry is lost (Koopman et al. 1994). Therefore, if aptamers were non-specifically binding to apoptotic cells, such binding rates would be increased upon staurosporine treatment. Since MSC are non-hematopoietic stem cells that can directly or indirectly modulate immune responses, it was important to evaluate the aptamer effect on human PBMCs (Wang et al., 2018) and to verify the effects on apoptosis in aptamer-stained cells.

We standardized experimental staurosporine concentration at 2 $\mu\text{g/mL}$, since higher concentrations did not further change cell mortality. We diluted the drug in dimethyl sulfoxide (DMSO) and used the solvent as negative control for death measurement after 2 hours. For all the samples, tested time points were 30 minutes, 1 hour and 2 hours after the staurosporine exposure at 37°C. Upon treatment with DMSO (Figure 9A), only MSC showed significant annexin V staining in the autofluorescence unbiased population (30%) compared to lymphocytes and monocytes populations (less than 10%) after 2 hours of experiment. Thus, results for the staurosporine treatment suggested that MSC had more apoptotic potential, although displaying a constant level of staining over the time during the main experiment. Besides that, lymphocytes and monocytes slightly and drastically increased their apoptotic potential within the last hour of incubation, respectively.

To complete the cell death assay, we checked the apoptotic potential for cells stained with aptamers. We used APT10 to investigate the relation between the binding profile and cell death severity. The results (Figure 9B) showed a significant increase (from 34% to 52%) in apoptotic potential for APT10-stained MSC, 2 hours after death induction compared to the time point control (0 hour - not enough time for the staurosporine-induced effect).

On the other hand, apoptotic cell death of lymphocytes and monocytes stained for APT10 remained constant over time (15% and 90% of average, respectively). Despite monocytes showed a constant aptamer staining for 90% of cells, this result might be related to other cellular mechanisms than apoptotic death, such as the Ca^{2+} -dependent activated state that enhances annexin V staining. Annexins are proteins that interact with calcium-dependent membrane lipids due to many reasons, including calcium channel activities, endo and exocytosis, cytoskeleton-anchorage and membrane trafficking (Lizarbe et al., 2013). Macrophages are described to react with foreign molecules, assuming an activated state resultant from different causes, such as phagocytosis, vacuole production and internal calcium

variation (Petricevich et al., 2008). Such characteristics contribute to 90% monocyte population binding rate from annexin V and DNA aptamers. This aptamer-related binding is more likely to result from mechanisms such as phagocytosis than from an aptamer-binding specificity. Moreover, aptamer may act as a foreign molecule that enables the Ca^{2+} -dependent activated state.

Therefore, the MSC-aptamer staining increases due to death mechanisms of uptake or endocytosis. The non-specific aptamer internalization may result in binding to sites that are not specific for the target cell, increasing the variables that can influence target binding and apoptotic effects, which should be excluded from the binding analysis.

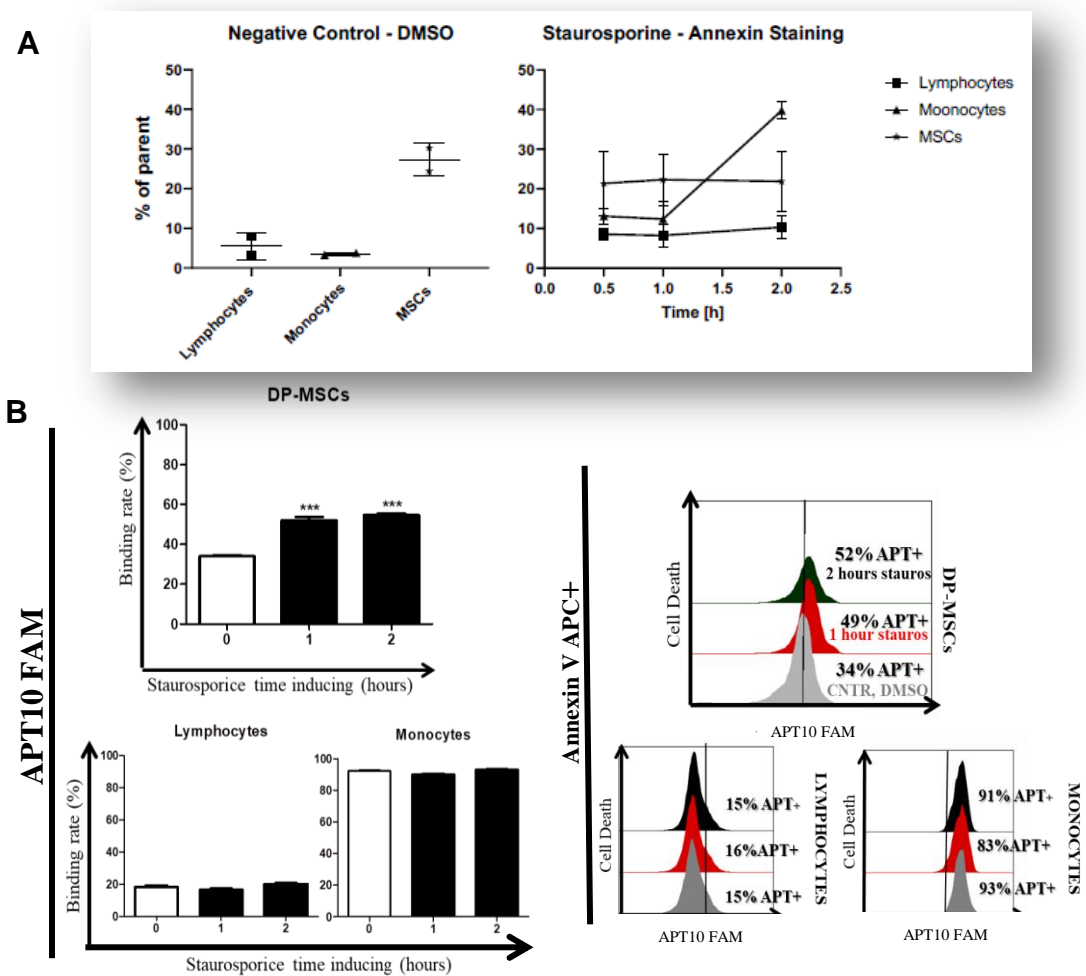


Figure 9. Quantitative flow cytometry analysis of apoptosis induction by staurosporine. A) DMSO effect in cell death after 2 hours as a negative control (left) and evaluation of apoptotic potential of staurosporine treated

cells over time (right), with higher amount of DP-MSC apoptotic stained cells; B) Plot showing APT10-stained cells (6-FAM conjugated) over time (left) for DP-MSC after 2 hours of staurosporine induction; cell death histograms (right) represented by annexin V (APC conjugated) of APT10 stained and treated cells (DP-MSC, lymphocytes and monocytes). Flow cytometry data with $p < 0.05$ relative to control, $n = 3$. Analysis of variance one-way ANOVA followed by the Dunnett posthoc test.

Cell death assay to induce controlled and quantifiable apoptosis by staurosporine exposure was performed with the annexin V ligand. Such approach is frequently used to assess apoptosis as annexin V strongly binds to extracellular exposed phosphatidylserine (PS) when membrane asymmetry is lost (Engeland et al. 1998). Since apoptotic potential was increased over time (2 hours), aptamers might bind to exposed epitopes on apoptotic cells. In the negative control (DMSO), only MSC were efficiently stained by annexin V, evidencing their delicate stem cell nature. However, for the staurosporine treatment, cell death induction of aptamer-bound monocytes and lymphocytes remained constant, suggesting that aptamer binding does not increase apoptosis in these cells. The analysis is additionally hampered, as it was found that even viable monocytes show a considerable amount of annexin V-binding at exposed PS sites (Appelt et al. 2004). On the other hand, annexin V binding can also be increased due to calcium (Ca^{2+}) elevation in the course of cell activation (Rysavy et al. 2014). Therefore, for the further experiments, only negative annexin V-viable cells would be analyzed although activated cells could also be included, veiling the true apoptotic state of the cells.

5.4 Binding efficiency and specificity between viable cells and candidate aptamers

Based on quantitative analyses of aptamers staining to DP-MSC and AD-MSC, we chose four candidate aptamers to check the cell binding-efficiency, since cells demonstrated increased binding rate to aptamers when induced to apoptosis. The candidate aptamers APT1,

APT3, APT10 and APT15 were evaluated by flow cytometry to investigate the aptamer-staining efficiency with DP-MSCs, UC-MSCs and PBMCs following exclusion of apoptotic/activated cells. For this analysis, we also used a non-specific aptamer (CNTR APT) to analyze the cell-binding specificity, since its sequence is composed by a random ssDNA that was not selected for any of the tested cell types.

Thus, we studied the cell-aptamer staining excluding apoptotic/activated cells via annexin V labeling (APC conjugated). In this way, in Figure 10 we can identify viable cells stained by the candidate aptamers through the binding rate analysis when we select only the APT/ 6-FAM positive subpopulations and eliminate the annexin/APC positive subpopulations. We can see from the graphs a greater staining for all cell types when they are bound to APT10 and APT15. In a quantitative analysis of the aptamer-binding capacity, the mean staining of viable lymphocytes was very low for all the aptamers (2.0% for APT10; 0.9% for APT15 and 0.2% for CNTR APT). On the other hand, MSC and monocytes displayed enhanced staining efficiencies compared to the non-specific aptamer. For MSC, we found a binding rate for APT1, APT3, APT10, APT15 and CNTR APT of 4%, 4.8%, 32.6, 23.6 and 2.5% for DP-MSCs and 4.3%, 4%, 49.9%, 42.5% and 5% for UC-MSCs, respectively.

In contrast to MSC, monocytes had a high binding rate for all aptamers in all flow cytometry analysis. The average of aptamer-stained monocytes were 40.4% for APT1, 47.6% for APT3, 87.2% for APT10, 64% for APT15 and 34.5% for CNTR APT.

Therefore, APT10 and APT15 binding showed significant statistical differences compared to CNTR APT for all cell types, except APT15 for lymphocytes. In this way, MSC showed a higher specificity for APT10 in comparison to CNTR APT, since the fold increase was 16X for DP-MSCs and 10X for UC-MSCs, over only 2.5 fold increase for monocytes.

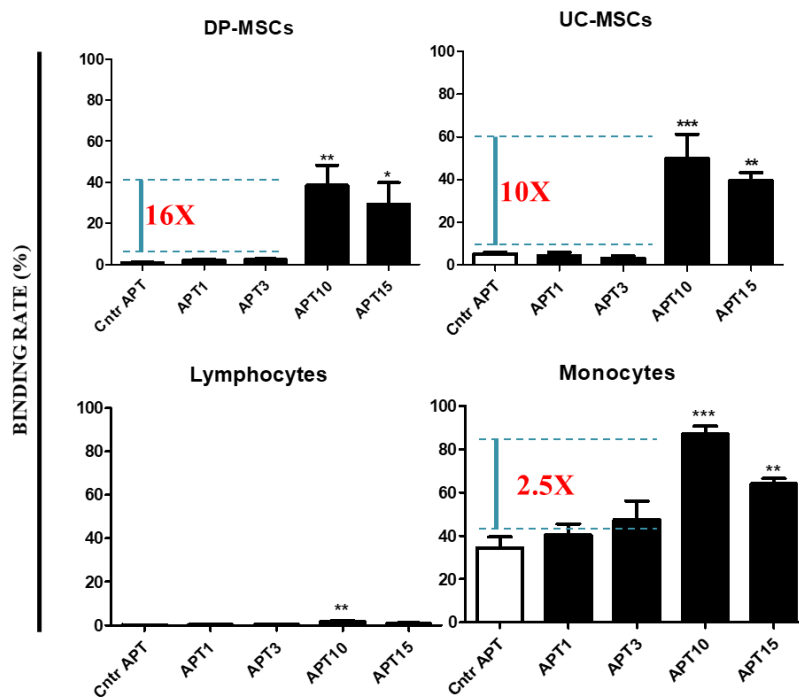


Figure 10. Binding rate efficiencies and specificities of candidate aptamers to lymphocytes, monocytes and MSC. Human cell types were stained with aptamers APT1, APT3, APT10, APT15 and CNTR APT (6-FAM conjugated) and annexin V (APC conjugated) for the quantification of viable cells. To exclude early apoptotic cells co-stained by aptamers, dot plots for DP MSC, UCMSC and PBMCs were gated for aptamer- positive and annexin V-negative populations (APT+/Annexin-). APT10 showed significantly increased binding compared to that of the non-specific aptamer (CNTR APT) for DP-MSC, UC-MSC and monocytes, with a 16X, 10X and 2.5X rate efficiencies, respectively. $p < 0.05$ in relation to control aptamer; $n = 3$. Analysis of variance one-way ANOVA followed by the Dunnett posthoc test.

The pseudocolor dot plot shows differences in the viable cell population when they are stained by aptamers (Figure 11). In this case, we can see singular examples of DP-MSC, UC-MSC, lymphocytes and monocytes stained by APT10, APT15 and CNTR APT. We can see the shift of the non-apoptotic positive population stained with aptamers on the Q1 quadrant (aptamer⁺ axis/annexinV⁻ axis) for MSC/lymphocytes, and the Q2 quadrant (aptamer⁺ axis/annexinV⁺ axis) for monocytes. All dot plot image data were compared to those of the unstained cell population (Q4 quadrant). Therefore, when viable cells (annexinV⁻ population) were positive for aptamer labeling (aptamer-6FAM⁺ population), 20% to 50% of the MSC

populations were recognized by APT10 and APT15 against 1% stained by CNTR APT. For the PBMCs population, 1.4% to 2.5% of lymphocytes were stained by APT10 and APT15 against 0.1% are stained by CNTR APT binding. However, analysis of the monocyte population, which are all positive for annexin V, revealed that 80% to 94% of the cells were stained by APT10 and APT15, in comparison to 30% positive for CNTR APT binding.

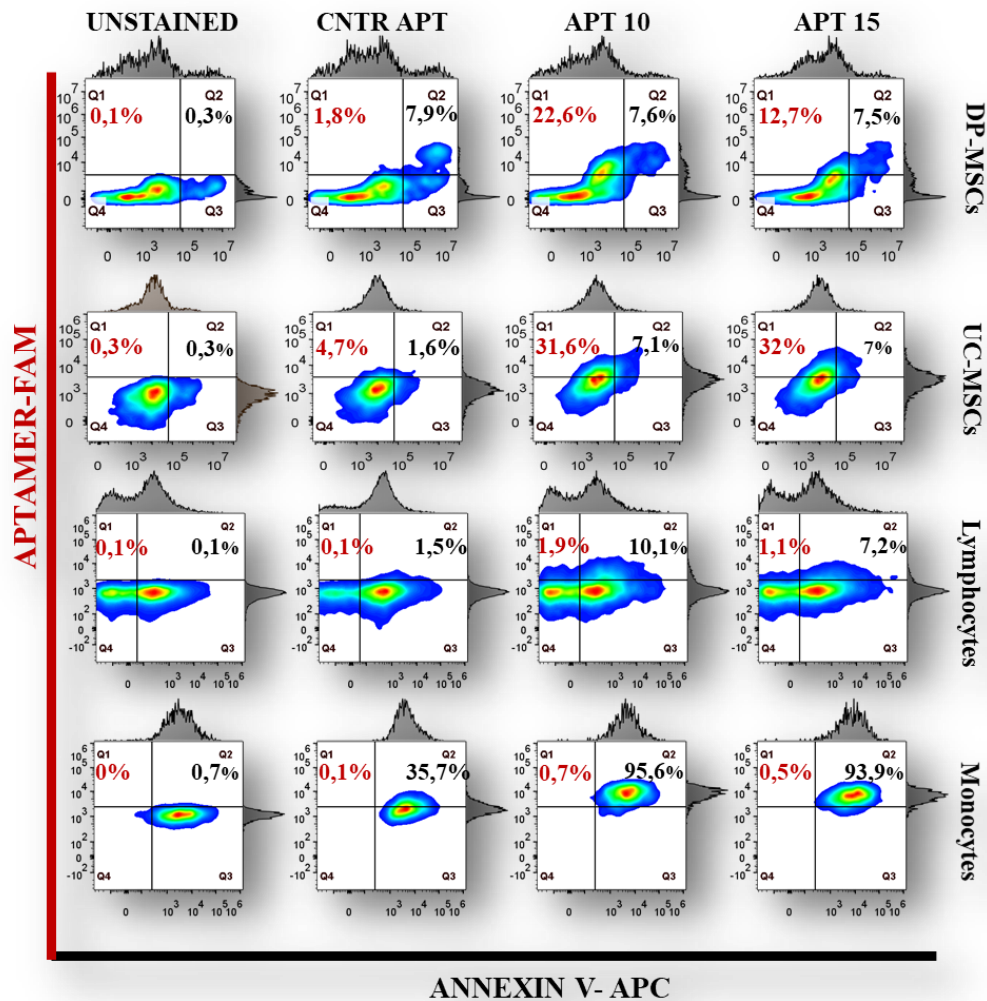


Figure 11. Flow cytometry analysis of binding rates (%) of aptamers to DP-MSC, UC-MSC, PBMCs and monocytes. (A) Quantification of viable DP-MSC by CNTR APT, APT10 and APT15 (fluorescence emission in the FITC channel - Q1); (B) Quantification of viable UC-MSC by CNTR APT, APT10 and APT15 (Q1 discrimination); (C) Quantification of viable PBMCs by CNTR APT, APT10 and APT15 (Q1 discrimination); (D) Quantification of the viable population of monocytes discriminated by annexin V (Q2) to exclude early apoptotic cells co-stained

The whole positive staining for annexin V can be explained by an activated state or an early apoptotic influence presented by monocytes. Moreover, these results showed good staining for APT10-stained MSC and monocyte cells. The lower specificity rate observed in monocytes can be related to an overexpression of monocyte-MSC shared markers, to which APT10 could be binding. According to what was demonstrated by Gonçalves et al. (2017), interactions between MSC's cellular membrane and monocytes regulate immune responses that are important for a successful transplantation therapy using MSC. Since monocytes and their progeny dendritic cells (DC) are key players in innate and adaptive immunity, they have three main functions: phagocytosis, antigen presentation, and cytokine production (Jakubzick et al. 2017). It is known that monocyte-derived DCs feature receptor molecules for intracellular non-self DNA, as Toll-like receptor 9 (TLR9) and mechanisms to take up extracellular DNA via antimicrobial peptide LL37. Thus, it is very unlikely that classical monocytes purposefully take up DNA (Chamilos et al. 2012). This might be explained by the extensive CD11c expression, which hints to an abundant DC-like phenotype in the monocyte compartment, contributing to the aptamer uptake. Such uptake mechanisms would be unspecific and generic for DNA oligonucleotides. Taken together, it is likely that APT10 gets ingested by activated monocyte-derived DCs, leading to intracellular staining (Colling et al., 2013).

5.5 Analysis of aptamer binding sites on MSC

The aptamers selected by Cell-SELEX are supposed to bind to surface membrane epitopes in human MSC. Therefore, based on our flow cytometry results of aptamer-binding rates to different cell types, we analyzed the aptamer-binding specificity to MSC and PBMC by confocal microscopy and immunofluorescence. First, we checked the staining of adhered DP-MSC bound to APT1 and APT9 (6-FAM) by immunofluorescence (Figure 12). We could

observe increased staining of APT9 compared to APT1 in DP-MSK. Moreover, we used the DNA blue fluorescent dye (Hoechst) to check the nuclear unspecific staining caused by aptamer binding to cell membrane (Figure 12A). DP-MSK were stained for aptamers (green color) and for the nucleus (Hoechst, blue color). When we merged the emission channels, we found some staining of DP-MSK bound to APT9, apparently localized in the surface membrane by comparing brightfield (unstained cells, grey) to fluorescent images (stained cells, green). We also observed staining for fibroblasts, used as negative control to compare to the APT9 binding profile in the green channel (Figure 12B). Fibroblasts did not bind to APT9, as concluded from the comparison of the overlapping images. These results corroborate our data concerning APT9 binding rate to MSC and fibroblasts, similar to the results for APT1 staining, which showed lower binding to MSC.

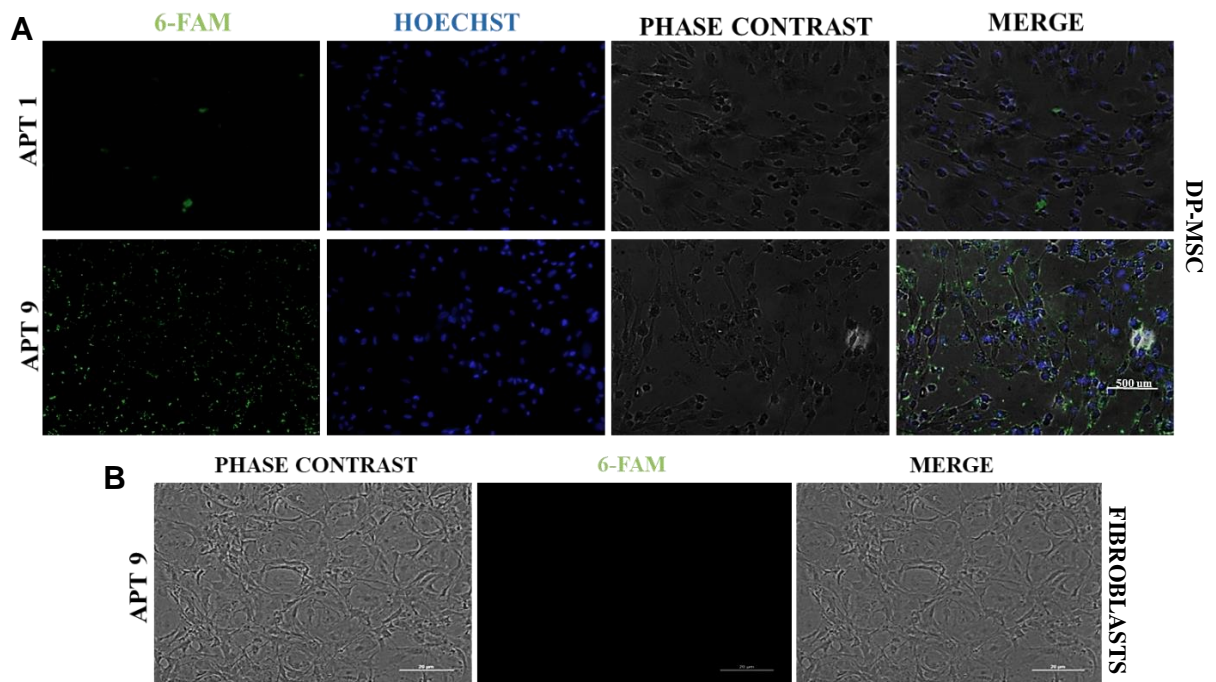


Figure 12. Immunofluorescence of DP-MSK and fibroblasts stained with aptamers. A) DP-MSK immunofluorescence analysis for APT1 and APT9 staining (6-FAM; green); *Hoechst* fluorescent dye (HOECHST, blue) used for nuclear DNA staining; Phase Contrast (unstained cells, grey) images were added for staining overlay (Merge); scale bar = 500 μm; B) Fibroblasts stained with APT9 showed no fluorescence emission; scale bar = 20 μm. 20X Nikon Eclipse TE300.

Furthermore, because cells feature a huge variety of surface proteins, Cell-SELEX yields many sequences with comparable affinities for a whole set of epitopes. The greater interest is to determine the aptamer-target-interaction location on MSC, whereas the unknown epitopes might differ from the already known markers CD29, CD73, CD90 or CD105. Since immunofluorescence experiments corroborated the results of aptamers binding rate to MSC, we decided to check the co-staining between aptamers and the MSC surface marker CD90 in DP-MSC (Figure 13).

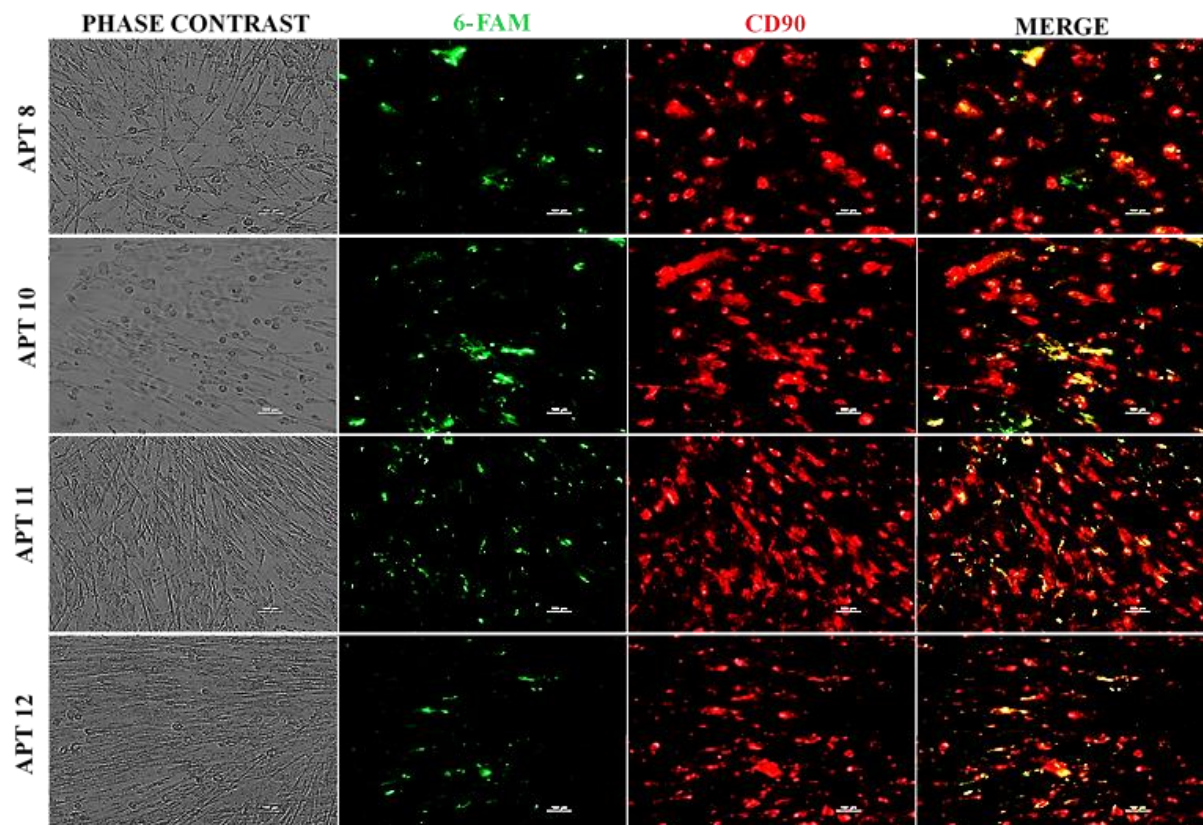


Figure 13. Co-staining analysis of DP-MSC bound to aptamers and antibodies against specific surface marker epitopes by immunofluorescence microscopy. Intensity analysis of DP-MSC stained with APT8, APT10, APT11 and APT12 (6-FAM conjugated, green) and anti-CD90 surface marker (APC conjugated, red). Phase contrast resolution was used to overlap immunofluorescence staining (merge) of CD90 surface marker and candidate aptamers with higher binding rate observed by flow cytometry. Scale bar = 100 μ m; 20X Nikon Eclipse TE300.

Adhered DP-MSCs were stained with APT8, APT10, APT11, APT12 (6-FAM) and anti-CD90 (APC conjugated) for the co-staining analysis by immunofluorescence microscopy. In this way, we can see cells co-stained with aptamers (green) and CD90 surface marker (red) when the images are merged (orange/light; co-staining). Moreover, we can also observe aptamer staining of epitopes that were not shared with CD90 marker and that were apparently located in the intracellular space (Phase Contrast). Based on this data, we could corroborate the aptamer binding to the plasma membrane, since there was a shared surface marker staining. However, we needed specific images to confirm the location of the aptamer staining in the cells.

Therefore, we performed Z-stack images by confocal microscopy (Figure 14) of adhered UC-MSCs stained with APT10 and CNTR APT (6-FAM), which showed the greater specific binding rate by flow cytometry. The possible unspecific binding of DNA aptamers due to their nucleic acid nature (negative charge) was excluded given that the random control aptamer (CNTR APT) did not stain MSC (Figure 14A). On the other hand, we saw similar staining of UC-MSCs and DP-MSCs for APT10. Because of that, we performed Z-stack images to further analyze this feature internally. Since we could see from Z-stack images that APT10 apparently bound to cell surface membrane, we checked the shared staining of CD90 surface marker from a zoomed image of MSC bound to APT10 (Figure 14B). The most common cells found in a processed lipoaspirate tissue are blood cells (Zuk et al, 2001), then cellular heterogeneity showed by MSC population can be also explained by derived-like subpopulation of immune cells inserted in a whole population of MSC.

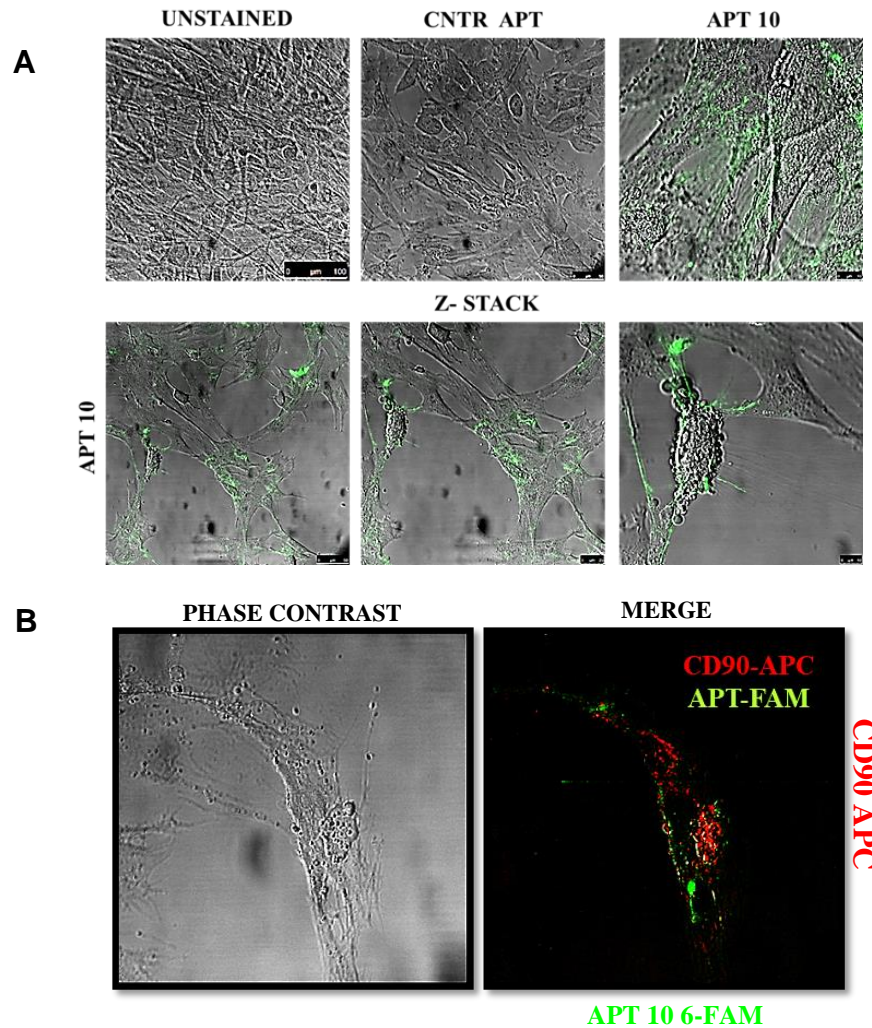


Figure 14. Confocal images of live and adhered UC-MSC, stained with a panel of aptamers and anti-CD90 surface marker antibodies. A) Confocal microscopy analysis of viable UC-MSC adhered in a plastic slide chamber stained with APT10 and non-specific CNTR APT (6-FAM conjugated, green color), followed by a Z-stack approximate image of UC-MSC bound to APT10; B) Z-stack phase contrast image of UC-MSC co-stained with anti-CD90 (APC, red) surface marker and APT10. 40x pictures captured by Confocal Leica SP5 microscope.

The non-specific control aptamer (CNTR APT) showed no binding staining to UC-MSC, suggesting no affinity of DNA to cell surface molecules. All selected aptamers for MSC bound to the adhered cells, but APT10 displayed the highest and most defined levels of staining. Albeit APT1, APT3, APT9 and APT15 showed staining to some degree, its location remained arbitrary. APT10 signals were mostly observed at the cell edges, extending out to

the spindle-shaped plasma membranes. Thus, we also found cells with altered morphology (including membrane vesicles), reflecting non-intact MSC. On the other hand, Figure 14 shows the middle layer of a single cell bound to APT10, which is probably restricted to the cell surface, where CD90 surface marker was stained in the plasma membrane. Staining of APT10 in the border location, as observed for CD90, corroborates the hypothesis of this candidate aptamer binding to the surface membrane of MSC.

Previous flow cytometry experiments showed that APT10 and APT15 stained PBMCs. This could be explained by two hypothesis: 1. PBMCs and MSC share common surface antigens that are recognized by Cell-SELEX selected aptamers; or 2. monocytes actively internalize the DNA oligonucleotides, contributing to unspecific binding. To test whether the selected aptamers are ingested by phagocytosis or if they bind to surface epitopes, PBMCs were analyzed by confocal microscopy after aptamer incubation. We used PBMCs in suspension bound to aptamers and we detected a staining of some of these cells when they are bound to APT10 (Figure 15A). No staining was observed from aptamer-unstained cells, CNTR APT or APT15 cells. From all the tested aptamers, only APT10 was markedly bound to the cells. The other aptamers showed slight staining, not robustly present throughout the sample. A Z-stack was applied to single cells in the APT10 sample, showing that fluorescence is restricted to the plasma membrane.

Due to the lack of specific cell lineage markers, it was not clear which cell type was observed. To tackle this issue, monocytes were sorted by FACS with anti-CD14 antibody APC conjugated) from whole blood containing PBMCs (Figure 15B). The live CD14⁺ cell population was stained with APT10 and analyzed by confocal microscopy. Indeed, monocytes were efficiently stained with APT10 when compared to the unstained control. The previously reported intracellular staining of PBMCs was also observed in the current staining analysis of monocytes. The results suggested an active internalization mechanism of DNA

oligonucleotides performed by monocytes, since the non-specific CNTR APT resulted in high staining of monocytes as determined by flow cytometry.

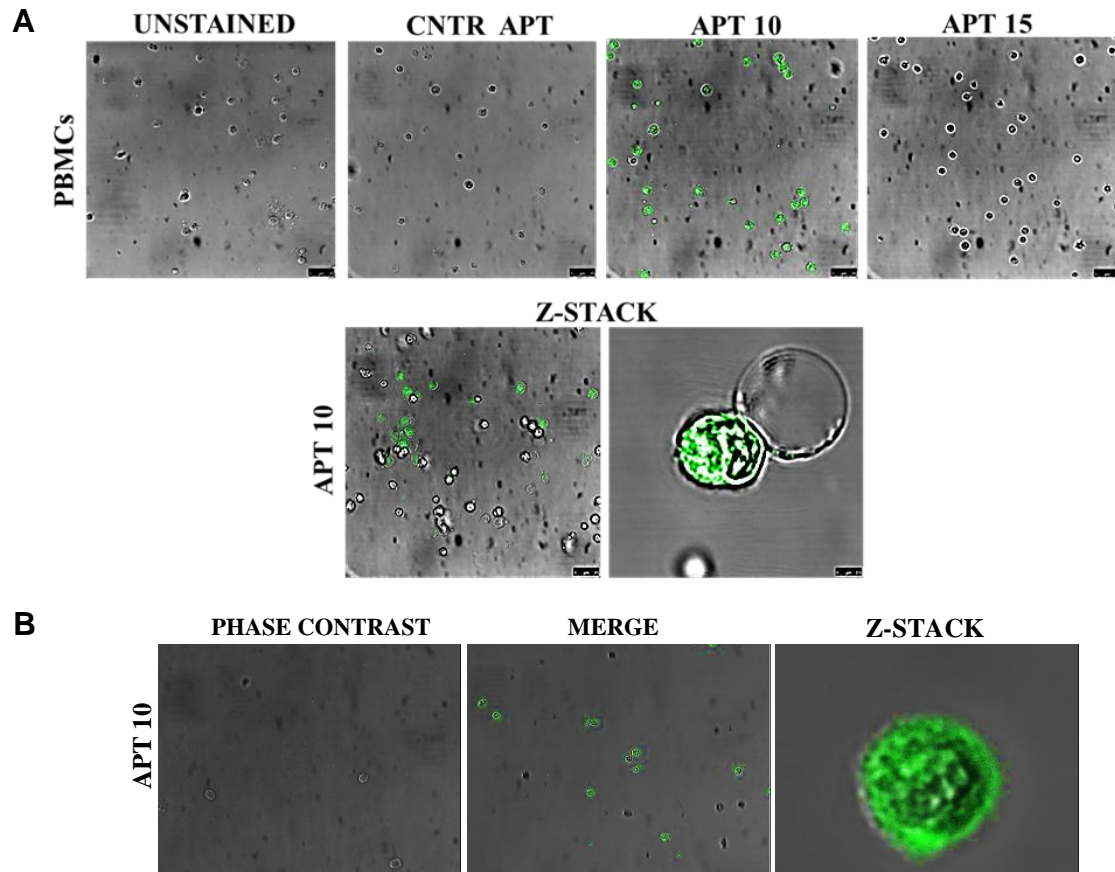


Figure 15. Confocal microscopy of live PBMCs and isolated monocytes stained with a panel of aptamers. A) Viable and freshly isolated PBMCs were stained with APT10, APT15 and CNTR APT and analyzed by immunofluorescence. As only APT10-stained PBMCs showed affinity to the cells, they were submitted to a Z-stack zoom imaging. B) Analysis of isolated monocytes (CD14+ population separated by FACS) stained with APT10, which revealed a corroborated internal cellular staining of APT10 exhibit by Z-stack images. 40x images captured on Confocal Leica SP5 microscope.

Therefore, we found by confocal image microscopy that APT10 binds to monocytes and MSC most efficiently. Moreover, APT1, APT3, APT9 and APT15 did not bind to PBMCs. When analyzed for binding to MSC, only a slight staining at undefined sites or no staining was observed. From Z-stack recordings, APT10-staining appeared to be localized in the intracellular space of monocytes and on the plasma membrane of MSC. A proportion of

stained MSC featured advanced vesicles (Figure 14A), which typically occurs during cell death via apoptosis (Coleman et al. 2001). Annexin V cell death experiments showed that APT-MSC-staining increased with apoptotic potential. This suggests that APT10 binding is not restricted to viable cells.

Candidate aptamers were developed for MSC by Cell-SELEX, meaning that they should target membrane epitopes and therefore be localized at the plasma membrane. However, monocytes bound to APT10 in the entire cell area, including intracellular sites. Because of that, results suggest that there might be common extracellular and intracellular MSC receptors bound by APT10, that might be also expressed in monocytes. Nevertheless, the confocal images did not show staining for non-specific aptamer binding, which stands in contrast to a mechanism restricted to phagocytic uptake.

Further support for the results comes from flow cytometry analysis, since the efficiency rate of candidate aptamers is higher for MSC than for monocytes. This staining discrepancy between confocal microscopy and flow cytometry may be due to the weak brightness of 6-FAM and higher sensitivity for the fluorescence dye of the flow cytometer. However, APT10 was found to bind to MSC population and CD14⁺ monocytes in both flow cytometry and fluorescence microscopy analysis. Thus, whilst MSC are efficiently stained at the plasma membrane compared to the whole cell labelling of monocytes, the binding site for APT10 on MSC surface membrane may reveal an unknown MSC epitope to be characterized.

5.6 Hematopoietic stem cell labeling in PBMCs

Considering that the candidate APT10 showed staining for MSC and PMBCs by both flow cytometry and immunofluorescence techniques, we checked if PBMCs would present any specific stem cell surface marker. HSCs are stem cells with pluripotency and self-renewal properties involved in the generation of all types of blood cells. Furthermore, these cells are

important immunological players in the transplantation context, as they interact with the T-cell class of receptors (via HLA system) (Ng and Alexander, 2017).

HLA antigens are characterized by polymorphic glycoproteins that present a binding site recognized by immune cells' receptors. Although reports emphasize that HLA antigens are expressed by HSCs, HLA-DR complexes can be released by T-cells and B-cells when macrophages are present in the environment (Jendro et al., 1991). CD45 marker is a receptor-linked protein tyrosine phosphatase that is responsible for T-cell activation, and also a marker of leukocytes. Furthermore, it is also a negative antigen for the characterization of MSC (Altin and Sloan, 1997). CD14 is a membrane associated protein produced by monocytes, macrophages and dendritic cells, that acts as a myeloid differentiation marker (Marcos, et al. 2010). CD117 is a tyrosine kinase receptor responsible for cancer cell progression and maintenance of stem cells (Foster, 2018).

Given that, we investigated the affinity profile of aptamer-stained PBMCs regarding the surface markers CD117 and HLA-DR (expressed by HSCs), CD45 (expressed by leucocytes) and CD14 (expressed by monocytes).

Lymphocytes stained with aptamers (CNTR, APT10 and APT15) and the described antibodies were identified by flow cytometry (SSC-A scatter versus FSC-A scatter) (Figure 16). Apoptotic cells were excluded from the analysis via annexin V labeling (APC conjugated) using the "Unstained" density plots as reference (Fig 16: v, vi, vii and i).

LYMPHOCYTES

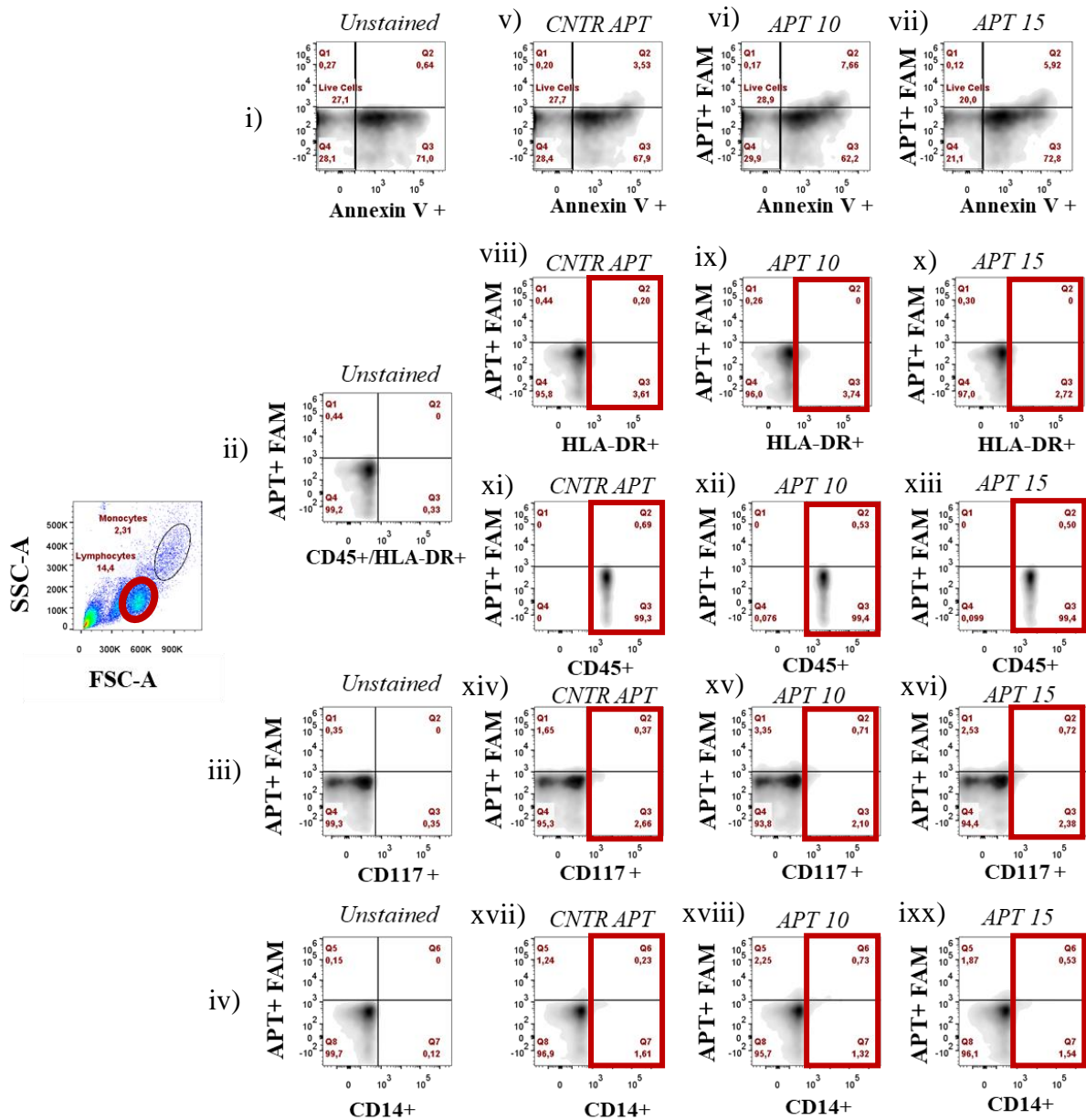


Figure 16. Characterization of stemness surface marker and aptamer staining in human lymphocytes by flow cytometry. PBMCs were stained with APT10, APT15 and CNTR APT and viable lymphocytes (annexin V negative population, 26% of the total cells) were analyzed for immunostaining with anti-CD117, HLA-DR (HSCs marker), CD45 (leucocyte marker) and CD14 (monocyte marker) antibodies. Flow cytometry density plots show 94% CD45⁺ (xi, xii and xiii) cells and 1.5 to 4% of CD14⁺ (xvii, xviii and ix), CD117⁺ (xiv, xv and xvi) and HLA-DR⁺ cells (viii, ix and x). Lymphocyte population exhibit low stemness profile and a 0.5 to 3% aptamer staining.

Annexin V negative population was evaluated concerning APT10, APT15 and CNTR APT staining (6-FAM conjugated). 99.4% of viable lymphocytes (26% of the lymphocyte population) were CD45⁺ (Fig 16 xi, xii, xiii), whilst presenting very low positivity for the tested aptamers (0.6%). 2% of monocyte CD14⁺ co-stained for aptamers (1.4 - 3%), which evidences a low CD14⁺ cells contamination in the whole population (Fig 16 xvii, xviii and ix). For the HSC analysis, only 3% of the cells were positive for CD117 (Fig 16 xiv, xv and xvi) and HLA-DR (Fig 16 viii, ix and x) antigens. 3.5% and 0.5% of these cells were labeled by aptamers, respectively. Therefore, the CD45⁺ lymphocyte population shows weak staining for all aptamers, indicating that this population is not recognized by aptamers.

We also analyzed the monocyte population when they were CD45⁺, HLA-DR⁺, CD117⁺ and CD14⁺ and positive for CNTR APT, APT10 and APT15 labeling (Figure 17). As described above, the analysis of SSC-A and FSC-A scatter plots showed the size and granularity of monocytes. Given that, basically all the monocyte population (99%) might be in an activated state (annexin V-binding can be increased due to Ca²⁺ elevation), this population presented 99% of HLA-DR⁺ (Fig 17 v, vi and vii), CD45⁺ (Fig 17 viii, ix and x) and CD14⁺ (Fig 17 xiv, xv and xvi) cells.

On the other hand, only HLA-DR⁺ cells similarly bound to aptamers as previously verified (34.3% of CNTR APT⁺, 72.3% APT10⁺ and 75.1% APT15⁺).

In CD45⁺ population, 26.9%, 65.5% and 69.9% were CNTR APT⁺, APT10⁺ and APT15⁺, respectively. Regarding the CD14⁺ population, 6.4%, 34.9% and 31% of the cells were respectively co-stained with CNTR APT, APT10 and APT15. Finally, 24 to 29.9% of the monocytes population were positive for the HSC marker CD117, while simultaneously staining for CNTR APT, APT10 and APT15 in a rate of 4.4%, 11.6% and 9.8%, respectively. Since only 2.5-5% of HLA-DR⁺, CD45⁺, CD117⁺ and CD14⁺ cell populations bound to the

analyzed aptamers, we hypothesized that the selected aptamer could be phagocytised/uptaken by these cells.

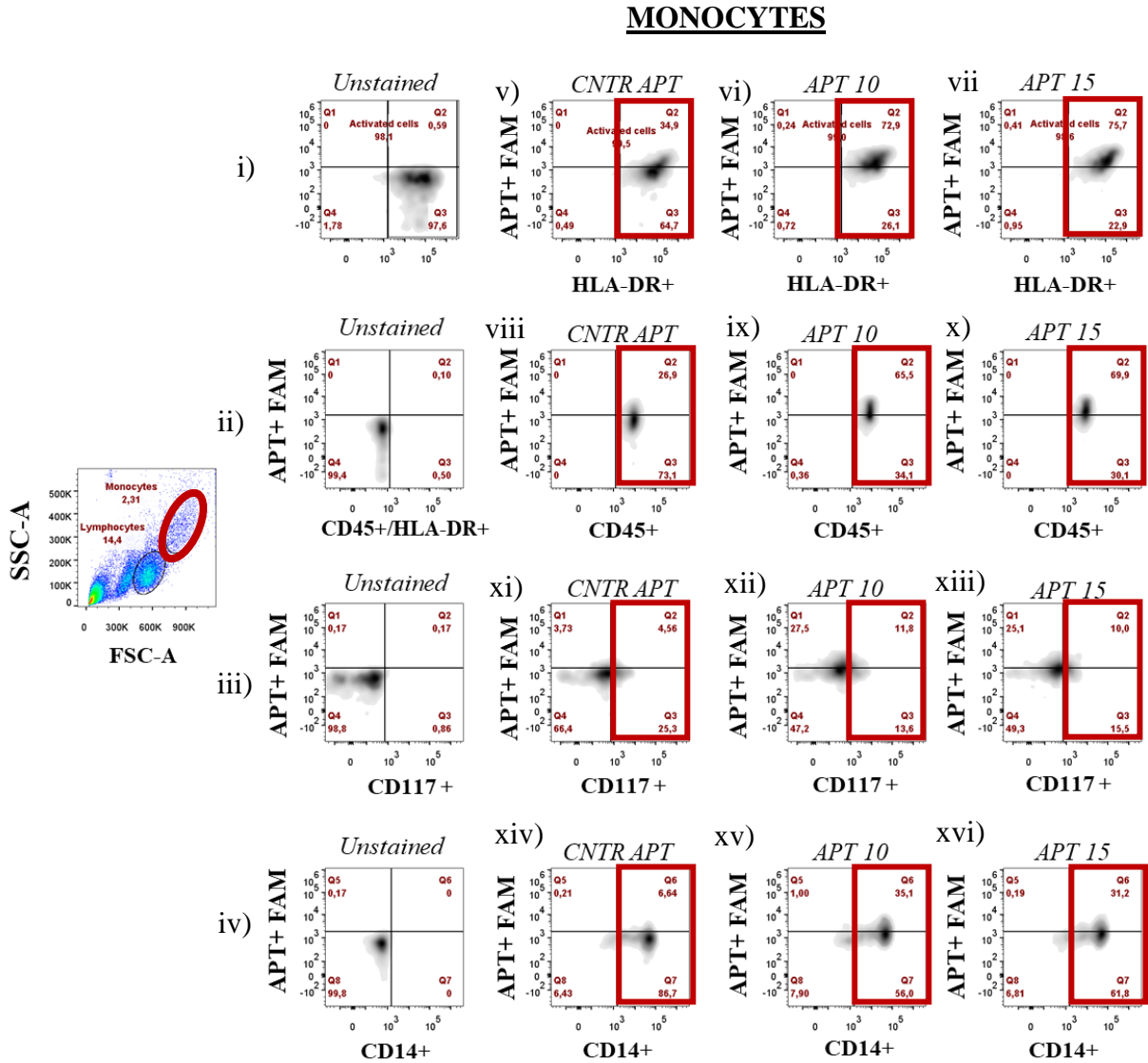


Figure 17. Characterization of stemness surface marker and aptamer binding in human monocytes cells by flow cytometry. PBMCs were stained for APT10, APT15 and CNTR APT. Activated monocytes (annexin V positive population, 30 - 99% of the total cells) were analyzed regarding CD117⁺, HLA-DR⁺, CD45⁺ and CD14⁺ populations. Flow cytometry density plots showed for these populations a 99% of staining for CD45 (viii, ix and x), CD14 (xiv, xv and xvi) and HLA-DR (v, vi and vii) markers and 30% of cells positive for CD117 (xi, xii and xiii) cell population. Further, 4 (CNTR APT) to 75% monocytes APT labeled with aptamers.

On the other hand, we observed the same increasing pattern of the binding rate of these cells when they are bound to APT10 and APT15. Since MSC are known to demonstrate immunoregulatory properties by releasing cytokines and grow factors as a result of their interactions with immune cells, the results suggest that selected aptamers might interact with unknown epitopes co-expressed by both MSC and monocytes. The aptamer staining might also be enhanced via phagocytosis/internalization, since the highest specificity binding rates (10-16%) were obtained when the aptamers bound to MSC (Figure 10).

Cell-cell interactions between MSC and immune cells showed to modulate immune suppression, which also influences inflammatory processes, such as hematopoietic stem cell engraftment and MSC differentiation (Wang et al., 2018). Thus, it is possible that surface markers shared by MSC, HSCs, monocytes and other immune cells might be antigens that interact with aptamers.

5.7 Confirmation of the surface profile of FACS-sorted aptamer-stained MSC

The aptamer-MS C characterization indicated APT10 and APT15 as promising markers for MSC. In view of that, we wanted to demonstrate if the MSC population bound to those aptamers retained the CD90+/CD105+ profile. Therefore, MSC were stained with APT10 and APT15. The aptamer-positive populations were isolated and recovered by FACS. The collected “aptamer-sorted MSC” were immunolabeled for MSC markers (CD90 and CD105) and monocyte marker (CD14), and submitted to a standard flow cytometry analysis.

In order to confirm the binding potential of MSC to aptamers, “aptamer-sorted MSC” were analyzed under three different conditions: 1. concomitant analysis and FACS isolation (Fresh “aptamer-sorted MSC”, Figure 18); 2. FACS isolation followed by two weeks in culture (Cultured “aptamer-sorted MSC”, Figure 19); and 3. a second FACS isolation after two weeks in culture (Fresh “aptamer-sorted MSC” after cultivation, Figure 20). The MSC

cell population was defined as described before (SSC-A scatter versus FSC-A scatter). After debris, doublets and apoptotic cells exclusion, aptamer positive cells (6-FAM fluorescent emission) were identified and isolated by FACS.

After labeling and isolating MSC bound to aptamers by FACS, a restaining of fresh “aptamer-sorted MSC” was done using anti-surface marker antibodies (CD90 and CD105). These fresh isolated cells were analyzed by flow cytometry to check the the population stemness profile (Figure 18). It was found that 99% of cells were positively labeled for MSC CD90⁺ and CD105⁺ populations. Conversely, only 2.2 to 7.6% of the cell population was positive for the CD14 monocyte marker. Additionally, the fresh “aptamer-sorted MSC” maintained the aptamer staining verified prior to FACS isolation, suggesting that the possible target should bind the aptamers in a stemness way.

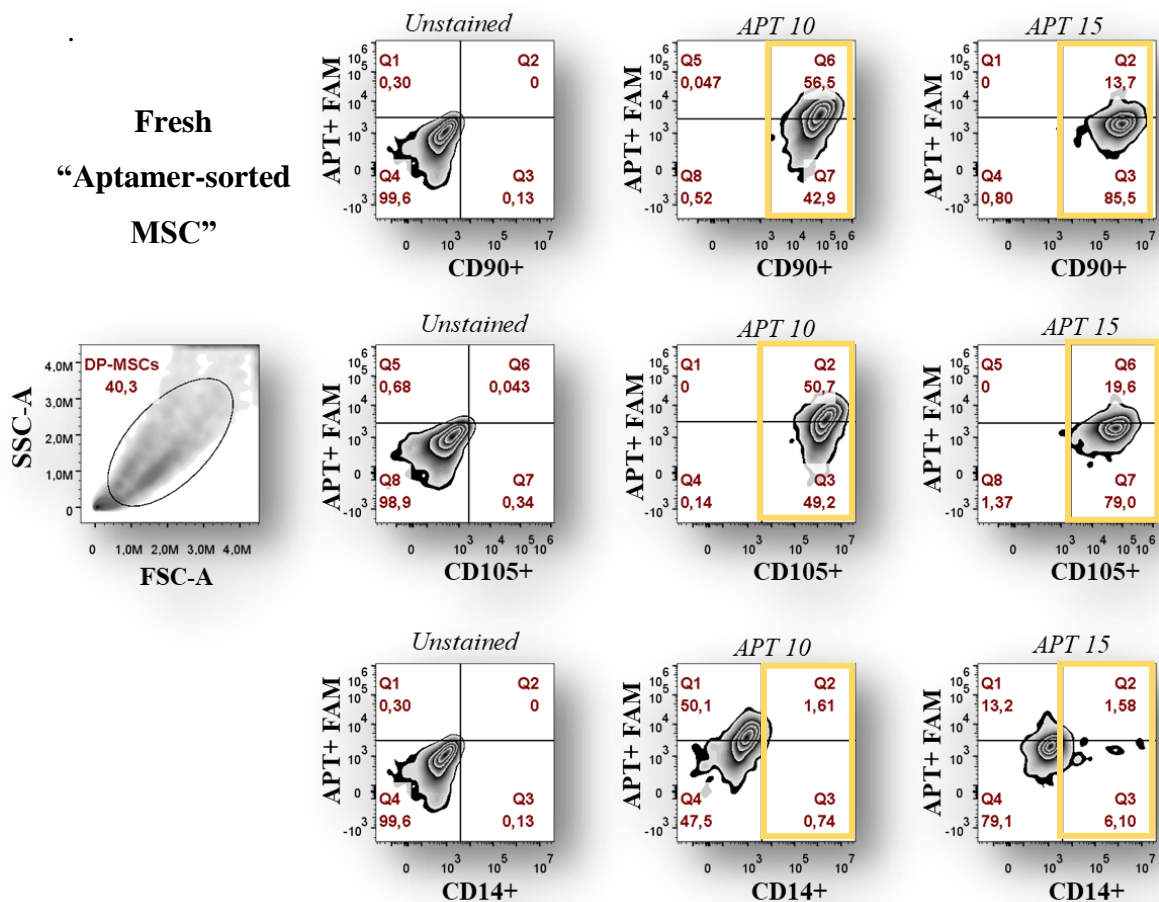


Figure 18. Flow cytometry analysis of MSC surface marker profiles of freshly isolated aptamer-positive population of MSC by flow cytometry. Fresh aptamer-sorted MSC stained with APT10 and APT15 by FACS.

The positive aptamer population were isolated and the flow cytometry results showed that restrained cells are 99% labeled for CD90 and CD105 antigens. For the CD14 monocyte marker, only 2-7% of cells were stained. Remaining aptamer transitory staining was also observed after isolation of fresh aptamer-stained MSC.

After the first FACS isolation of the MSC population bound to APT10 and APT15, the cells were recovered and kept in sterile conditions for proliferation during two weeks. Then, these first time-sorted cells were stained for CD90, CD105 and CD14 surface markers immunofluorescence for profile evaluation by flow cytometry (Figure 19). Differently from the freshly sorted cells, it was observed that aptamer-isolated MSC lose their binding to aptamers effectiveness after cultivation, but keep their MSC surface profile. This can be conclude since the whole population (99%) was stained by anti-CD90 and CD105 immunofluorescence. The negative labeling for the monocyte surface marker CD14 (less than 1%) ensured that APT10 and APT15 bound specifically to MSC.

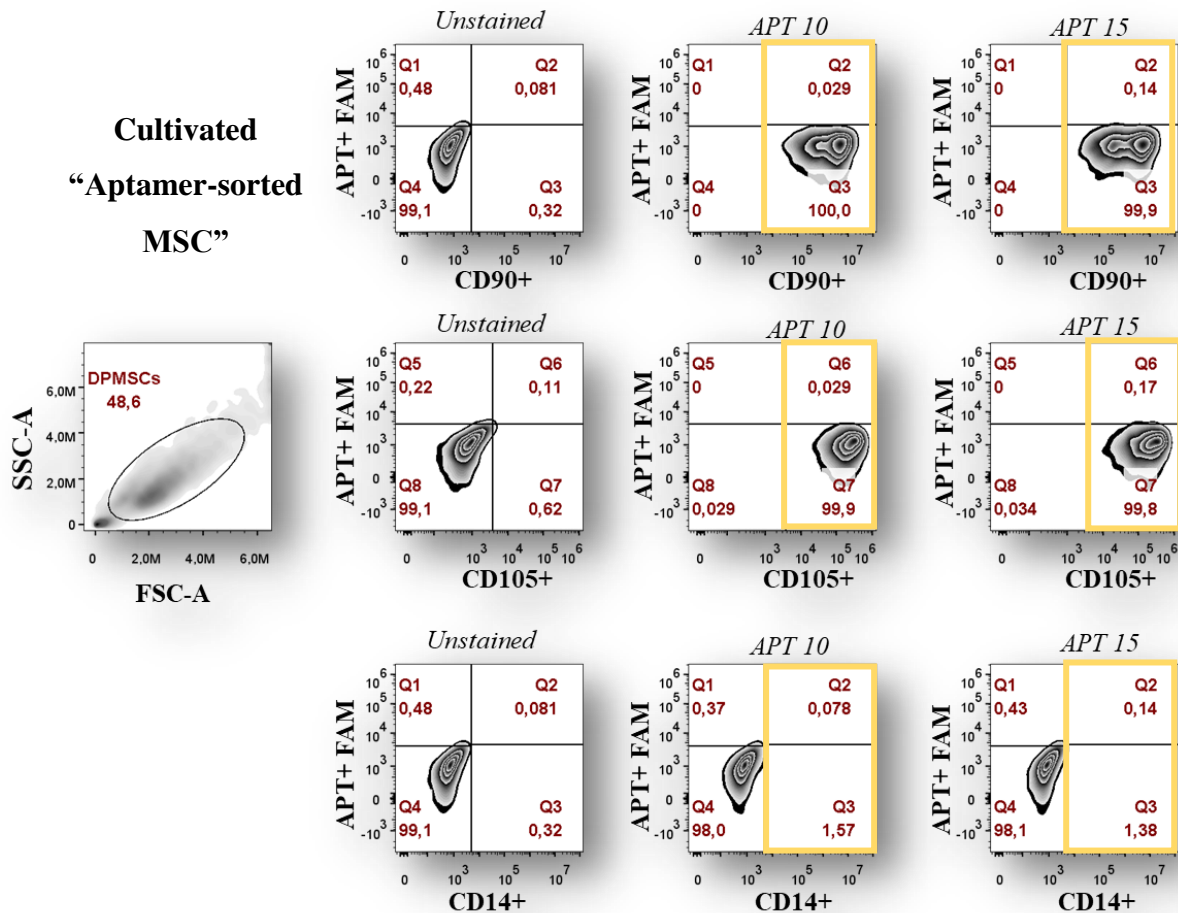


Figure 19. Flow cytometry analysis of MSC surface marker profiles after *in vitro* culture of aptamer-sorted MSC. Aptamer-sorted MSC isolated and recovered by FACS were cultivated *in vitro* and analyzed regarding CD90, CD105 and CD14 surface markers by flow cytometry. APT10 and APT15-sorted population showed a loss of aptamer staining after *in vitro* cultivation but remained the MSC marker profile, with 99% of staining for CD90⁺ and CD105⁺ cells and 1% labeled for CD14 monocyte marker.

Since “aptamer-sorted MSC” lost the aptamer staining after their *in vitro* cultivation, a second time isolation of these sorted MSC was performed by FACS. Those cells were retained with APT10 and APT15, isolated and recovered for their surface marker profile verification (Figure 20). The new fresh “aptamer-sorted MSC” were analyzed for CD90, CD105 and CD14 expression by flow cytometry. 90% of APT10-sorted MSC were CD90⁺ and CD105⁺, while not expressing the monocyte surface marker CD14. Analysis of the

“APT15-sorted MSC” after cultivation showed 92% of CD90⁺ cells and 72% of CD105⁺ population. Additionally, 2.4% of APT15-sorted MSC expressed the monocyte marker CD14, indicating a possible weak differentiation process.

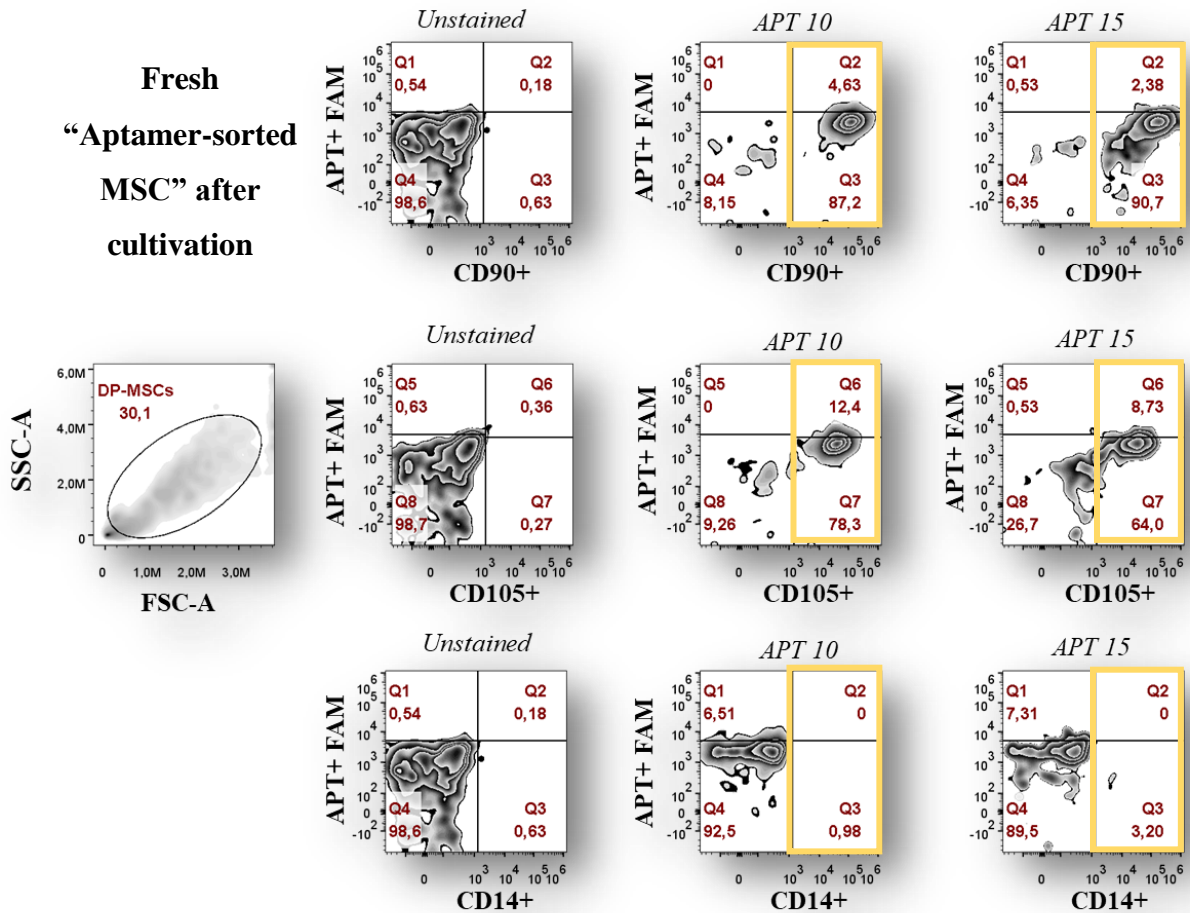


Figure 20. Flow cytometry analysis of MSC surface marker profiles of fresh aptamer-restained MSC after *in vitro* cultivation. Aptamer-sorted MSC recovered by FACS and cultivated *in vitro* were isolated for a second time using APT10 and APT15. These new fresh aptamer-stained cells were analyzed regarding CD90, CD105 and CD14 surface markers by flow cytometry. Fresh APT10-sorted population stained 90% of CD90⁺ and CD105⁺ cells; fresh APT15-sorted cells were and 92% and 72% stained for CD90 and CD105; aptamer-sorted MSC lost some staining after *in vitro* cultivation even after their restaining for FACS experiment (3-11% for APT10 stained cells and 2-7% for APT15 stained cells).

These results showed a shift in aptamer staining after cell sorting, since the labeling decreases after the isolation and cultivation processes (Figure 20). Thus, when sorted cells

were positive for CD90 marker, APT10 and APT15 presented a staining of 3.9% and 2.2% respectively.

On the other side, CD105⁺ population showed 11.4% and 7.7% of APT10 and APT15 staining. Regarding the unstained MSC (Figure 20), it was observed a heterogeneous cell population that disappeared after the aptamer staining and isolation of the cells. In this way, besides aptamer-sorted MSC having preserved the CD90⁺ and CD105⁺ phenotypes, they are still able to proliferate, replicating the stem cell population. Therefore, MSC antigens bound to aptamer might be in some way involved in a microenvironment, which maintains stemness capacities of MSC. A recent study by Grasso et al. (2016) showed that different subsets of populations (tumorigenic CD133⁺ and CD133⁻ cells) derived from sorting experiments preserved their functions. At the same time, it was showed that CD133⁻ population isolated from human melanoma cell lines preserves the CD133⁺ phenotype characteristics (by *in vitro* and *in vivo* methods) This could be due to the inclusion of several sorting experiments for the complete subpopulations purification to reduce the heterogeneity influence of isolated cells (Grasso et al., 2016). Another study (Nefitel et al., 2019) analyzed four different populations of glioblastoma cells (sorted) showing that they varied in the same four states, even after their isolation. These cell subpopulations kept their heterogeneity when analyzed after an *in vivo* procedure, possibly due to an association with genetic drivers that converge to the same cellular stages.

Therefore, when aptamer-stained cells are subjected to sorting experiments, it is supposed that they may recover the heterogeneity of the provided initial MSC populations. This occurs due to their genetic capacity of recovering to an initial cell state of heterogeneity (meaning undifferentiated coexisting with progenitor cells). It is known that MSC have a heterogeneous microenvironment, in which progenitors cells are present in a quiescent state (Klimczak and Kozłowska, 2015). Considering that, MSC are not a homogeneous population,

sorted-aptamer stained cells maintained their MSC phenotypic profile. Moreover, recovered cells did not show any CD14⁺ population, indicating that aptamers do not bind specifically to monocytes.

5.8 Differentiation potential of isolated aptamer-stained MSC

Since aptamer-stained MSC maintained their surface marker profile after sorting experiments, it was performed a cell sorting procedure (FACS) of aptamer-stained DP-MSCs using the aptamers APT1, APT3, APT10 and APT15 for the MSC. APT1 and APT3 were included in order to investigate if a small binding rate would mean that any specific target is interacting with aptamer. The “aptamer-sorted MSC” were recovered and cultivated during two weeks under sterile conditions for a differentiation study of these aptamer-MSCs population. MSC that were not subjected to the sorting isolation were used as undifferentiated (UND) and differentiated (CTL) controls for osteogenesis, chondrogenesis and adipogenesis differentiation, the mean phenotypes induced by MSC. Aptamer-sorted MSC and non-sorted MSC (CTL) were kept in specific optimal cell culture conditions for each type of differentiation for 14 days. Undifferentiated cells (UND) were cultivated in stemness cell culture conditions.

Differences in cell morphology of the adhered MSC, as described by Allameh et al. (2016), were verified during the differentiation period (Figure 21). Non-sorted UND cells remained with the same morphology profile on both day 0 and day 14 of differentiation. In the meanwhile, non-sorted CTL presented a differentiated shape profile. APT-sorted MSC showed the same pattern of CTL differentiation, which could be confirmed by quantitative and qualitative analyses of the specific cell types staining. All samples were fixed on day 14 of differentiation. Osteogenic, chondrogenic and adipogenic-differentiated MSC were stained with alizarin red S, toluidine blue and oil red-O, respectively. Analysis was performed using

the TissueFAXS equipment, based on a high resolution brightfield microscopy image that is integrated to single cell labeling quantification.

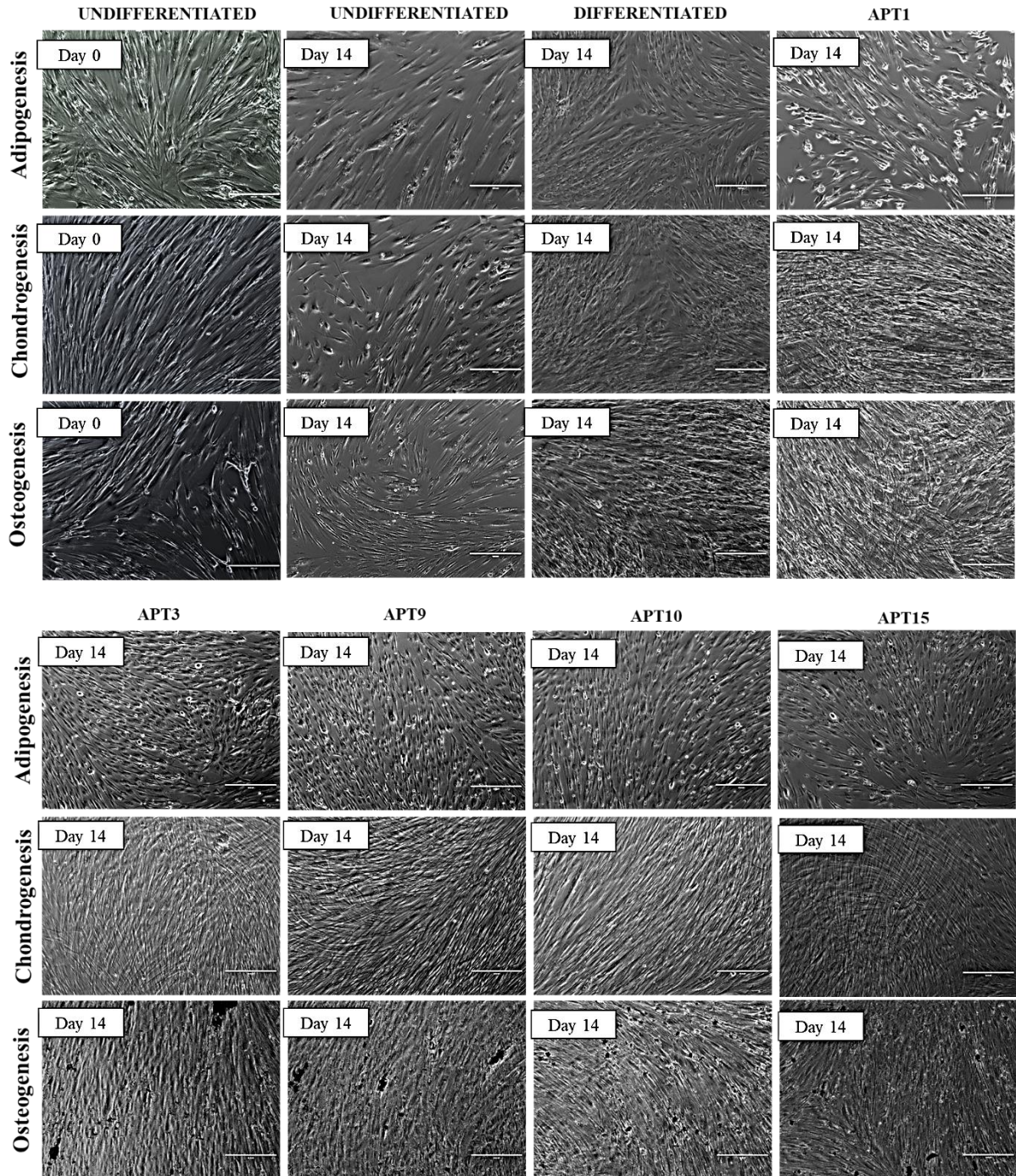


Figure 21. Cellular differentiation of heterogeneous MSC and aptamer-sorted MSC. *In vitro* differentiation assay of adhered derived-MSC under specific conditions during 14 days. Non-sorted differentiated MSC (positive control) and aptamer-sorted MSC were induced to differentiate into chondrocytes, adipocytes and osteocytes cells. Non-sorted undifferentiated MSC were used as negative control. APT1, APT3, APT10 and

APT15 were used for FACS cell isolation and differentiation processes were captured by brightfield microscopy; n=3.

The differentiation potential was investigated (Figure 21) by an image analysis to quantify the intensity of histochemical stained cells, which is based on a mask created by the software StrataQuest® (multishade mask - detected by color tonalities). The detecting colors used for this analysis were red for osteogenic-derived MSC, dark-brown dots for adipogenic-derived MSC and dark-purple for chondrogenic-derived MSC. These masks were all established by a comparison between UND and CTL controls (negative and positive) and they were used to quantify single cells in a tissue environment (tissue cytometry) according to their staining intensity.

Chondrogenic differentiation secrete an extracellular matrix composed of anionic proteoglycan and glycosaminoglycan molecules, which interacts with a cationic toluidine blue dye that produces a purple tone for cartilaginous tissue (Bergholt et al., 2019 and Terry et al., 2000). Adipogenic induction is identified by the occurrence of lipid vacuoles. Oil red O is a lipophilic dye that reacts with fat and produces a reddish color stain (Bumbrah, et al., 2019). Osteogenic differentiation can be identified based on the mineralization of a calcium matrix that interacts with the alizarin red S dye, forming calcified deposits (Shah et al., 2016). CTL and APT-derived MSC samples showed higher tendency to be differentiated compared to UND sample, which had not been induced to differentiation into chondrocytes, adipocytes and osteocytes. CTL, APT3, APT9 and APT15-sorted MSC underwent differentiation, and APT-sorted MSC displayed a tendency of enhanced differentiation into the three cell types. Moreover, the mean color intensity of APT3-derived MSC and APT15-derived MSC was significantly higher compared to the intensity of CTL-differentiated MSC into osteocyte and adipocyte phenotypes, respectively.

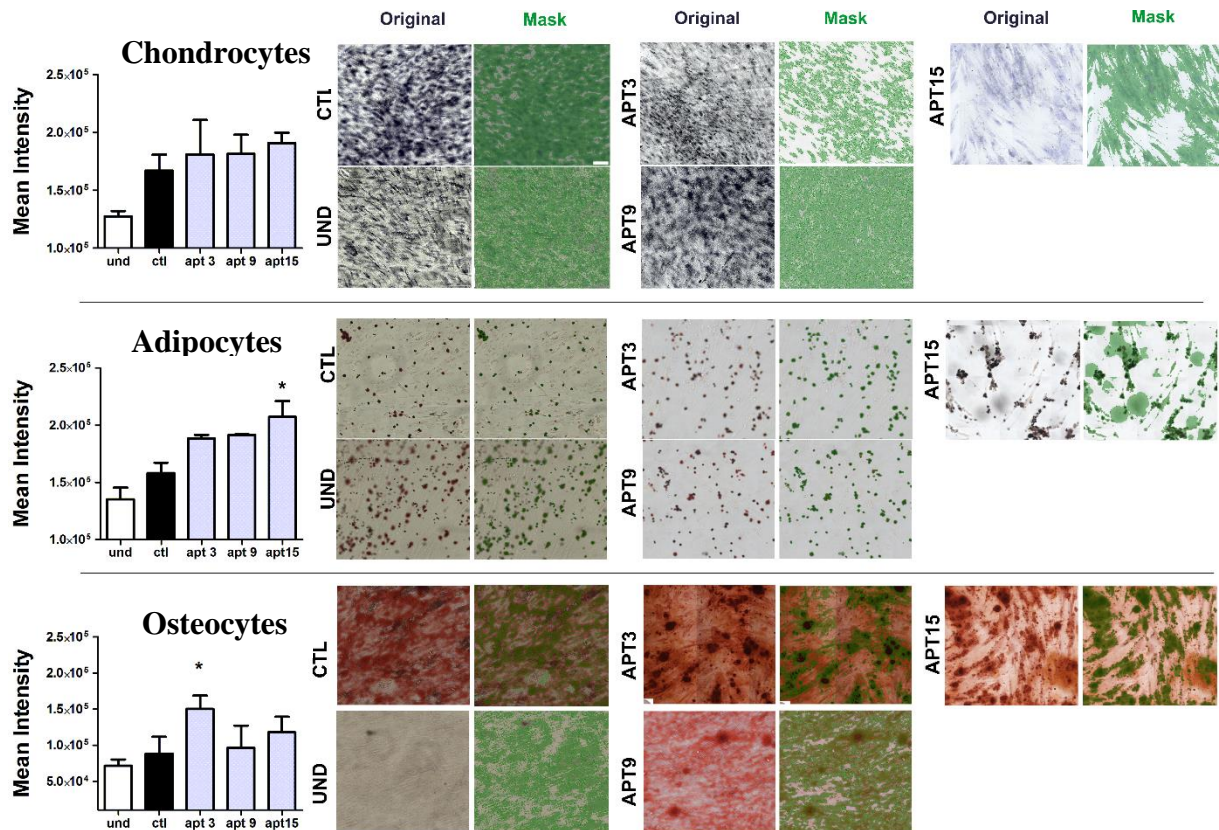


Figure 22. Differentiation potential of MSC quantified by tissue cytometry. Quantification of chondrogenesis, adipogenesis and osteogenesis process originated from sorted and non-sorted DP-MSC. Comparison between the undifferentiated MSC (UND) as negative control, the differentiated cells from non-sorted MSC (CTL) as positive control, and differentiated cells from aptamer-sorted MSC (In this figure, APT3, APT9 and APT15-sorted MSC). Mean intensity units are Mask-based on the color tonalities of the induced cell types (purple for chondrocytes, reddish-brown for adipocytes and red for osteocytes). Analysis procedured by TissueFAXS method, statistical analysis (CTR as control) with Bonferroni post hoc test, n=3

The other APT-derived MSC samples, such as APT1 and AP10 sorted cells (n=1), were not available for triplicate analysis due to their sensitiveness to differentiation medium. Even though, they presented a tendency to produce a better differentiation performance than conventional differentiation of MSC (Figure 23). When determining the efficiency of chondrogenesis, adipogenesis and osteogenesis induction, all APT-derived MSC showed higher mean color intensities compared to undifferentiated controls. The exception is given by APT10-derived MSC differentiated into adipocytes, since they showed a lower mean staining

intensity in comparison to UND samples. However, because this experiment has only one replicate, we cannot reach a conclusion.

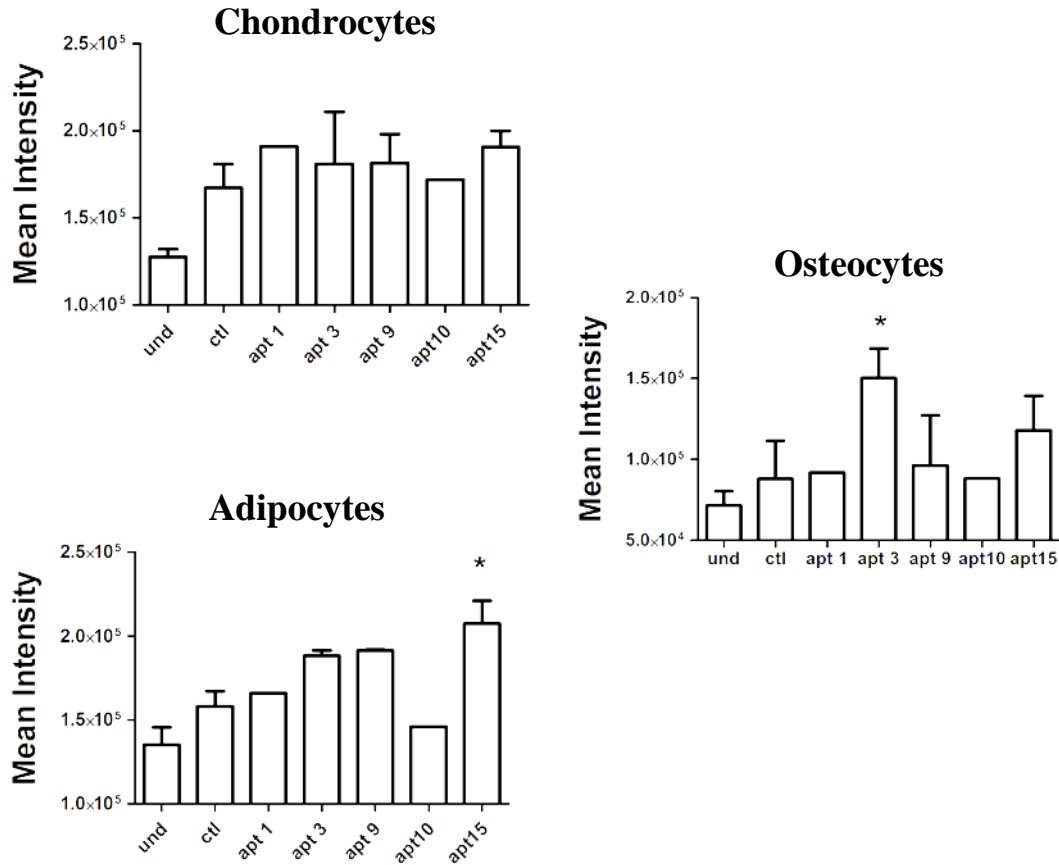


Figure 23. Mean color intensity comparison for aptamer-sorted and non-sorted differentiated MSC determined by tissue cytometry. Quantification of chondrocytes, adipocytes and osteocytes originated from DP-MSC by mean color intensity comparison between undifferentiated MSC (UND), differentiated cells from not sorted MSC (CTL) and differentiated cells from aptamer-sorted MSC (APT1, APT3, APT9, APT10 and APT15-sorted MSC).

The differentiation potential of APT-derived MSC was better for APT3 and APT15-sorted MSC, as they showed increased tendency to differentiate compared to UND and CTL controls. This was mainly significant regarding APT3-derived MSC differentiation into osteocytes and APT15-derived MSC differentiation into adipocytes. Even though, all aptamers maintained the capacity to undergo differentiation process. These results are

important to assume that interactions between aptamers and specific cell surface targets, as previously shown, maintain cell function above expectations.

Recently, aptamers sparked therapeutic interest because of their vast applications, such as the first aptamer approved drug. Maccugen® is an aptamer that binds to vascular endothelial growth factor (VEGF), replace antibodies in their use as high-affinity binders, leading to therapeutic effects (Zhou and Rossi, 2016). Furthermore, aptamers have been selected as molecular probes, pharmaceutical drugs and diagnostic tools for diseases based on their interaction with proteins of therapeutic or diagnostic relevance, such as the prostate-specific membrane antigen (PSMA), coagulation factor IXa (FIXa), human epidermal growth factor receptor 2 (HER-2) and protein tyrosine kinase 7 (PTK7). In view of the high-affinity binding characteristics of aptamers, these will benefit from specific cell targeting and isolation for therapeutic applications. MSC-based therapies might be explored by aptamers that recognize specific targets expressed by MSC, and the importance of biomarkers discovery was explored in this work.

5.9 Identification of surface proteins bound to aptamers

It has been defined that aptamers were presenting an interesting result for the interaction with MSC from different origins. After all necessary characterizations for pattern determination between aptamers and MSC, the specific antigen that was interacting with aptamers was sought.

Based on our results, we decided to analyze which biomarkers would bind to APT10,. In this way, APT10 and CNTR APT sequences were used to exclude the interaction with unspecific antigens. These sequences were chemically synthesized with a biotin molecule coupled to the 5' end of the DNA oligonucleotides. This biotin molecule was also separated by

an 18 carbon chain from the first nucleotide belonged to the strand, as the aptamer sequences synthesized before.

The biotin-aptamers were attached to a streptavidin molecule immobilized in agarose bead for a Pull Down assay. To make sure this interaction was correctly performed, standard experiments (using biotin-APT10 sequence) were performed to find the better conditions for the aptamer coupling (Figure 24). After following the protocol procedures for the incubation of aptamer (5 μ M) and streptavidin (0.6 μ g) at 25°C, the binding between biotin-aptamer and streptavidin molecules was verified.

Biotin-streptavidin has a non-covalent interaction that forms a strong complex composed by biotin vitamin molecule and streptavidin bacterial protein, which may be disrupted under elevated temperatures (Holmberg et al., 2005). This high binding affinity brings an advantage to detect proteins that interact with biotinylated DNA ligands.

Therefore, denaturation conditions at 25°C were tested and analyzed in a 10% polyacrylamide gel electrophoresis (Figure 24A). After biotin-coupled APT10 binding to the streptavidin agarose bead, unbound biotin-aptamer was analyzed after the first bead washing (Lane 2) until there was no more unbound DNA (Lane 3). Since the biotin-aptamer was strongly complexed to the beads, two elution conditions were tested: 6M urea solution (Lane 4) and 10% SDS-6M urea solution (Lane 6) at 25°C. Both conditions revealed none or very weak disruption of biotin-coupled aptamers from the agarose beads (Lanes 5 and 7). To confirm the immobilized aptamer status, we also included in the polyacrylamide gel 1 μ M biotin-APT10 (positive control, Lane A). Results allowed to conclude that denaturation at 25°C did not break the biotin-streptavidin complexes.

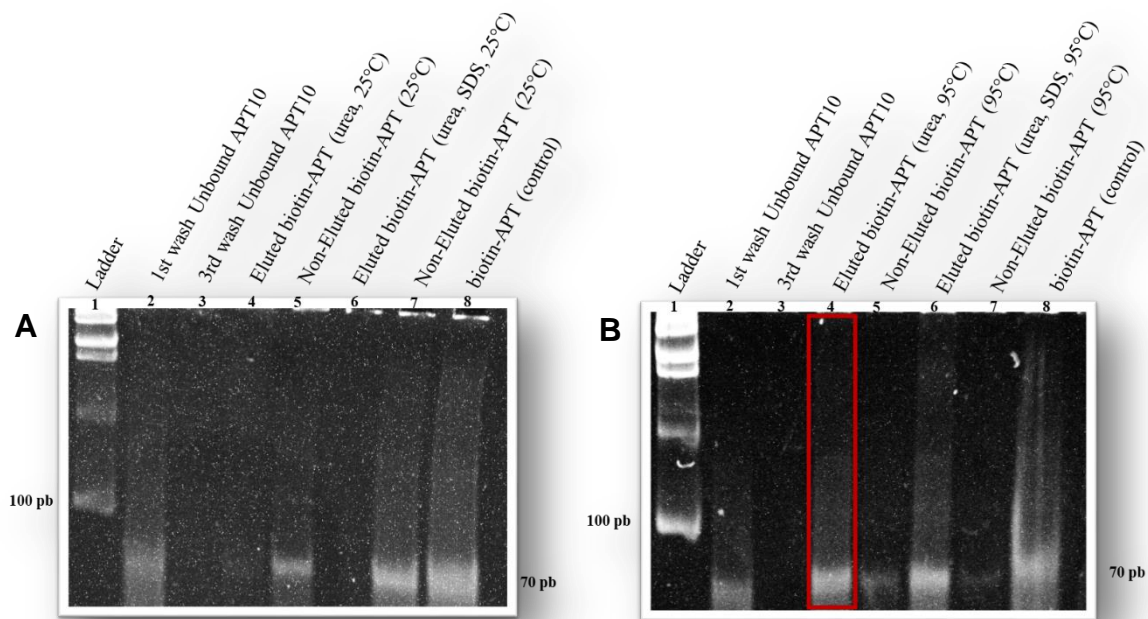


Figure 24. Confirmation of biotin-aptamer DNA binding to streptavidin-immobilized beads for affinity chromatography assays. 10% polyacrylamide gel electrophoresis was performed to select the standard conditions to analyze the link between biotin-APT10 and streptavidin molecules immobilized in agarose for pull down assay. A) Unbound biotin-APT after 1st and 3rd washes (Lanes 2 and 3) from the molecule complexes; elution of biotin-APT by denaturation at 25°C (Lane 4: 6M urea solution, Lane 6: 10% SDS + 6M urea solution); remained biotin-aptamer on agarose beds (Lane 7). B) Unbound biotin-APT after 1st and 3rd washes (Lanes 2 and 3) from the molecule complexes; elution of biotin-APT by denaturation at 95°C (Lane 4: 6M urea solution, Lane 6: 10% SDS + 6M urea solution); remained biotin-aptamer on agarose beads (Lane 7). The pure biotin-APT10 sequence (70 bp) was used as DNA staining-positive control in the polyacrylamide gel; 100 bp DNA Ladder (Thermo Fisher Scientific)

For the second denaturation condition (Figure 24B), a 10% polyacrylamide gel electrophoresis confirmed the binding between biotin-APT10 and streptavidin molecules after the first and third washes (Lanes 2 and 3). After an elution of the biotin-aptamer at 95°C, both conditions (6M urea solution and 10% SDS-6M urea solution) resulted in a recovery of the biotin-aptamer sequences (Lanes 4 and 6, respectively). Moreover, the Lanes 5 and 7 exhibit a low proportion of biotin-aptamer that remained linked to streptavidin molecules, confirming

the restoration of biotin-aptamer from the streptavidin agarose beads. Pure biotin-APT10 was used in the polyacrylamide gel as a positive control for DNA presence.

Since the biotin-aptamer DNA was confirmed to be associated with streptavidin molecules, the correct conditions for the pull down assay were established. We adapted our protocol according to SAPA assay (streptavidin-agarose pull down assay), which has been used to detect proteins from a nuclear extract (Wu, 2016).

For the pull down assay, we first detached DP-MSC from the culture plate using TryPLE enzyme, which presents a gentle activity to decrease the impact on the cell surface membrane. We tested three protein extraction conditions (Figure 25A): trypsin treatment, 0.1% triton X-100 detergent, and a sonication process. Differently from the previous experiment, we did not use ionic buffers mixed to soft detergents as the final method, since such a protocol had been developed for nuclear proteins, and not plasma membrane epitopes. Therefore, as we needed to find exclusive extracellular proteins, cells were rapidly sonicated incubated with protease inhibitor, after the plasma membrane recovering process. After the cellular membrane lysate incubation with the biotin-aptamer-streptavidin complexes, the antigens that bound to APT10 and CNTR APT were eluted under denatured conditions and submitted to 16% SDS-polyacrylamide gel electrophoresis. After this experiment, we could identify the protein extract (proteins not bound to the APT-streptavidin complex), the washing steps to eliminate the unbound proteins, and the eluted proteins for each condition. For the both trypsin and Triton reagent conditions, there were no differences in protein content between APT10 and CNTR APT eluted samples. However, the sonication process resulted in a different protein content for APT10 and CNTR APT samples standing out as the best procedure. Following the sonication protocol, proteins were extracted from the gel (Figure 25) (black square area) and analyzed by mass spectrometry.

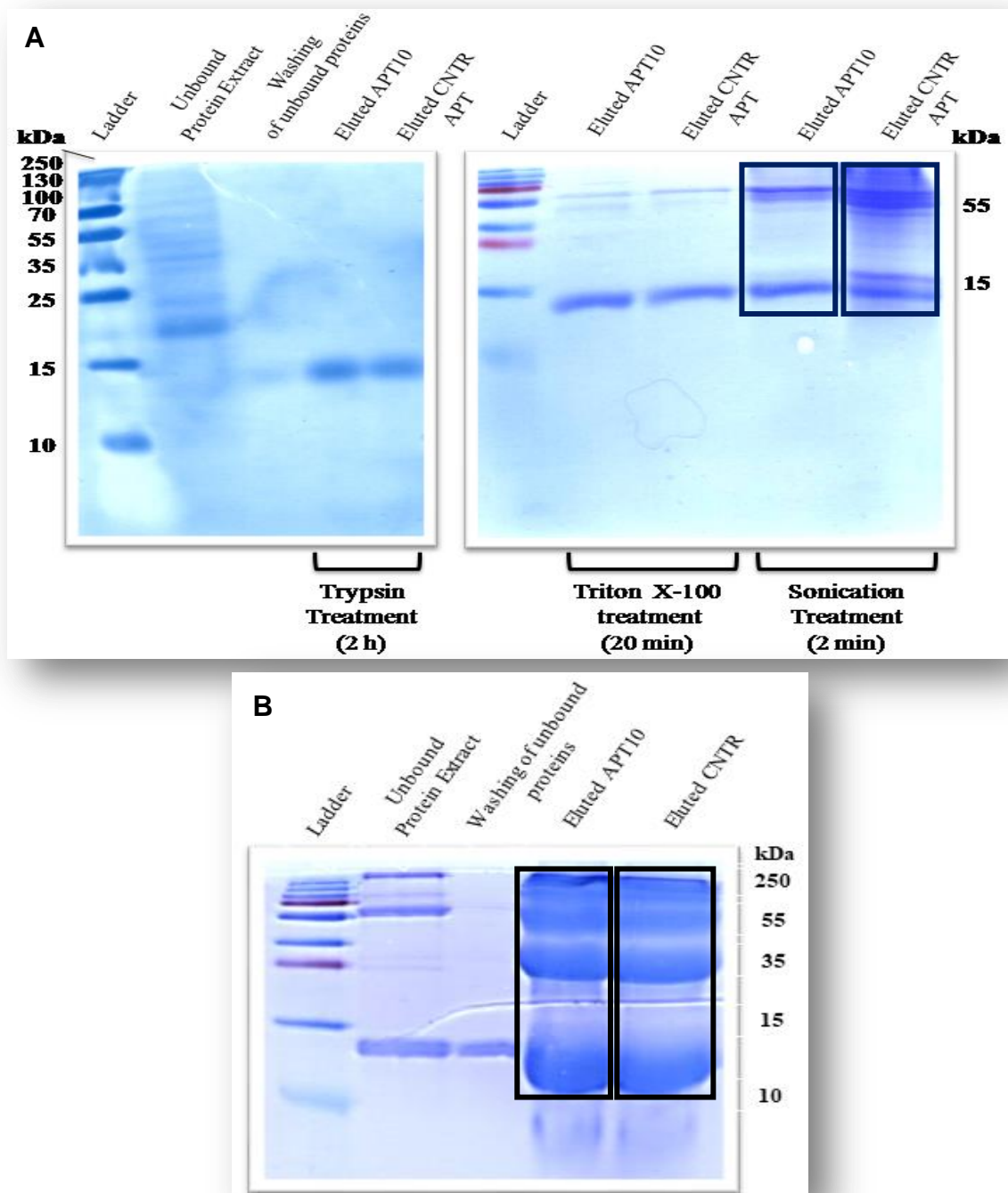


Figure 25. Verification of membrane surface proteins bound to aptamers in a pull down assay with DP-MSC and blood cell lysates. 16% SDS-PAGE analysis of proteins linked to biotin-aptamer-streptavidin complexes in a pull down assay. A) Protein pattern obtained from a pull down assay that used DP-MSC lysates acquired under 3 conditions: 0.25% trypsin treatment, 0.1% Triton X-100, and sonication. All procedures were applied for streptavidin-immobilized APT10 and CNTR APT. The sonication protocol resulted in the unbound proteins extract (which did not bound to aptamer complexes), the unbound proteins in washing steps, and the eluted proteins in APT10 and CNTR APT samples. B) Protein pattern obtained from a pull down assay that used

blood cell lysates by sonication protocol treatment. The results show the unbound proteins extract, the unbound proteins in washing steps and the eluted proteins in APT10 and CNTR APT samples. All eluted proteins shown by the black square area were recovered from the gel and sent to mass spectrometry analysis. PageRuler Prestained Protein Ladder (Thermo Scientific).

We introduced human blood cells as another negative control for the pull down assay and mass spectrometry analysis, since it is necessary to validate the results here reported, and because MSC might be in contact with these microenvironment situations. Fresh human blood cells were submitted to the same pull down protocol as used for DP-MSC and were analyzed in a 16% SDS-polyacrylamide gel (Figure 25B). The gel revealed the unbound proteins that did not interacted to the aptamer-streptavidin-membrane lysate, the washing steps of unbound proteins, and the eluted proteins that were binding to APT10 and CNTR APT samples. These antigens bound to aptamers were recovered from the polyacrylamide gel and submitted to mass spectrometry analysis. APT10 and CNTR APT bound to a higher amount of proteins, which could not be discriminated by the SDS-PAGE. In fact, we used PBMCs as a negative control for most of our results, but as observed before, there are possible antigens that might be co-expressed by immune cells and MSC. Therefore, to identify specific biomarkers of MSC, it is necessary to exclude proteins that may bind to the negative controls: CNTR APT and blood cells.

5.10 Analysis of MSC biomarkers bound to specific aptamers

The proteins obtained by pull down assay coupled to a SDS-PAGE trypsin-digest were sent to a mass spectrometry analysis to identify biomarkers for MSC. The samples were divided into “APT10-proteins for MSC”, “CNTR APT-proteins for MSC”, “APT10-proteins for blood cells”, and “CNTR APT-proteins for blood cells”. Treated samples were analyzed by CEFAP Biomass facility (IB-USP) and protein identification was performed by Proteome

Discovery 1.4 software (SEQUEST search engine, Thermo Scientific). The analysis is based on NCBI Inr and Uniprot protein online data banks, which correlate amino acid sequences to the peptide mass spectrum results based on algorithms. Mass spectrometry analysis resulted in 2148 proteins for APT10 bound to the MSC lysate, 3550 proteins for CNTR APT bound to the MSC lysate, 1163 proteins for APT10 bound to the blood cell lysate and 1392 proteins for CNTR APT bound to the blood cell lysate. First, the proteins from the CNTR APT groups that appeared in the APT10 groups were eliminated, remaining only proteins specific to APT10 binding. The list of “APT10-proteins for MSC” that excluded the non-specific proteins shared with CNTR APT group is found in Attachment 1 (51 remained proteins). For the “APT10-proteins for blood cells”, 31 proteins were not shared with CNTR APT/blood cell group.

It was then necessary to eliminate the remaining proteins that appeared both in MSC and blood cell / APT10-groups. Therefore, 11 proteins only appearing in “APT10-proteins for MSC” were identified (Table 3) and evaluated in terms of functionality and location.

All proteins characterized as MSC antigens and with binding specificity to APT10 were verified on RSCB PDB and the Uniprot online data bank. We verified the function and location of these proteins, and a significant number of proteins were membrane proteins from the endoplasmic reticulum and Golgi complex. They were also composing cytoskeleton and cytoplasmic enzymes, meaning that they could be proteins binding to aptamers during an apoptotic stage or after aptamer internalization. Another possibility is the internalization via endocytosis, since there are studies showing that recognition by cell surface receptors might promote aptamer uptake (Zhou and Rossi, 2009).

Nevertheless, two promising proteins were identified with extracellular location on human MSC: Disintegrin and metalloproteinase domain-containing protein 17 (ADAM17) and VAMP3 (vesicle-associated membrane protein 3). Based on Uniprot data bank analysis,

ADAM17 is a transmembrane metallopeptidase (extracellular, transmembrane and cytoplasmic domains) with several functions including signaling pathway regulation of the transforming growth factor beta receptor (TGF- β), a receptor of the growth factor involved with the differentiation of MSC. VAMP3 is involved in vesicular transportation from the plasma membrane to Golgi complex via endocytosis. This protein has a transmembrane (is an anchor for a membrane protein), a cytoplasmic and a vesicular domains. Its involvement in immunity by its extracellular vesicles, which are known to be secreted by MSC, has already been reported (Uniprot data bank).

The amino acid sequence of human ADAM17 has two isoforms (depending on the alternative splicing), but the peptide sequence found by mass spectrometry (that binds to APT10) was: NYGKTILTKEADLVTTHELGHNFGEHDPDGLAECAPNEDQGGK (Figures 26A and 26B). ADAM 17 cleaves important cell surface proteins (Uniprot data bank).

For VAMP3, there is only one isoform and one amino acid sequence. The peptide sequence found by mass spectrometry was: LQQTQNQVDEVVDIMR (Figure 26C).

A MRQSLFLTSVVPFVLAAPRPPDDPGFGPHQRLEKLDLSDYDILSLSNIQQHSV
 RKRDLQSTHVTLLTFSALKRHFKLYLTSSTERFSQNFKVVVVDGKNESEYTVK
 WQDFFTGHVVGEPDSRVLAIHRDDVIIRINTDGAEYNIPLWRFVNDTKDKRML
 VYKSEDIKNVSRQLQSPKVCGYLKVDNEELLPKGLVDREPPEELVHRVKRRADPDP
 MKNTCKLLVADHRFYRYMGRGEESTTTNYLIELIDRVDDIYRNTSWDNAGFKGY
 GIQIEQIRILKSPQEVKPGKHYNMAKSYPNEEKDAWDVKMLLEQFSFDIAEEAS
 KVCLAHLFTYQDFDMGTLGLAYVGS PRANSHGGVCPKAYYSPVGKKNIYLNGLT
 STK**NYGKTILTKEADLVTTHELGHNFGEHDPDGLAECAPNEDQGGK**YVMYPIAV
 SGDHENKMFNSCKQSIYKTIESKAQECFQERSNKVCGNSRVDEGEEDPGIMY
 LNNDTCCNSDCTLKEGVQCSDRNSPCCCKNCQFETAQKKCQEAINATCKGVSYCTG
 NSSECPPPGNAEDDTVCLDLGKCKDGKCI PFCEREQOLESCACNETDNSCKVCCR
 DLSGRCVPYVDAEQKNLFLRKGKPTVGFCDMNGKCEKRVQDVIERFWD FIDQLS
 INTFGKFLADNIVGSVLVFSLIFWIPFSILVHCVDKLLDKQYESLSLHFPSNVEM
 LSSMDSASVRI IKFPFAPQTPGRLQAPVIPSAPAAPKLDHQRM DTIQEDPSTDS
 HMDDEGF EKDPFNSSTA AKSFEDLTDHPVTRSEKAASF KLQRQNRVDSKETEC

B MRQSLFLTSVVPFVLAAPRPDDPGFGPHQRLEKLDLSLLSDYDILSLSNIQQHVS
 RKRDLQSTHVELLLTFSALKRHFKLYLTSSSTERFSQNFKVVVVDGKNESEYTVK
 WQDFFTGHVVGEPDSRVLAHIRDDDVIIRINTDGAEYNIIEPLWRFVNDTKDKRML
 VYKSEDIKNVSRQLQSPKVCGYLKVDNEELLPKGLVDREPPPEELVHRVKRRADPDP
 MKNTCKLLVVADHRFYRYMGRGEESTTTNYLIELIDRVDDIYRNTSWDNAGFKGY
 GIQIEQIRILKSPQEVKPGKHYNMAKSYPNEEKDAWDVKMLLEQFSFDIAEEAS
 KVCLAHLFTYQDFDMGTLGLAYVGSFRANSHGGVCPKAYYSPVGKKNIYLNGLT
 STK**NYGKTI**L**TKEADLV**T**THELGHNFGAEHDPDGLAECAPNEDQGGK**YVMYPIAV
 SGDHENKMFNSNCSKQSIYKTIESKAQECFQERSNKVCGNSRVDEGEECDPGIMY
 LNNDTCCNSDCTLKEGVQCSDRNSPCKKNCQFETAQKCKQEAINATCKGVSYCTG
 NSSECPPPGNAEDDTVCLDLGKCKDGKCI PFCEREQQLESCACNETDNSCKVCCR
 DLSGRCPYPVDAEQKNLFLRKGPCTVGFCDMNGKCEKRVQDVIERFWDFIDQLS
 INTFGKFLADNIVGSVLVFSLIFWIPFSILVHCV

C MSTGPTAATGSNRR**LQQTQNQVDEVVDIMR**VNVDKVLERDQKLSELDDRADALQA
 GASQFETSAAKLKRKYWWKNCKMWAIGITVLVIFIIIIIVVVVSS

Figure 26. Amino acid sequences of ADAM 17 and VAMP3 proteins found by spectrometry mass for MSC. Proteins ADAM17 and VAMP3 amino acid sequences found by mass spectrometry for APT10 derived samples from the pull down assay with MSC. A) Isoform A of ADAM17 human protein, which is altered by alternative splicing. B) Isoform B of ADAM17 protein. Both isoforms contain the peptide sequence (red: residues 389-432) found by mass spectrometry. C) The only isoform sequence of VAMP3 human protein and its peptide sequence found by mass spectrometry (red: residues 15-30). Information and sequence provided by Uniprot online data bank.

Table 4.: Description of proteins identified by mass spectrometry when bound to the complex “APT10-MSC surface lysate” after a pull down assay.

Accession number	Protein description
P61803	Dolichyl-diphosphooligosaccharide--protein glycosyltransferase subunit DAD1 OS=Homo sapiens OX=9606 GN=DAD1 PE=1 SV=3 - [DAD1_HUMAN]
Q15836	Vesicle-associated membrane protein 3 OS=Homo sapiens OX=9606 GN=VAMP3 PE=1 SV=3 - [VAMP3_HUMAN]
P78559	Microtubule-associated protein 1A OS=Homo sapiens OX=9606 GN=MAP1A PE=1 SV=6 - [MAP1A_HUMAN]
P21964	Catechol O-methyltransferase OS=Homo sapiens OX=9606 GN=COMT PE=1 SV=2 - [COMT_HUMAN]
Q15645	Pachytene checkpoint protein 2 homolog OS=Homo sapiens OX=9606 GN=TRIP13 PE=1 SV=2 - [PCH2_HUMAN]

O00303	Eukaryotic translation initiation factor 3 subunit F OS=Homo sapiens OX=9606 GN=EIF3F PE=1 SV=1 - [EIF3F_HUMAN]
Q86Y82	Type-1 angiotensin II receptor-associated protein OS=Homo sapiens OX=9606 GN=AGTRAP PE=1 SV=1 - [ATRAP_HUMAN]
Q8TCJ2	Dolichyl-diphosphooligosaccharide--protein glycosyltransferase subunit STT3B OS=Homo sapiens OX=9606 GN=STT3B PE=1 SV=1 - [STT3B_HUMAN]
P78536	Disintegrin and metalloproteinase domain-containing protein 17 OS=Homo sapiens OX=9606 GN=ADAM17 PE=1 SV=1 - [ADA17_HUMAN]
P46778	60S ribosomal protein L21 OS=Homo sapiens OX=9606 GN=RPL21 PE=1 SV=2 - [RL21_HUMAN]
Q9UGP8	Translocation protein SEC63 homolog OS=Homo sapiens OX=9606 GN=SEC63 PE=1 SV=2 - [SEC63_HUMAN]

Therefore, the peptide sequence of ADAM17 represents a part of the catalytic site of this enzyme (Maskos et al., 1998), to which APT10 supposedly binds in MSC surface area. VAMP3 should have an affinity to APT10, which is associated with MSC-secreted extracellular vesicles or internalization of the aptamer (Rani et al., 2015).

5.11 Bioinformatic analysis of APT10 binding to ADAM17 and VAMP3

ADAMs are single-pass transmembrane proteins with a characteristic modular domain organization. ADAM17 has an ectodomain that contains an N-terminal signal sequence and an adjacent pro-domain, followed by metalloproteinase, disintegrin, and cysteine-rich domains (Figure 27A). Docking of the aptamer on the ADAM17's surface (Table 4) was generated based on the metalloprotease domain's crystallized structure, while a homology model of the cysteine-rich and disintegrin domains were considered for discussion. ADAM10 structure suggests that the cysteine-rich domain prevents access of protein substrates to the active site, which results in auto inhibition (Seegar et al., 2017). Similarly, ADAM17 inhibited state was modelled by including the disintegrin and cysteine-rich domains (Figure 27B), delimiting the surface where a potential inhibitory aptamer could interact (Figure 27C).

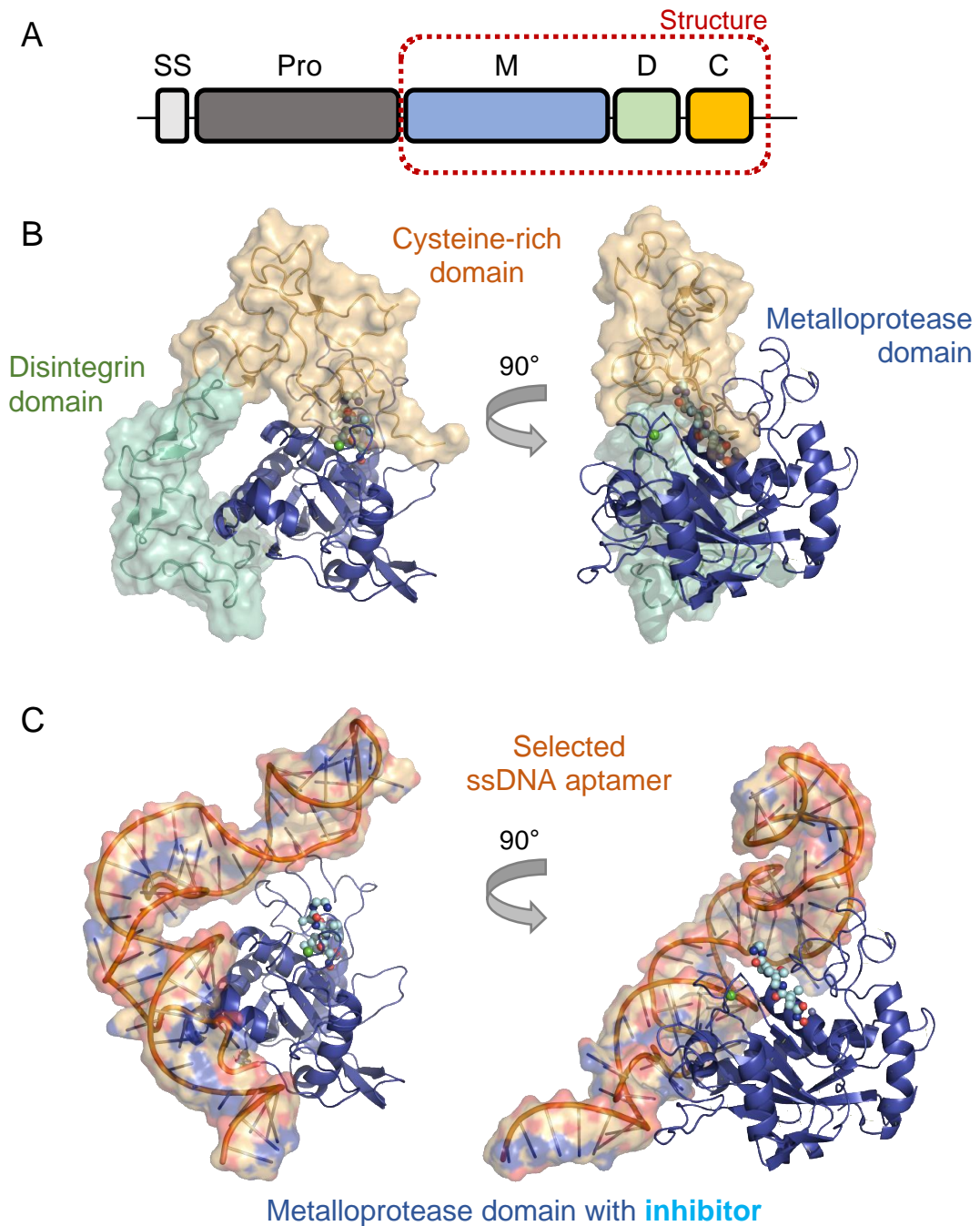


Figure 27. Modeling of ADAM17 interaction with aptamer 10. A) ectodomain organization evidencing the following features: SS, signal sequence; Pro, pro-domain; M, metalloproteinase (blue); D, disintegrin (green); C, cysteine-rich (light orange); The red box encompasses the portion of the protein visualized in the structural model. B) Structural model of ADAM17's based on ADAM10 homologue and the respective structure co-crystallized with the inhibitor (cyan ball and sticks model); C) ADAM17's metalloprotease domain and its suggested interaction with the ssDNA aptamer.

Table 5.: Scoring information of ADAM17 and aptamer interaction, as predicted by HDock.

Lowest energy structure was chosen for structural interpretation.

Rank	Docking Score	Ligand rmsd (Å)
1	-269.03	59.36
2	-245.87	62.91
3	-244.24	55.03
4	-237.63	58.69
5	-235.63	66.83
6	-235.43	59.59
7	-233.58	58.36
8	-233.52	60.07
9	-229.51	52.81
10	-229.37	57.3

ADAM17 or TACE is a tumor necrosis factor (TNF α) converting enzyme that participate in several transmembrane ectodomains cleavage, and is associated with resultant signaling processes (Granato et al., 2018). ADAM enzymes are catalytic Zn²⁺-dependent and has both proteolytic and adhesion properties. 21 types of ADAM were described for human species and some of them may lose their enzymatic potential according to the different phases of cellular cycle, which can be related to the decrease in extracellular [Zn²⁺] (Gooz, 2010). ADAM17 is involved in inflammatory processes. It is reported as an enzyme for adhesion substrates: TNF α and TNF α receptors, IL-6 receptor, IL-15 receptor, L-selection and others molecules (Tang et al., 2011). TGF- β is another substrate for the ADAM17 enzyme, since the peptidase cleaves this transmembrane growth factor and inhibits TGF- β signaling processes (Malapeira et al. 2011). TGF- β is involved in the differentiation process of MSC through cell interactions and extracellular signaling factors, meaning that several cascade pathways develop and influence chondrogenesis, adipogenesis and osteogenesis (Grafe et al., 2018). All these factors corroborate the APT10 binding to MSC, since the undifferentiated state of these cells is promoted by ADAM17, inhibiting the TGF- β signaling process during differentiation.

Moreover, when these ADAM17-expressed stem cells are bound to APT10 and are isolated by sorting methods, the new set of subpopulation has their ADAM17 catalytic site blocked by APT10. Consequently, MSC remain multipotent for later differentiation induction. Thus, it is possible that there is a reactivation of TGF- β signaling as suggested by the tendency of enhanced differentiation potential of MSC, when the cells bound to aptamers have been isolated. Furthermore, our results also showed that after cycles of aptamer-sorting isolation, the aptamer binding rate decreases for these sorted-MSCs. Nevertheless, MSC remained labeled with fluorescent aptamers after hours of the isolation experiment, meaning APT10 was still bound to the catalytic site of ADAM17, and MSC were halted from undergoing spontaneous differentiation.

In parallel, vesicle-associated membrane protein 3 (VAMP3, Q15836) sequence was modelled as full-length, using rat VAMP2 (sequence identity of 78% and 99% similarity in covered regions). VAMP3 acts in the regulation of endocytosis and belongs to a transmembrane complex of proteins named soluble N-ethylmaleimide-sensitive factor activating protein receptor (SNAREs), which are involved in content transportation into intracellular localities (Zhu et al., 2017). Two structures from VAMP2 were used as template in order to generate models with different protein conformations: the VAMP2 alone model (based on the NMR structure 2KOG, Ellena et al., 2009) and the VAMP2 within the SNARE complex (3HD7, resolution: 3.4 Å, Stein et al., 2009). As the structural model of human VAMP3 is not available, its binding with APT10 presented a tricky understanding in terms of binding location in the secondary structures (Figure 28).

MSC contain extracellular vesicles that play important roles in the communication of cells related to immune processes, and in cell differentiation (Phan et al., 2018). Moreover, MSC release soluble cytokines and other molecules that depend on the microenvironment of their location (Leuning et al., 2018). In this way, it is hypothesized that APT10 binds to the

VAMP3 membrane vesicle since the derived-MSD protein influences the extracellular membrane sites of MSD according to immune and inflammatory responses. These signaling cascades might result in specific endocytosis and exocytosis transportation (Harrel et al, 2019). In our results, there was considerable binding rate for aptamers and monocytes that correlates to the regulation of activation and proliferation of immune cells.

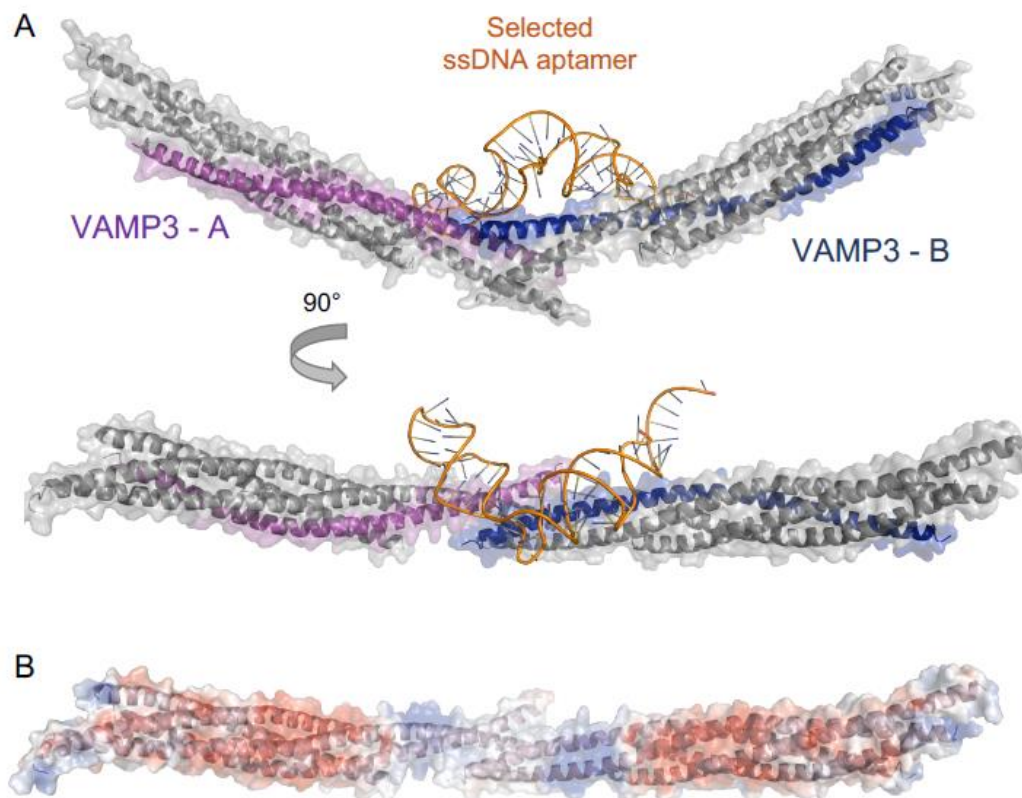


Figure 28. VAMP3 interaction with aptamer 10 model. A) Structural model of human VAMP3's based on rat VAMP2 homologue and the respective structure co-crystallized with ssDNA aptamer; B) VAMP3's SNARE final complex based on rat VAMP2 homologue protein, which revealed a tricky understanding due the complexity and lack of information regarding human VAMP3.

5. CONCLUSION

Aptamers selected to identify MSC from different origins presented important results regarding binding features and biomarker discovery. Aptamer-target interaction increased accordingly with the apoptosis induction of cells, based on the enhanced internalization potential of the ssDNA ligands. However, immunofluorescence microscopy and tissue cytometry were precise to show the binding sites of aptamers, which were external for MSC and both internal and external for monocytes. On the other hand, lower specificity binding rate exhibited by monocytes (2.5X) compared to MSC (10-16X) suggests unspecific interactions between aptamers and monocytes. Aptamer-sorting of MSC proved the maintenance of CD90 and CD105 surface markers, besides showing that MSC yet exhibit aptamer staining after recovering subpopulations of cells and the maintenance of a multipotent population able to differentiate into various cellular phenotypes. Pull-down assays identified ADAM17 and VAMP3 transmembrane proteins that interact with APT10. These possible biomarkers are supposedly involved in stemness potential. ADAM17 may act in undifferentiated MSC due to the possible inhibition of TGF β differentiation signaling. When bound to APT10, the active site of ADAM17 is blocked, increasing multipotency differentiation potential of aptamer-sorted MSC. In addition, VAMP3 interaction with APT10 reveals specificity of the microenvironment, where MSC are present, since this protein is involved in the endocytosis and exocytosis of different molecules. Moreover, it is known that the MSC secretome plays a great role in immune responses and differentiation mechanisms. Overall, the herein identified proteins will be subject for further investigations aiming the improvement of MSC-based therapies.

PERSPECTIVES

Based on the obtained results, further work might be developed, considering the importance of the MSC biomarkers identified by aptamer binding, as described above:

- ❖ To determine binding kinetics between aptamers and purified ADAM17 and VAMP3;
- ❖ To investigate effects of APT10 on ADAM17 enzymatic activity;
- ❖ To demonstrate the differences in immune environment and responses when MSC are aptamer-purified;
- ❖ To test aptamer 10-treated MSC *in vivo* for cell regeneration therapy.

7. REFERENCES

- ALT E, YAN Y, GEHMERT S, SONG YH, ALTMAN A, GEHMERT S, VYKOUKAL D, BAI X. FIBROBLASTS SHARE MESENCHYMAL PHENOTYPES WITH STEM CELLS, BUT LACK THEIR DIFFERENTIATION AND COLONY-FORMING POTENTIAL. *BIOLOGY OF THE CELL*. 2011; 103(4):197-208.
- ALTIN JG, SLOAN EK. THE ROLE OF CD45 AND CD45-ASSOCIATED MOLECULES IN T CELL ACTIVATION. *IMMUNOLOGY & CELL BIOLOGY* 1997 OCT;75(5):430-45.
- ALLAMEH A, JAZAYERI M, ADELIPOUR M. IN VIVO VASCULARIZATION OF ENDOTHELIAL CELLS DERIVED FROM BONE MARROW MESENCHYMAL STEM CELLS IN SCID MOUSE MODEL. *CELL J*. 2016 JUL-SEP; 18(2): 179–188.
- APPELT U, SHERIFF A, GAIPL US, KALDEN JR, VOLL RE, HERRMANN M. VIABLE, APOPTOTIC AND NECROTIC MONOCYTES EXPOSE PHOSPHATIDYL- SERINE: COOPERATIVE BINDING OF THE LIGAND ANNEXIN V TO DYING BUT NOT VIABLE CELLS AND IMPLICATIONS FOR PS-DEPENDENT CLEARANCE. *CELL DEATH & DIFFERENTIATION*. 2005; 12(2):194-6.
- BAER PC, GEIGER H. ADIPOSE-DERIVED MESENCHYMAL STROMAL/STEM CELLS: TISSUE LOCALIZATION, CHARACTERIZATION, AND HETEROGENEITY. *STEM CELLS INTERNATIONAL*. 2012; 2012:812693.
- BAGHAEI K, HASHEMI SM, TOKHANBIGLI S, RAD AA, ASSADZADEH-AGHDAEI H, ABDOLHAMI SHARIFIAN A, ZALI MR. ISOLATION, DIFFERENTIATION, AND CHARACTERIZATION OF MESENCHYMAL STEM CELLS FROM HUMAN BONE MARROW. *GASTROENTEROL HEPATOL BED BENCH*. 2017; 10(3): 208–213.
- BARRY FP, MURPHY JM. MESENCHYMAL STEM CELLS: CLINICAL APPLICATIONS AND BIOLOGICAL CHARACTERIZATION. *INTERNATIONAL JOURNAL OF BIOCHEMISTRY & CELL BIOLOGY*. 2004; 36(4):568-84.
- BERGHOLT NL, LYSDAHL H, LIND M, FOLDAGER CB. A STANDARDIZED METHOD OF APPLYING TOLUIDINE BLUE METACHROMATIC STAINING FOR ASSESSMENT OF CHONDROGENESIS. *CARTILAGE*. 2019; 10 (3):370-374.
- BIESIADA M, PURZYCKA KJ, SZACHNIUK M, BLAZEWICZ J, ADAMIAK RW. AUTOMATED RNA 3D STRUCTURE PREDICTION WITH RNACOMPOSER. *METHODS MOL BIOL*. 2016; 1490:199–215.
- BLIAKHER MS, FEDOROVA IM, LOPATINA TK, ARKHIPOV SN, KAPUSTIN IV, RAMAZANOVA ZK, KARPOVA NV, IVANOV VA, SHARAPOV NV.. ACILACT AND IMPROVEMENT OF THE HEALTH STATUS OF SICKLY CHILDREN. *VESTNIK ROSSIYSKOI AKADEMII MEDITSINSKIKH NAUK*. 2005; (12):32-5.
- BYDŁOWSKI SP, JANZ FL. ADVANCES IN HEMATOPOIETIC STEM CELL RESEARCH: HEMATOPOIETIC STEM CELL IN ACUTE MYELOID LEUKEMIA. *INTech*. 2012; 12: 261-276.
- BUMBRAH GS, SODHI GS, KAUR J. OIL RED O (ORO) REAGENT FOR DETECTION OF LATENT FINGERMARKS: A REVIEW. *EGYPTIAN JOURNAL OF FORENSIC SCIENCES*. 2019; 9(3).
- CAN A. A CONCISE REVIEW ON THE CLASSIFICATION AND NOMENCLATURE OF STEM CELLS. *TURKISH JOURNAL OF HEMATOLOGY*. 2008; 25: 57–59.

CHAMILOS G, GREGORIO J, MELLER S, LANDE R, KONTOYIANNIS DP, MODLIN RL, GILLIET M. CYTOSOLIC SENSING OF EXTRACELLULAR SELF-DNA TRANSPORTED INTO MONOCYTES BY THE ANTIMICROBIAL PEPTIDE LL37. *BLOOD*. 2012; 120 (18):3699-707.

CHANG YM, DONOVAN MJ, TAN W. USING APTAMERS FOR CANCER BIOMARKER DISCOVERY. *JOURNAL OF NUCLEIC ACIDS*. 2013:817350.

CATHERINE AT, SHISHIDO SN, ROBBINS-WELTY GA, DIEGELMAN-PARENTE A. RATIONAL DESIGN OF A STRUCTURE-SWITCHING DNA APTAMER FOR POTASSIUM IONS. *FEBS OPEN BIO*. 2014; 4:788-95.

COLEMAN ML, SAHAI EA, YEO M, BOSCH M, DEWAR A, OLSON MF. MEMBRANE BLEBBING DURING APOPTOSIS RESULTS FROM CASPASE-MEDIATED ACTIVATION OF ROCK I. IN: *NATURE CELL BIOLOGY*. 2001 APR;3(4):339-45.

COLLIN M, MCGOVERN N, HANIFFA M. HUMAN DENDRITIC CELL SUBSETS. *IMMUNOLOGY*. 2013; 140(1):22-30.

CHETTY R, GATTER K.. CD3: STRUCTURE, FUNCTION, AND ROLE OF IMMUNOSTAINING IN CLINICAL PRACTICE. IN: *THE JOURNAL OF PATHOLOGY*. 1994; 173(4):303-7.

DANIELS DA, CHEN H, HICKE BJ, SWIDEREK KM, GOLD LA TENASCIN-C APTAMER IDENTIFIED BY TUMOR CELL SELEX: SYSTEMATIC EVOLUTION OF LIGANDS BY EXPONENTIAL ENRICHMENT. *PROCEEDINGS OF THE NATIONAL ACADEMY OF SCIENCES OF THE UNITED STATES OF AMERICA*. 2003; 100(26):15416-21.

DARMOSTUK M, RIMPELOVA S, GBELCOVA H, RUMI T. CURRENT APPROACHES IN SELEX: AN UPDATE TO APTAMER SELECTION TECHNOLOGY. *BIOTECHNOLOGY ADVANCES*. 2015; 33 (6 Pt 2):1141-61.

DOMINICI M, LE BLANC K, MUELLER, SLAPER-CORTENBACH, MARINI F, KRAUSE D, DEANS R, KEATING A, PROCKOP DJ, HORWITZ E. MINIMAL CRITERIA FOR DEFINING MULTIPOTENT MESENCHYMAL STROMAL CELLS. *THE INTERNATIONAL SOCIETY FOR CELLULAR THERAPY POSITION STATEMENT. CYTOTHERAPY*. 2006; 8(4):315-7.

VAN ENGELAND M, NIELAND LJ, RAMAEKERS FC, SCHUTTE B, REUTELINGSPERGER CP. ANNEXIN V-AFFINITY ASSAY: A REVIEW ON AN APOPTOSIS DETECTION SYSTEM BASED ON PHOSPHATIDYLSERINE EXPOSURE. *CYTOMETRY*. 1998; 31(1):1-9.

ELLENA JF, LIANG B, WIKTOR M, STEIN A, CAFISO DS, JAHN R, TAMM LK DYNAMIC STRUCTURE OF LIPID-BOUND SYNAPTOBREVIN SUGGESTS A NUCLEATION-PROPAGATION MECHANISM FOR TRANS-SNARE COMPLEX FORMATION. *PROC NATL ACAD SCI USA*. 2009; 106(48):20306-11.

FRIEDENSTEIN AJ, CHAILAKHJAN RK, LALYKINA KS THE DEVELOPMENT OF FIBROBLAST COLONIES IN MONOLAYER CULTURES OF GUINEA-PIG BONE MARROW AND SPLEEN CELLS. *CELL AND TISSUE KINETICS*. 1970; 3(4):393-403.

FOSTER BM, ZAIDI D, YOUNG TR, MOBLEY ME, KERR BA. CD117/C-KIT IN CANCER STEM CELL-MEDIATED PROGRESSION AND THERAPEUTIC RESISTANCE. *BIOMEDICINES*. 2018; 6(1). pii: E31.

GEISSMANN F, MANZ MG, JUNG S, SIEWEKE MH, MERAD M, LEY K. DEVELOPMENT OF MONOCYTES, MACROPHAGES, AND DENDRITIC CELLS. *SCIENCE*. 2010; 327(5966):656-61.

GEISSMANN F, JUNG S, LITTMAN DR. BLOOD MONOCYTES CONSIST OF TWO PRINCIPAL SUBSETS WITH DISTINCT MIGRATORY PROPERTIES. *IMMUNITY*. 2003; 19(1):71-82.

GIORDANO RJ, CARDÓ-VILA M, LAHDENRANTA J, PASQUALINI R, ARAP W. BIOPANNING AND RAPID ANALYSIS OF SELECTIVE INTERACTIVE LIGANDS. *NATURE MEDICINE*. 2001; 7(11):1249-53.

GONÇALVES, FDC, LUK F, KOREVAAR SS, BOUZID R, PAZ AH, LÓPEZ-IGLESIAS C, BAAN CC, MERINO A, HOOGDUIJN MJ. MEMBRANE PARTICLES GENERATED FROM MESENCHYMAL STROMAL CELLS MODULATE IMMUNE RESPONSES BY SELECTIVE TARGETING OF PRO-INFLAMMATORY MONOCYTES. *SCIENTIFIC REPORTS*. 2017; 7(1):12100.

GOOZ M. ADAM-17: THE ENZYME THAT DOES IT ALL. *CRITICAL REVIEWS IN BIOCHEMISTRY AND MOLECULAR BIOLOGY*. 2010; 45 (2):146-69

GRAFE I, ALEXANDER S, PETERSON JR, SNIDER TN, LEVI B, LEE B, MISHINA Y. TGF-B FAMILY SIGNALING IN MESENCHYMAL DIFFERENTIATION. *COLD SPRING HARB PERSPECT BIOL*. 2018; 10 (5)PII: A022202.

GRANATO DC, E COSTA RAP, KAWAHARA R, YOKOO S, ARAGÃO AZ, DOMINGUES RR, PAULETTI BA, HONORATO RV, FATTORI J, FIGUEIRA ACM, OLIVEIRA PSL, CONSONNI SR, FERNANDES D, LAURINDO F, HANSEN HP, ET AL. THIOREDOXIN-1 NEGATIVELY MODULATES ADAM17 ACTIVITY THROUGH DIRECT BINDING AND INDIRECT REDUCTIVE ACTIVITY. *ANTIOXIDANTS & REDOX SIGNALING*. 2018; 29 (8):717-734.

GRASSO C, ANAKA M, HOFMANN O, SOMPALLAE R, BROADLEY K, HIDE W, BERRIDGE MV, CEBON J, BEHREN A, MCCONNELL MJ. ITERATIVE SORTING REVEALS CD133+AND CD133-MELANOMA CELLS AS PHENOTYPICALLY DISTINCT POPULATIONS. *BMC CANCER*. 2016; 16(1):726.

HARRELL CR, FELLABAUM C, JOVICIC N, DJONOV V, ARSENIJEVIC N, VOLAREVIC V. MOLECULAR MECHANISMS RESPONSIBLE FOR THERAPEUTIC POTENTIAL OF MESENCHYMAL STEM CELL-DERIVED SECRETOME. *CELLS*. 2019; 8(5). pii: E467.

HAZIOT A, CHEN S, FERRERO E, LOW MG, SILBER R, GOYERT SM.. THE MONOCYTE DIFFERENTIATION ANTIGEN, CD14, IS ANCHORED TO THE CELL MEMBRANE BY A PHOSPHATIDYLINOSITOL LINKAGE. *THE JOURNAL OF IMMUNOLOGY*. 1988; 141(2):547-52.

HERMANN T, PATEL DJ. ADAPTIVE RECOGNITION BY NUCLEIC ACID APTAMERS. *SCIENCE*, 2000; 287(5454):820-5.

HOLMBERG A, BLOMSTERGREN A, NORD O, LUKACS M, LUNDEBERG J, UHLÉN M. THE BIOTIN-STREPTAVIDIN INTERACTION CAN BE REVERSIBLY BROKEN USING WATER AT ELEVATED TEMPERATURES. *ELECTROPHORESIS* 2005; 26(3):501-10

HOLMES, N. CD45: ALL IS NOT YET CRYSTAL CLEAR. *IMMUNOLOGY*. 2006; 117(2):145-55.

HUANG SY, ZOU X. KNOWLEDGE-BASED SCORING FUNCTION FOR PROTEIN-RNA INTERACTIONS DERIVED FROM A STATISTICAL MECHANICS-BASED ITERATIVE METHOD. *NUCLEIC ACIDS RES*. 2014; 42(7):E55.

JACOBSON MP, PINCUS DL, RAPP CS, DAY TJ, HONIG B, SHAW DE, FRIESNER RA. A HIERARCHICAL APPROACH TO ALL-ATOM PROTEIN LOOP PREDICTION. *PROTEINS: STRUCTURE, FUNCTION, AND BIOINFORMATICS*. 2004; 55(2):351-67.

JAKUBZICK CV, RANDOLPH GJ, HENSON PM. MONOCYTE DIFFERENTIATION AND ANTIGEN-PRESENTING FUNCTIONS. *NATURE REVIEWS IMMUNOLOGY*. 2017; 17(6):349-362.

JEDDI I, SAIZ L. THREE-DIMENSIONAL MODELING OF SINGLE STRANDED DNA HAIRPINS FOR APTAMER-BASED BIOSENSORS. *SCIENTIFIC REPORTS*. 2017; 26;7 (1):1178.

JENDRO M, GORONZY JJ, WEYAND CM. STRUCTURAL AND FUNCTIONAL CHARACTERIZATION OF HLA-DR MOLECULES CIRCULATING IN THE SERUM. *AUTOIMMUNITY*. 1991; 8(4):289-96.

KABIR J, LOBO M, ZACHARY I. STAUROSPORINE INDUCES ENDOTHELIAL CELL APOPTOSIS VIA FOCAL ADHESION KINASE DEPHOSPHORYLATION AND FOCAL ADHESION DISASSEMBLY INDEPENDENT OF FOCAL ADHESION KINASE PROTEOLYSIS. IN: *BIOCHEMICAL JOURNAL* 2002;367(Pt 1):145-55.

KEEFE AD, PAI S, ELLINGTON A. APTAMERS AS THERAPEUTICS. *NATURE REVIEWS. DRUG DISCOVERY*. 2010; 9 (7):537-50.

KOOPMAN G, REUTELINGSPERGER CP, KUIJTEN GA, KEEHNEN RM, PALS ST, VAN OERS MH. ANNEXIN V FOR FLOW CYTOMETRIC DETECTION OF PHOSPHATIDYLSERINE EXPRESSION ON B CELLS UNDERGOING APOPTOSIS. *BLOOD* 1994; 84(5):1415-20.

KLIMCZAK A, KOZLOWSKA U. MESENCHYMAL STROMAL CELLS AND TISSUE-SPECIFIC PROGENITOR CELLS: THEIR ROLE IN TISSUE HOMEOSTASIS. *STEM CELLS INTERNATIONAL*. 2016; 2016: 4285215.

LAURIDSEN LH, SHAMAILEH HA, EDWARDS SL, TARAN E, VEEDU RN RAPID ONE-STEP SELECTION METHOD FOR GENERATING NUCLEIC ACID APTAMERS: DEVELOPMENT OF A DNA APTAMER AGAINST A-BUNGAROTOXIN. *PLoS ONE*. 2012; 7 (7): e41702.

LEUNING DG, BEIJER NRM, DU FOSSÉ NA, VERMEULEN S, LIEVERS E, VAN KOOTEN C, RABELINK TJ, BOER J. THE CYTOKINE SECRETION PROFILE OF MESENCHYMAL STROMAL CELLS IS DETERMINED BY SURFACE STRUCTURE OF THE MICROENVIRONMENT. *SCIENTIFIC REPORTS*. 2018; 8(1):7716.

LIN, F. ADIPOSE TISSUE-DERIVED MESENCHYMAL STEM CELLS: A FAT CHANCE OF CURING KIDNEY DISEASE? *KIDNEY INTERNATIONAL*. 2012; 82(7):731-3.

LIZARBE MA, BARRASA JI, OLMO N, GAVILANES F, TURNAY J. ANNEXIN-PHOSPHOLIPID INTERACTIONS. FUNCTIONAL IMPLICATIONS. *INTERNATIONAL JOURNAL OF MOLECULAR SCIENCES*. 2013; 14(2):2652-83.

LU XJ, OLSON WK.: A SOFTWARE PACKAGE FOR THE ANALYSIS, REBUILDING AND VISUALIZATION OF THREE-DIMENSIONAL NUCLEIC ACID STRUCTURES. *NUCLEIC ACIDS RES* 2003; 31(17):5108-21.

LUSCOMBE NM, LASKOWSKI RA, THORNTON JM. NUCPLOT: A PROGRAM TO GENERATE SCHEMATIC DIAGRAMS OF PROTEIN-NUCLEIC ACID INTERACTIONS. *NUCLEIC ACIDS RES*. 1997; 25:4940-5.

MALAPEIRA J, ESSELENS C, BECH-SERRA JJ, CANALS F, ARRIBAS J. ADAM17 (TACE) REGULATES TGF β SIGNALING THROUGH THE CLEAVAGE OF VASORIN. *ONCOGENE*. 2011; 30(16):1912-22.

MARIMUTHU C, TANG TH, TOMINAGA J, TAN SC, GOPINATH SC. SINGLE-STRANDED DNA (ssDNA) PRODUCTION IN DNA APTAMER GENERATION. *THE ANALYST*. 2012; 137(6):1307-15.

MARCOS V, LATZIN P, HECTOR A, SONANINI S, HOFFMANN F, LACHER M, KOLLER B, BUFLER P, NICOLAI T, HARTL D, GRIESE M. EXPRESSION, REGULATION AND CLINICAL SIGNIFICANCE OF SOLUBLE AND MEMBRANE CD14 RECEPTORS IN PEDIATRIC INFLAMMATORY LUNG DISEASES. *RESPIRATORY RESEARCH*. 2010;11:32.

MASKOS K, FERNANDEZ-CATALAN C, HUBER R, BOURENKOV GP, BARTUNIK H, ELLESTAD GA, REDDY P, WOLFSON MF, RAUCH CT, CASTNER BJ, DAVIS R, CLARKE HR, PETERSEN M, FITZNER JN, CERRETTI DP, ET AL. CRYSTAL STRUCTURE OF THE CATALYTIC DOMAIN OF HUMAN TUMOR NECROSIS FACTOR-A-CONVERTING ENZYME. *PNAS* 1998; 95(7):3408-12.

MCDONALD IK, THORNTON JM. SATISFYING HYDROGEN BONDING POTENTIAL IN PROTEINS. *J MOL BIOL.* 1994; 238(5):777-93.

NEFTEL C, LAFFY J, FILBIN MG, HARA T, SHORE ME, RAHME GJ, RICHMAN AR, SILVERBUSH D, SHAW ML, HEBERT CM, DEWITT J, GRITSCH S, PEREZ EM, GONZALEZ CASTRO LN, LAN X, ET AL. AN INTEGRATIVE MODEL OF CELLULAR STATES, PLASTICITY, AND GENETICS FOR GLIOBLASTOMA. *CELL.* 2019; 178(4):835-849.E21.

NERY AA. HUMAN ADIPOSE MESENCHYMAL STEM CELL SEPARATION BY DNA APTAMERS FOLLOWED BY THE CHARACTERIZATION OF THE OBTAINED PHENOTYPES FROM NEURONAL DIFFERENTIATION. DOCTORAL THESIS. 2013; 13P.

NERY AA, NASCIMENTO IC, GLASER T, BASSANEZE V, KRIEGER JE, ULRICH H. HUMAN MESENCHYMAL STEM CELLS: FROM IMMUNOPHENOTYPING BY FLOW CYTOMETRY TO CLINICAL APPLICATIONS. *CYTOOMETRY. PART A : THE JOURNAL OF THE INTERNATIONAL SOCIETY FOR ANALYTICAL CYTOLOGY.* 2013; 83(1):48-61.

NERY AA, WRENGER C, ULRICH H. RECOGNITION OF BIOMARKERS AND CELL SPECIFIC MOLECULAR SIGNATURES: APTAMERS AS CAPTURE AGENTS. *JOURNAL OF SEPARATION SCIENCE.* 2009; 32(10):1523-30.

NEUDORFER J, SCHMIDT B, HUSTER KM, ANDERL F, SCHIEMANN M, HOLZAPFEL G, SCHMIDT T, GERMEROOTH L, WAGNER H, PESCHEL C, BUSCH DH, BERNHARD H. REVERSIBLE HLA MULTIMERS (STREPTAMERS) FOR THE ISOLATION OF HUMAN CYTOTOXIC T LYMPHOCYTES FUNCTIONALLY ACTIVE AGAINST TUMOR- AND VIRUS-DERIVED ANTIGENS. *JOURNAL OF IMMUNOLOGICAL METHODS .* 2007;320(1-2):119-31.

NIMJEE SM, RUSCONI CP, SULLENGER BA. APTAMERS: AN EMERGING CLASS OF THERAPEUTICS. *ANNUAL REVIEW OF MEDICINE.* 2005; 56:555-83.

NG AP, ALEXANDER WS. HAEMATOPOIETIC STEM CELLS: PAST, PRESENT AND FUTURE. *CELL DEATH DISCOV.* 2017; 3:17002.

NG EW, ADAMIS AP. ANTI-VEGF APTAMER (PEGAPTANIB) THERAPY FOR OCULAR VASCULAR DISEASES. *ANNALS OF THE NEW YORK ACADEMY OF SCIENCES.* 2006; 1082:151-71.

OHUCHI S.. CELL-SELEX TECHNOLOGY. *BIORESEARCH OPEN ACCESS.* 2012;1(6):265-72.

PEREIRA RL, NASCIMENTO IC, SANTOS AP, OGUSUKU IEY, LAMEU C, MAYER G, ULRICH H. APTAMERS: NOVELTY TOOLS FOR CANCER BIOLOGY. *ONCOTARGET.* 2018; 9 (42):26934-26953.

PETRICEVICH VL, REYNAUD E, CRUZ AH, POSSANI L D. MACROPHAGE ACTIVATION, PHAGOCYTOSIS AND INTRACELLULAR CALCIUM OSCILLATIONS INDUCED BY SCORPION TOXINS FROM TITYUS SERRULATUS. *CLINICAL & EXPERIMENTAL IMMUNOLOGY.* 2008; 154(3): 415–423.

PHAN J, KUMAR P, HAO D, GAO K, FARMER D, WANG A. ENGINEERING MESENCHYMAL STEM CELLS TO IMPROVE THEIR EXOSOME EFFICACY AND YIELD FOR CELL-FREE THERAPY. *JOURNAL OF EXTRACELLULAR VESICLES.* 2018; 7(1):1522236.

POPENDA M, SZACHNIUK M, ANTCZAK M, PURZYCKA KJ, LUKASIAK P, BARTOL N, BLAZEWCZ J, ADAMIAK RW. AUTOMATED 3D STRUCTURE COMPOSITION FOR LARGE RNAs. *NUCLEIC ACIDS RES.* 2012; 40(14): e112.

RANI S, RYAN AE, GRIFFIN MD, RITTER T. MESENCHYMAL STEM CELL-DERIVED EXTRACELLULAR VESICLES: TOWARD CELL-FREE THERAPEUTIC APPLICATIONS. *MOLECULAR THERAPY.* 2015; 23(5): 812–823.

RYSAVY NM1, SHIMODA LM, DIXON AM, SPECK M, STOKES AJ, TURNER H, UMEMOTO EY. BEYOND APOPTOSIS: THE MECHANISM AND FUNCTION OF PHOSPHATIDYL SERINE ASYMMETRY IN THE MEMBRANE OF ACTIVATING MAST CELLS. *BIOARCHITECTURE.* 2014; 4 (4-5):127-37.

ROOS K, WU C, DAMM W, REBOUL M, STEVENSON JM, LU C, DAHLGREN MK, MONDAL S, CHEN W, WANG L, ABEL R, FRIESNER RA, HARDER ED. OPLS3E: EXTENDING FORCE FIELD COVERAGE FOR DRUG-LIKE SMALL MOLECULES. *J CHEM THEORY COMPUT* 2019; 15(3):1863-1874.

SEEGAR TCM, KILLINGSWORTH LB, SAHA N, MEYER PA, PATRA D, ZIMMERMAN B, JANES PW, RUBINSTEIN E, NIKOLOV DB, SKINIOTIS G, KRUSE AC, BLACKLOW SC. STRUCTURAL BASIS FOR REGULATED PROTEOLYSIS BY THE A-SECRETASE ADAM10. *CELL.* 2017; 171(7):1638-1648.E7.

SEELAM PP, MITRA A, SHARMA P. PAIRING INTERACTIONS BETWEEN NUCLEOBASES AND LIGANDS IN APTAMER:LIGAND COMPLEXES OF RIBOSWITCHES: CRYSTAL STRUCTURE ANALYSIS, CLASSIFICATION, OPTIMAL STRUCTURES, AND ACCURATE INTERACTION ENERGIES. *RNA.* 2019; 25(10):1274-1290

SCHRÖDINGER L. PYMOL, THE PYMOL MOLECULAR GRAPHICS SYSTEM. N.D.

SHAH KM, STERN MM, STERN AR, PATHAK JL, BRAVENBOER N, BAKKER AD. OSTEOCYTE ISOLATION AND CULTURE METHODS. *BONEKEY REPORTS.* 2016; 5:838

STEIN A, WEBER G, WAHL MC, JAHN R. HELICAL EXTENSION OF THE NEURONAL SNARE COMPLEX INTO THE MEMBRANE. *NATURE.* 2009; 460 (7254):525-8.

TANG J, ZARBOCK A, GOMEZ I, WILSON CL, LEFORT CT, STADTMANN A, BELL B, HUANG LC, LEY K, RAINES EW. ADAM17-DEPENDENT SHEDDING LIMITS EARLY NEUTROPHIL INFLUX BUT DOES NOT ALTER EARLY MONOCYTE RECRUITMENT TO INFLAMMATORY SITES. *BLOOD.* 2011; 118 (3): 786–794.

TERRY DE, CHOPRA RK, OVENDEN J, ANASTASSIADES TP. DIFFERENTIAL USE OF ALCIAN BLUE AND TOLUIDINE BLUE DYES FOR THE QUANTIFICATION AND ISOLATION OF ANIONIC GLYCOCONJUGATES FROM CELL CULTURES: APPLICATION TO PROTEOGLYCAN AND A HIGH-MOLECULAR-WEIGHT GLYCOPROTEIN SYNTHESIZED BY ARTICULAR CHONDROCYTES. *ANALYTICAL BIOCHEMISTRY.* 2000; 285(2):211-9.

ULRICH H, WRENGER C. DISEASE-SPECIFIC BIOMARKER DISCOVERY BY APTAMERS. *CYTOMETRY. PART A: THE JOURNAL OF THE INTERNATIONAL SOCIETY FOR ANALYTICAL CYTOLOGY.* 2009; 75(9):727-33.

VERHOECKX K, COTTER P, LÓPEZ-EXPÓSITO I, KLEIVELAND C, LEA T, MACKIE A, REQUENA T, SWIATECKA D, WICHERS H, KLEIVELAND CR. PERIPHERAL BLOOD MONONUCLEAR CELLS. IN: THE IMPACT OF FOOD BIOACTIVES ON HEALTH. *SPRINGER;* 2015. CHAPTER 15.

WANG M1, YUAN Q1, XIE L1. MESENCHYMAL STEM CELL-BASED IMMUNOMODULATION: PROPERTIES AND CLINICAL APPLICATION. *STEM CELLS INTERNATIONAL.* 2018; 2018:3057624.

WAGERS AJ, WEISSMAN IL. PLASTICITY OF ADULT STEM CELLS. *CELL*. 2004; 116(5):639-48.

WU J, WANG C, LI X, SONG Y, WANG W, LI C, HU J, ZHU Z, LI J, ZHANG W, LU Z, YANG CJ. IDENTIFICATION, CHARACTERIZATION AND APPLICATION OF A G-QUADRUPLEX STRUCTURED DNA APTAMER AGAINST CANCER BIOMARKER PROTEIN ANTERIOR GRADIENT HOMOLOG 2. *PLOS ONE*. 2012; 7(9):E46393.

WU KK. ANALYSIS OF PROTEIN-DNA BINDING BY STREPTAVIDIN-AGAROSE PULLDOWN *METHODS IN MOLECULAR BIOLOGY*. 2006; 338:281-90.

YAN Y, ZHANG D, ZHOU P, LI B, HUANG SY. HDOCK: A WEB SERVER FOR PROTEIN-PROTEIN AND PROTEIN-DNA/RNA DOCKING BASED ON A HYBRID STRATEGY. *NUCLEIC ACIDS RES*. 2017; 45(W1):W365-W373.

YOSHIMURA T, ARIMURA N, KAIBUCHI K. SIGNALING NETWORKS IN NEURAL POLARIZATION. *J. NEUROSCI*, 2006; 26 (42):10626-30.

ZHOU J, ROSSI J. APTAMERS AS TARGETED THERAPEUTICS: CURRENT POTENTIAL AND CHALLENGES. *NATURE REVIEWS DRUG DISCOVERY*. 2017; 16(6):440.

ZHOU J, ROSSI JJ. THE THERAPEUTIC POTENTIAL OF CELL-INTERNALIZING APTAMERS. *CURRENT TOPICS IN MEDICINAL CHEMISTRY*. 2009; 9(12):1144-57.

ZHU JJ, LIU YF, ZHANG YP, ZHAO CR, YAO WJ, LI YS, WANG KC, HUANG TS, PANG W, WANG XF, WANG X, CHIEN S, ZHOU J. VAMP3 AND SNAP23 MEDIATE THE DISTURBED FLOW-INDUCED ENDOTHELIAL MICRORNA SECRETION AND SMOOTH MUSCLE HYPERPLASIA. *PNSA*. 2017; 114 (31):8271-8276.

ZUK PA, ZHU M, MIZUNO H, HUANG J, FUTRELL JW, KATZ AJ, BENHAIM P, LORENZ HP, HEDRICK MH. MULTILINEAGE CELLS FROM HUMAN ADIPOSE TISSUE: IMPLICATIONS FOR CELL-BASED THERAPIES. *TISSUE ENGINEERING*. 2001; 7: 211-228.

ZUKER M. MFOLD WEB SERVER FOR NUCLEIC ACID FOLDING AND HYBRIDIZATION PREDICTION. *NUCLEIC ACIDS RES*. 2003; 31 (13), 3406-15.

8. LISTA DE ANEXOS

8.1 Súmula Curricular

DADOS PESSOAIS

Nome: Ana Paula de Jesus Santos

Local e data de nascimento: São Paulo - Brasil, 28/09/1988

EDUCAÇÃO

Colégio: ETEC Guaracy Silveira, São Paulo, 2006

Universidade: Universidade de São Paulo, Ribeirão Preto, 2012

Graduação (Química)

OCUPAÇÃO

Universidade de São Paulo, São Paulo, SP - Brasil, 2014 - 2020

Doutorado direto em Bioquímica

Universidade Técnica de Munique, Munique, Bavária - Alemanha , 2018-2019

Doutorado Sanduíche

8.2 Publicações

1. OLIVEIRA-GIACOMELLI, A.; ALBINO, C. M., DE SOUZA, H. D.; CORRÊA-VELLOSO, J.; SANTOS, A. P.; ULRICH, H. P2Y6 and P2X7 receptor antagonism exerts neuroprotective/ neurodegenerative effects in an animal model of Parkinson's disease. *Frontiers in Cellular Neuroscience*. 18;9:500, 2019.
2. PEREIRA, R. L.; NASCIMENTO, I. C.; SANTOS, A. P.; OGUSUKU, I. E. Y.; LAMEU C.; MAYER, G.; ULRICH, H. Aptamers: Novelty Tools for Cancer Biology. *Oncotarget*, 9:26934-26953, 2018.
3. ULRICH, H.; RATAJCZAK, M. Z.; SCHNEIDER, G., ADINOLFI E.; ORIOLI E.; FERRAZOLI E. G.; GLASER T.; CORRÊA-VELLOSO J.; MARTINS P. C. M.; COUTINHO F.; SANTOS A. P. J.; PILLAT M. M.; SACK U.; LAMEU C. Kinin and Purine Signaling Contributes to Neuroblastoma Metastasis. *Frontiers in*

Pharmacology, 9:500, 2018.

ANEXO I

Accession	Description (Proteins found to DP-MSK bound to APT10)
P07437	Tubulin beta chain OS=Homo sapiens OX=9606 GN=TUBB PE=1 SV=2 - [TBB5_HUMAN]
P01891	HLA class I histocompatibility antigen, A-68 alpha chain OS=Homo sapiens OX=9606 GN=HLA-A PE=1 SV=4 - [1A68_HUMAN]
Q15286	Ras-related protein Rab-35 OS=Homo sapiens OX=9606 GN=RAB35 PE=1 SV=1 - [RAB35_HUMAN]
Q86Y82	Syntaxin-12 OS=Homo sapiens OX=9606 GN=STX12 PE=1 SV=1 - [STX12_HUMAN]
P52597	Heterogeneous nuclear ribonucleoprotein F OS=Homo sapiens OX=9606 GN=HNRNPF PE=1 SV=3 - [HNRNPF_HUMAN]
Q9Y4E6	WD repeat-containing protein 7 OS=Homo sapiens OX=9606 GN=WDR7 PE=1 SV=2 - [WDR7_HUMAN]
P56192	Methionine--tRNA ligase, cytoplasmic OS=Homo sapiens OX=9606 GN=MARS PE=1 SV=2 - [SYMC_HUMAN]
Q86Y82	Type-1 angiotensin II receptor-associated protein OS=Homo sapiens OX=9606 GN=AGTRAP PE=1 SV=1 - [ATRAP_HUMAN]
Q8TCJ2	Dolichyl-diphosphooligosaccharide--protein glycosyltransferase subunit STT3B OS=Homo sapiens OX=9606 GN=STT3B PE=1 SV=1 - [STT3B_HUMAN]
P50552	Vasodilator-stimulated phosphoprotein OS=Homo sapiens OX=9606 GN=VASP PE=1 SV=3 - [VASP_HUMAN]
O95255	Multidrug resistance-associated protein 6 OS=Homo sapiens OX=9606 GN=ABCC6 PE=1 SV=2 - [MRP6_HUMAN]
Q9Y262	Eukaryotic translation initiation factor 3 subunit L OS=Homo sapiens OX=9606 GN=EIF3L PE=1 SV=1 - [EIF3L_HUMAN]
Q8N6C5	Immunoglobulin superfamily member 1 OS=Homo sapiens OX=9606 GN=IGSF1 PE=1 SV=3 - [IGSF1_HUMAN]

O15061	Synemin OS=Homo sapiens OX=9606 GN=SYNM PE=1 SV=2 - [SYNEM_HUMAN]
Q15417	Calponin-3 OS=Homo sapiens OX=9606 GN=CNN3 PE=1 SV=1 - [CNN3_HUMAN]
Q6ZU65	Ubinuclein-2 OS=Homo sapiens OX=9606 GN=UBN2 PE=1 SV=2 - [UBN2_HUMAN]
O15127	Secretory carrier-associated membrane protein 2 OS=Homo sapiens OX=9606 GN=SCAMP2 PE=1 SV=2 - [SCAM2_HUMAN]
A6NI86	Golgin subfamily A member 6-like protein 10 OS=Homo sapiens OX=9606 GN=GOLGA6L10 PE=3 SV=4 - [GG6LA_HUMAN]
O75431	Metaxin-2 OS=Homo sapiens OX=9606 GN=MTX2 PE=1 SV=1 - [MTX2_HUMAN]
Q8IZY2	ATP-binding cassette sub-family A member 7 OS=Homo sapiens OX=9606 GN=ABCA7 PE=1 SV=3 - [ABCA7_HUMAN]
Q15822	Neuronal acetylcholine receptor subunit alpha-2 OS=Homo sapiens OX=9606 GN=CHRNA2 PE=1 SV=2 - [ACHA2_HUMAN]
P78536	Disintegrin and metalloproteinase domain-containing protein 17 OS=Homo sapiens OX=9606 GN=ADAM17 PE=1 SV=1 - [ADA17_HUMAN]
O95714	E3 ubiquitin-protein ligase HERC2 OS=Homo sapiens OX=9606 GN=HERC2 PE=1 SV=2 - [HERC2_HUMAN]
Q9UPX6	UPF0258 protein KIAA1024 OS=Homo sapiens OX=9606 GN=KIAA1024 PE=2 SV=3 - [K1024_HUMAN]
P20645	Cation-dependent mannose-6-phosphate receptor OS=Homo sapiens OX=9606 GN=M6PR PE=1 SV=1 - [MPRD_HUMAN]
Q8WX93	Palladin OS=Homo sapiens OX=9606 GN=PALLD PE=1 SV=3 - [PALLD_HUMAN]
P01111	GTPase NRas OS=Homo sapiens OX=9606 GN=NRAS PE=1 SV=1 - [RASN_HUMAN]
P46778	60S ribosomal protein L21 OS=Homo sapiens OX=9606 GN=RPL21 PE=1 SV=2 - [RL21_HUMAN]

Q9UGP8	Translocation protein SEC63 homolog OS=Homo sapiens OX=9606 GN=SEC63 PE=1 SV=2 - [SEC63_HUMAN]
O94933	SLIT and NTRK-like protein 3 OS=Homo sapiens OX=9606 GN=SLITRK3 PE=2 SV=2 - [SLIK3_HUMAN]
Q9BZF9	Uveal autoantigen with coiled-coil domains and ankyrin repeats OS=Homo sapiens OX=9606 GN=UACA PE=1 SV=2 - [UACA_HUMAN]
P04350	Tubulin beta-4A chain OS=Homo sapiens OX=9606 GN=TUBB4A PE=1 SV=2 - [TBB4A_HUMAN]
P68032	Actin, alpha cardiac muscle 1 OS=Homo sapiens OX=9606 GN=ACTC1 PE=1 SV=1 - [ACTC_HUMAN]
O00303	Eukaryotic translation initiation factor 3 subunit F OS=Homo sapiens OX=9606 GN=EIF3F PE=1 SV=1 - [EIF3F_HUMAN]
O14828	Secretory carrier-associated membrane protein 3 OS=Homo sapiens OX=9606 GN=SCAMP3 PE=1 SV=3 - [SCAM3_HUMAN]
P11279	Lysosome-associated membrane glycoprotein 1 OS=Homo sapiens OX=9606 GN=LAMP1 PE=1 SV=3 - [LAMP1_HUMAN]
P61803	Dolichyl-diphosphooligosaccharide--protein glycosyltransferase subunit DAD1 OS=Homo sapiens OX=9606 GN=DAD1 PE=1 SV=3 - [DAD1_HUMAN]
Q15836	Vesicle-associated membrane protein 3 OS=Homo sapiens OX=9606 GN=VAMP3 PE=1 SV=3 - [VAMP3_HUMAN]
P78559	Microtubule-associated protein 1A OS=Homo sapiens OX=9606 GN=MAP1A PE=1 SV=6 - [MAP1A_HUMAN]
P21964	Catechol O-methyltransferase OS=Homo sapiens OX=9606 GN=COMT PE=1 SV=2 - [COMT_HUMAN]
Q15645	Pachytene checkpoint protein 2 homolog OS=Homo sapiens OX=9606 GN=TRIP13 PE=1 SV=2 - [PCH2_HUMAN]

Q9P035	Very-long-chain (3R)-3-hydroxyacyl-CoA dehydratase 3 OS=Homo sapiens OX=9606 GN=HACD3 PE=1 SV=2 - [HACD3_HUMAN]
P55060	Exportin-2 OS=Homo sapiens OX=9606 GN=CSE1L PE=1 SV=3 - [XPO2_HUMAN]
Q8ND30	Liprin-beta-2 OS=Homo sapiens OX=9606 GN=PPFIBP2 PE=1 SV=3 - [LIPB2_HUMAN]
P21912	Succinate dehydrogenase [ubiquinone] iron-sulfur subunit, mitochondrial OS=Homo sapiens OX=9606 GN=SDHB PE=1 SV=3 - [SDHB_HUMAN]
O15400	Syntaxin-7 OS=Homo sapiens OX=9606 GN=STX7 PE=1 SV=4 - [STX7_HUMAN]
Q9H0U3	Magnesium transporter protein 1 OS=Homo sapiens OX=9606 GN=MAGT1 PE=1 SV=1 - [MAGT1_HUMAN]
P20674	Cytochrome c oxidase subunit 5A, mitochondrial OS=Homo sapiens OX=9606 GN=COX5A PE=1 SV=2 - [COX5A_HUMAN]
P49327	Fatty acid synthase OS=Homo sapiens OX=9606 GN=FASN PE=1 SV=3 - [FAS_HUMAN]
O43795	Unconventional myosin-Ib OS=Homo sapiens OX=9606 GN=MYO1B PE=1 SV=3 - [MYO1B_HUMAN]
Q14254	Flotillin-2 OS=Homo sapiens OX=9606 GN=FLOT2 PE=1 SV=2 - [FLOT2_HUMAN]

Anexo 1. Lista de proteínas relativa à ligação do aptâmero APT10 às DP-MS, obtida por espectrometria de massas.